Abrasion on Concrete Surfaces Caused by Hydraulic Loading with Water-Borne Sands

Mohammad Sabbir Hasan

A Thesis

In

The Department

Of

Building, Civil and Environmental Engineering

Presented in Partial Fulfilment of Requirements

For the Degree of Master of Applied Science (Civil Engineering) at

Concordia University

Montréal, Québec, Canada

August 2015

Concordia University

School of Graduate Studies

This is to certify that the thesis prepared

By: Mohammad Sabbir Hasan

Entitled: Abrasion on Concrete Surfaces Caused by Hydraulic Loading with Water-Borne Sands

and submitted in partial fulfilment of the requirements for the degree of

Master of Applied Science (Civil Engineering)

Complies with the regulations of the University and meets the accepted standards with respect to originality and quality.

Signed by the final examining committee:

Dr. Zhi Chen Chair

Dr. Ali Dolatabadi Examiner

Dr. Lan Lin Examiner

Dr. Samuel Li Co-Supervisor

Dr. Michelle Nokken Co-Supervisor

Approved by _____

Chair of the Department of Graduate Program Director

August, 2015 _____

Dean of Faculty

ABSTRACT

Abrasion on Concrete Surfaces Caused by Hydraulic Loading with Water-Borne Sands

Mohammad Sabbir Hasan

Hydraulic structures play an important role in regulation and transport of water in reservoirs as well as open channels. They are also useful for flow measurement. Examples of such structures include spillways, stilling basins, weirs, gates, and culverts. These structures commonly have concrete surfaces. Under the impacts of water flow, the concrete surfaces suffer inevitably from abrasive erosion. This is particularly problematic for ageing structures under the impacts of flowing water with suspended sediment in high concentrations. Severe abrasion can cause structural deterioration, leading to a shortened service life. It may not be possible to completely prevent abrasion in hydraulic structures. However, it is possible to reduce abrasion by using proper repairing materials. This study is aimed at investigating different types of repairing materials, with respect to their suitability as a protective layer on existing concrete surfaces. This study takes the experimental approach. Concrete specimens of cylindrical shape were cast using four types of materials: 1) a premium quality concrete mix of Portland cement, 2) latex modified repair material, 3) silica fume fibre-reinforced repair material, and 4) fly ash fibre-reinforced repair material. The concrete specimens were allowed to harden for a period of up to 28 days. A series of laboratory experiments were carried out, where the flat circular surface at the top of the concrete cylinders was subject to direct impact (for 3 to 9 hours) from a high-speed jet of a sand and water mixture from a nozzle. Material mass loss was determined as well as the depth of jet-induced abrasion on the top surface, abraded surface topography and abraded material volume, were measured using 3D scan technology. These measurements were analyzed using ArcGIS tools, and MATLAB functions. Evaluations of how well the concrete specimens resisted abrasive erosion were

determined through comparisons. The results show that in terms of abrasion resistance, the silica fume material is the best among the four types of materials, whereas the concrete mix is the poorest. The results also show that abrasion resistance of the concrete specimens increases when they have had sufficient time to age to their maximum structural integrity. A longer exposure to jet flow leads to higher abrasion. This study is perhaps the first to combine 3D scan and ArcGIS technologies to investigate abrasion depth and volume of different concrete materials. This study has led to the development of effective methods for data analysis and interpretation.

Acknowledgement

Prima facea, I am grateful to the Almighty God for the good health and wellbeing that were necessary to complete this research.

I would like to express my special appreciation and thanks to my supervisors Dr. Samuel Li and Dr. Michelle Nokken. Both of them have been a tremendous mentor for me. I am thankful for their aspiring guidance, invaluably constructive criticism and friendly advice during the research project. I am sincerely grateful to them for sharing their truthful and illuminating views on a number of issues related to the research project.

A special thanks to Dr. Attila Michael Zsaki, I am extremely grateful to him for his expert, sincere, valuable guidance and without his help it would not be possible to use 3D scan technology in my research project.

A special thanks to my family. Words cannot express how grateful I am with my mother and father for all of the sacrifices that they have made on my behalf. Their prayer for me was what sustained me thus far. I would also like to thank all of my friends who supported me in my study and incited me to strive towards my goal. At the end, I would like express special appreciation to my close friend Sarfaraz Alam for his generous support when there was no one to answer my queries.

Table of Contents

List of Figures

List of Tables

List of Symbols and Abbreviations

Symbols

a	Affected surface area	m^2
b	Average width of beam	mm
d	Average depth of beam	mm
D_{max}	Maximum aggregate size	mm
L	Span length	mm
P	Maximum applied load	N
P_v	Velocity losses in the transport hoses	m/s
p	Pressure of water jet on the sample surface	MPa
R	Modulus of Rupture	MPa
t	Test duration	min
U	An orthogonal matrix	
v	Velocity of water jet	m/s
$\vec{v}$	Non-zero eigenvector of **v**	
w_o	Critical threshold velocity	m/s
w_1	Mass of the sample	g
w/cm	Water cementing materials ratio	
x_1	Independent variable (age of concrete)	
x_2	Independent variable (compressive strength)	
ρ_w	Density of water	kg/m^3
ρ	Density of water-sand mix	kg/m^3
λ	Eigenvalue of B, which is a scalar	

λ	Aspect ratio	
μ	Velocity losses in the nozzle	m/s

Abbreviations

ACI	American Concrete Institute
ASTM	ASTM International
C_3S	Tricalcium aluminate
EMor	Epoxy mortar
FM	Fineness modulus
HPC	High performance concrete
HPFRC	High performance fibre-reinforced concrete
PC	Principal component
PMor	Polymer-modified cement mortar
SEM	Scanning electron microscope
SFmo	Silica fume mortar
SFco	Steel fibre concrete
SSD	Saturated surface dry
SVD	Singular value decomposition

1. Introduction

1.1 General Description

Durable materials are those which can last for a long span of time without significant deterioration. As a durable material lasts for long, it conserves resources, reduces waste and saves the environment from the negative impacts of repair and replacement. The durability of concrete is far more important than any other material on earth as concrete is the most widely used material in the world after water. The success of concrete lies in its ability to withstand the action of water without serious deterioration, making it an ideal material for building structures to control, store and transport water. Moreover, it is a versatile, strong and durable material which can be formed into a variety of shapes and sizes. Though concrete is most used building material, it consumes a lot of energy for its production, which is an obstacle in sustainable development. Many scientists and researchers have been working on concrete to make it more durable so that it can perform for a longer period. This effort will decrease the demand for the replacement of concrete which will automatically reduce the energy consumption for its production. Also, it will save money.

Concrete is a versatile construction material. One of the most attractive properties of concrete is that when it is newly mixed, it is plastic and malleable, but when it is hardened it becomes very strong and durable. These qualities make concrete unique from other materials. Concrete has various types of usage, such as for building skyscrapers, dams, bridges, sidewalks, highways, and houses. Depending on the use, purpose and environmental conditions, concrete might need some special qualities. That is why various types of concrete have evolved in the last decades for different purposes. For combatting freeze thaw effects, air entrained concrete was developed. There are many other types of concrete as well such as high performance concrete, lightweight

concrete, shotcrete, and roller compacted concrete. Every type of structure has its own issue. Hydraulic structures are submerged or partially submerged in a water body and interrupting the natural water flow. As it disrupts the natural flow of water, one of the major problems of hydraulic structures is abrasion due to water-borne particles like sand, gravel and any other debris. These suspended particles can cause severe damage to hydraulic concrete structures and shorten their life span. Moreover, in North America, a majority of the hydraulic structures are reaching their expected design life. It is not viable to replace them; costs are high and a huge amount of solid waste is generated. Concrete is not a green material, around 5% of greenhouse gases are emitted from cement industry alone. So repair and maintenance of structures is the best way to reduce use of concrete and make the world more sustainable thereby saving a lot of money.

Abrasion erosion damage leads to maintenance problems in hydraulic structures. Minor abrasion-erosion can easily be neglected, but severe abrasion can deteriorate the durability of concrete immensely. Abrasion-erosion damage is mostly caused by the rolling and grinding effect of water-borne particles such as silt, sand, gravel and other solid debris. To protect the hydraulic structures from abrasion, durable and abrasion resistant concrete mixtures are needed.

There are several factors which remarkably influence abrasion resistance of concrete. These factors can be categorized into two different groups, factors from the first group are solely related to the properties of concrete materials such as compressive strength, aggregate properties, water cement ratio, mixture proportions, uses of supplementary materials, fibre reinforcement, curing and surface finishing. Factors from the second group are related to the environment around the

hydraulic structures such as water flow velocity, size, shape and hardness of water-borne particles, impact angle, and frequency of impact attack.

To determine the abrasion resistance of concrete there are four distinguished ASTM standard methods. But among the four, only one method (ASTM C1138) is directly applicable for the abrasion in hydraulic structures. But according to several researchers (Liu 2007), this method is not good for abrasion due to impact. The main focus of this research is to measure the abrasion resistance of concrete due to impact. For this reason, another method has been used in this study, which is adopted from Liu et al. (2006).

1.2 Research Objectives

There are a few goals of this exploration study, destinations are given beneath.

1. The main goal of this study is to determine the abrasion resistance of four types of concrete repair materials which contains supplementary materials such as silica fume, fly ash, latex etc. These repair materials will be used to repair the concrete surfaces of various kind of hydraulic structures which are subjected to abrasion erosion due to water-borne sand.
2. Compare the abrasion resistance of various kind of repair materials in terms of abrasion mass loss, strength, volume loss and abrasion depth.
3. Evaluate the impact of supplementary materials such as silica fume, fly ash, latex polymer and impact of synthetic fibre (polypropylene microfirbe) on abrasion resistance and strength of concrete.
4. In past study, abrasion resistance of concrete was analyzed in terms of abrasion mass loss, compressive strength and abrasion depth. However, volume loss can be another medium to assess abrasion resistance with high accuracy. One of the major focus of this study is to

quantify volume loss utilizing 3D scan technology and processing the data in MATLAB and ArcGIS and establish a new methodology regarding of volume loss.

1.3 Organization of Thesis

This thesis contains of five chapters as follows:

- Chapter 1 begins with the concept of concrete durability, significance of concrete materials and then a background of the abrasion erosion problem of hydraulic structures was described. The scope of the research is also explained.
- Chapter 2 contains a detailed review of previous research related to concrete abrasion due water borne particles. The influence of different parameters such as compressive strength, w/cm ratio, admixtures, fibre reinforcement and finishing procedure on concrete abrasion resistant are described in detail on the basis of previous works.
- Chapter 3 describes the types and properties of concrete materials used, test procedures, methodology which was performed in the experimental program.
- Chapter 4 contains the data obtained from the test procedures. All the test results are discussed and compared with various parameters and compared with the findings of previous research.
- Chapters 5 and 6 present the conclusion of this study and some recommendation for future work.

2. Literature Review

2.1 Introduction

This chapter includes a detailed overview of available research on abrasion erosion in concrete hydraulic structures due to water borne particles such as sand and gravel. There are two types of factors concerning concrete abrasion, the first type one which is solely related to concrete properties such as w/cm ratio, concrete strength, aggregates, admixtures and the second type is related to environment such as velocity of water flow, impact angle, types of debris or water-borne particles. All these factors are discussed in this chapter. Moreover, the existing standard methods for measuring abrasion resistance are also discussed.

2.2 Abrasion of Concrete Surface

Erosion on the concrete structure surface is defined as a "progressive disintegration of solid by cavitation, abrasion or chemical action'' in the ACI Committee 210 report (ACI, 2003). There are basically three types of erosion processes which occur in concrete structures. They are:

1) Abrasion due to cavitation
2) Abrasion due to chemical attack
3) Abrasion due to erosion

2.2.1 Abrasion due to Cavitation

Cavitation damage can start at a point where there is a collapse in water flow due to a pressure change. Usually cavitation bubbles will grow and travel with the water flow and collapse due to a pressure field change. When cavitation bubbles explode close to or near a hard surface, the hard surface faces an extremely high pressure for a very short period of time on a very small area. These kind of high energy impacts are able to damage any kind of solid material. The cavitation process

in concrete is not well documented as metals, but the erosion progresses rapidly after a period of exposure when the surface slightly roughens with tiny cracks or pits. The possible reason behind this phenomenon is that the material beneath the surface is more vulnerable to attack the geometry of pits thereby weakening of the materials due to fatigue load. Frizell et al. (1991) mentioned that the erosion effect of 0.2 cavitation number is small enough to ignore. It this research, cavitation is not considered as it is small enough to be ignored.

2.2.2 Abrasion due to Chemical Attack

There are several types of compounds in hardened concrete, which are attacked by water, salt and acidic solutions, but in most cases the deleterious actions on an impermeable concrete surface is so slow that it can be ignored. There are certain cases in which it might accelerate deterioration and erosion of concrete at a rapid rate. Chemical attack is not the concern of this study so no consideration was made for this type of erosion in this study.

2.2.3 Abrasion due to Erosion

According to ACI ‘’*Abrasion erosion is a process of friction and impact of water borne particles such as silt, sand, gravel, rocks, ice and other kind of debris over a concrete surface of a hydraulic structure’’* (ACI 2003). The abrasion erosion impact can be easily recognized it creates a smooth, worn-appearing surface where erosion due to cavitation leaves small holes and pits on the surface. There are several factors which affect the rate of abrasion erosion and these factors can be categorized into two types. The first type is related to the characteristics of flow and water-borne particles and the second type is related to the properties of concrete itself. The major factors of the first type are size, shape, hardness and density of particles being transported in the water, the flow

velocity and impact angle of water on concrete surface. Bridge piers, spillway aprons, sluiceways, stilling basins and tunnel linings are most vulnerable to abrasion erosion (ACI 2003).

The abrasion action of a particle is divided into three stages. In the first stage, pre-abrasion peeling occurs by water molecules which depends mainly on flow velocity and associated hydraulic pressure. In the second stage the solid particles create an impact on the concrete surface and this impact is dependent on the particle size and hardness of water-borne particles. And in the third stage, abrasion erosion action occurs which is associated with the combined effects of the water borne particle hardness and shape, flow velocity and interfacial bonds of concrete materials (Liu et al., 2006). Figure 2-1 shows all three stages of abrasion process.

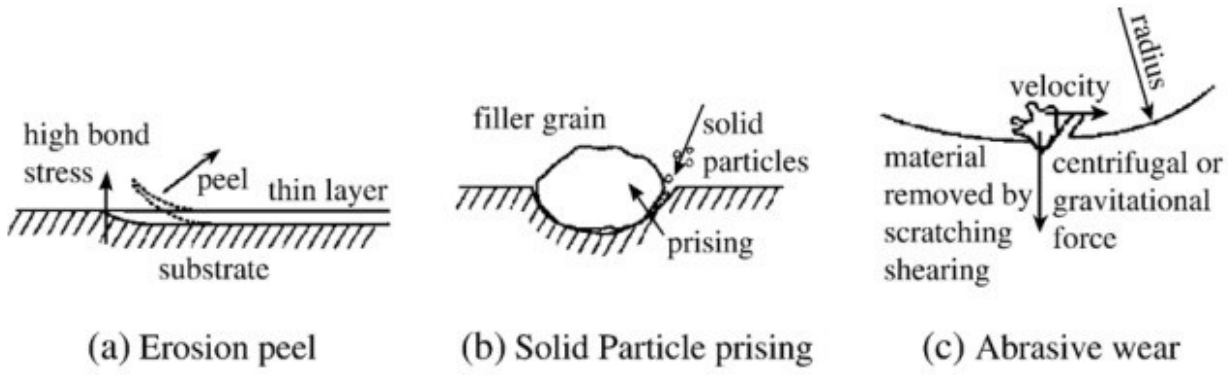

Figure 2-1: Abrasive action of water-borne particle on concrete surface (Liu et al., 2006).

2.3 Standard ASTM Test Methods for Determining Abrasion Resistance of Concrete

There are four standard ASTM test methods for measuring abrasion resistance of concrete. These methods are given below:

1) Abrasion resistance of concrete by sandblasting (ASTM C418)
2) Abrasion resistance of horizontal concrete surface (ASTM C779)

3) Abrasion resistance of concrete or mortar surfaces by the rotating-cutter method (ASTM C944)
4) Abrasion resistance of concrete – Underwater method (ASTM C1138)

2.3.1 Measurement of Abrasion Resistance of Concrete by Sandblasting (ASTM C 418)

ASTM C418 (ASTM 2012) uses the principle of producing abrasion by sandblasting, where concrete is subjected to impingement of air driven silica sand. This test method is a dry method where no water is used, though it can simulate the action of waterborne particles like sand and abrasives under traffic on a concrete surface. In this method, a cutting action is performed which tend to abrade the components of concrete severly which are less resistant. The sandblast apparatus consists of an injector-type gun, which has a high velocity air jet fed with a suitable controlled rate of flow for the abrasive sand (Figure 2-2). The abrasive should follow the specification of ASTM C 778 for sand which specifies that the sand should pass the No. 20 sieve and be retained on the No. 30 sieve. Before the test, the concrete specimen needs to be saturated and surface dried by immersion in water for 24h before the test and wiped with a damp cloth. After making the sample surface dry, the specimen should be kept under the sand blasting nozzle at a distance of 75 ± 2.5 mm. After the test, there will be loss of some concrete mass from the surface due to sand blasting. To determine the volume of abraded materials, an oil based clay is used as a filler to fill the cavities with a moderate amount of finger pressure. From the weight and specific gravity of clay it is possible to determine the mass of abraded portion easily. The adjusting parameters in this method are air pressure, gradation of sand, rate of feed of abrasive charge and the distance of the nozzle from the surface.

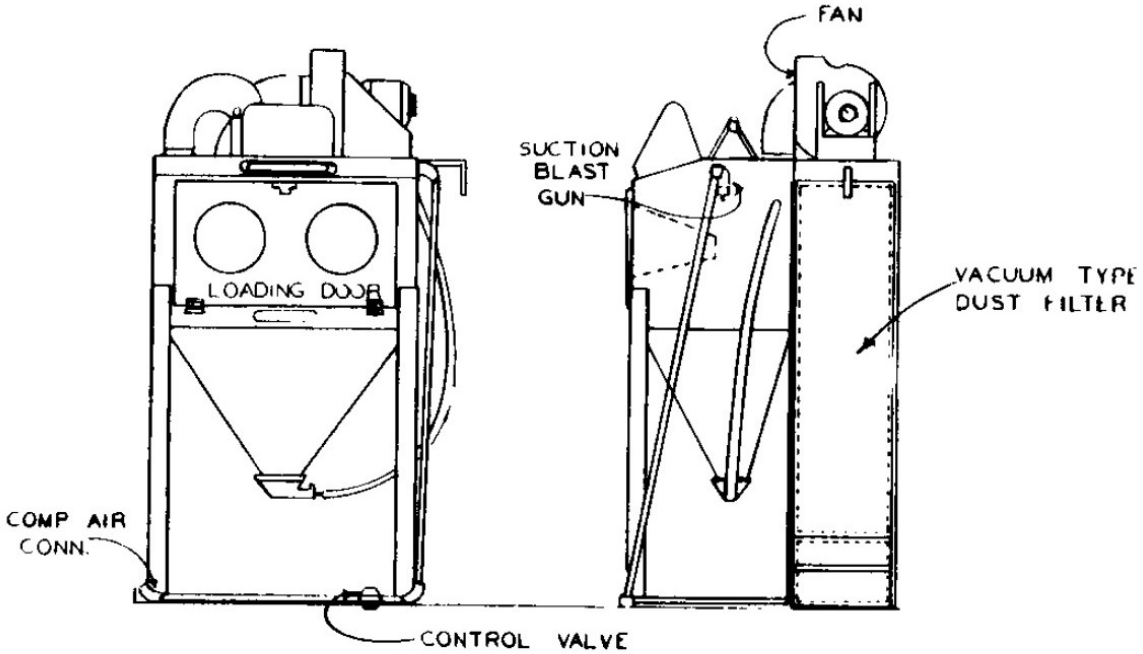

FIG. 2 Sand Blast Cabinet

Figure 2-2: Sand blasting cabinet. (ASTM C418 2012)

2.3.2 Measurement of Abrasion Resistance of Horizontal Concrete Surface (ASTM C 779)

There are three different available procedures in ASTM C 779 (ASTM 2012) to determine the relative abrasion resistance of horizontal concrete surface. These procedures depending on the type and degree of abrasive force and are used in determining the variations on concrete surface affected by mixture design, finishing procedure and surface treatment. The three procedures are:

A. The revolving-disk machine

B. The dressing-wheel machine

C. The ball-bearing machine

The revolving-disk machine abrades the concrete surface by generating frictional forces on the surface by rubbing and grinding. Figure 2-3 shows the image of the test apparatus.

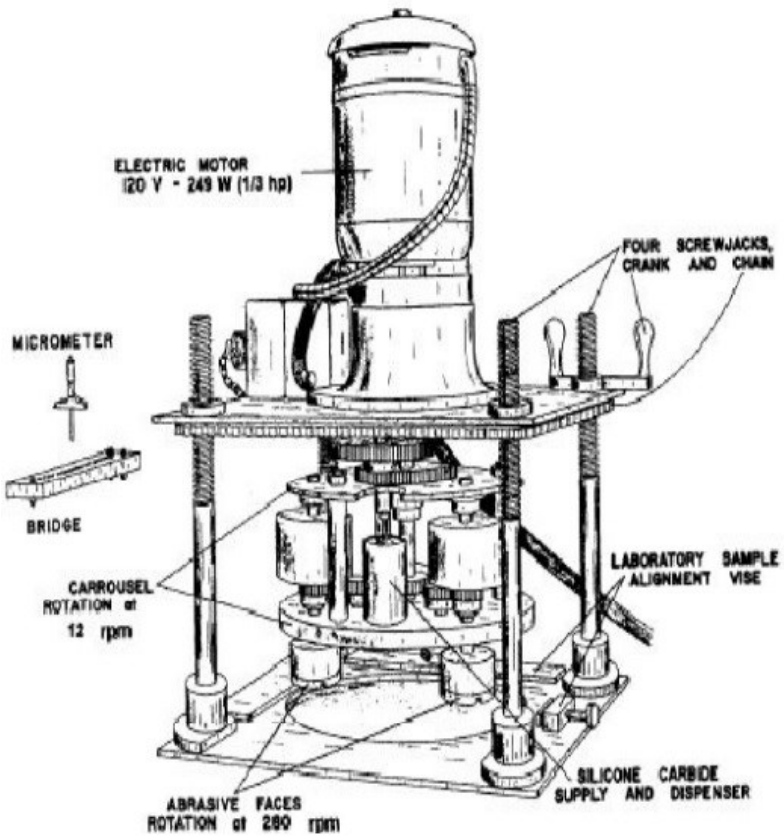

Figure 2-3: Revolving-Disks abrasion test apparatus (ASTM C779, 2012)

Rotating steel disks are in conjunction with abrasive grit sliding and scuffing is accomplished. Abrasive particles used in this method are silicon carbide supplied at the rate of 4-6 g/min. The duration of each test period is 30 minutes, which generally produces significant wear on most concrete surfaces, but if the duration of the test period could be changed from 30 to 60 mins it would provide better results.

The dressing wheel machine and revolving disk machine are similar. The key difference between these two are that three sets of seven dressing wheels mounted on the horizontal shafts take the place of the three rotating steel disks (Figure 2-4). No abrasive particles are used in this machine. With the help of a micrometer, initial and intermediate depths of the test path are measured. The test surface becomes irregular and rough after the test as harder aggregate particles stand out from

the softer paste and dressing wheel leaves a grooved of path on the tracked surface. Depth of wear occurring due to dressing wheel is more than double that occurring with the revolving-disk machine for the same amount of duration (Kumar et al. 2014). This dressing-wheel test method simulates rolling, pounding and cutting action of steel wheel.

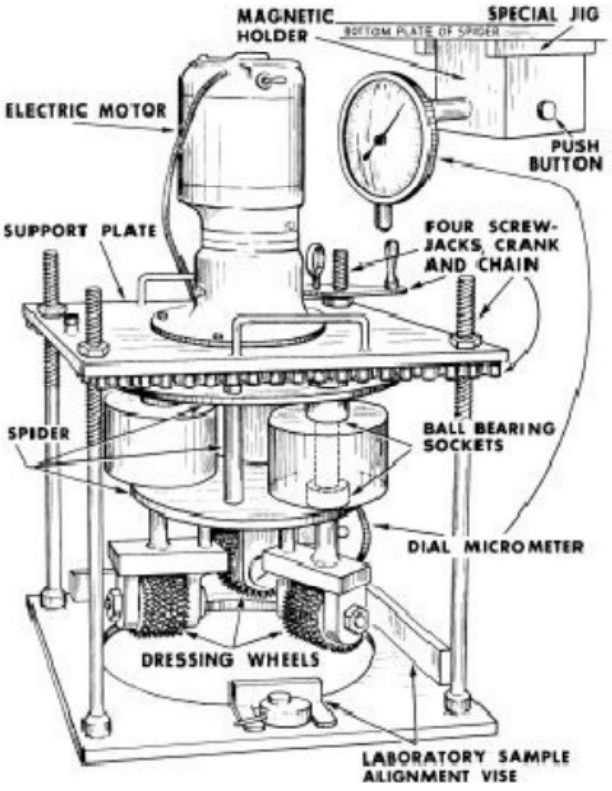

Figure 2-4: Dressing-wheel abrasion test apparatus (ASTM C779, 2012).

For the ball bearing procedure, a series of eight ball bearings rotate under load at a speed of 1000 rpm on a wet concrete surface (Figure 2-5). Water is used to move away the loose particles from the path and bring the ball bearings into contact with the sand and stone particles that still bonded with the concrete surface. Readings of abrasion depth are taken every 50 seconds with a micrometer mounted directly on the supporting shaft allowing readings on the fly. The duration of

each test is 20 minutes where readings are taken at every 50 s. The test is stopped when maximum depth of abrasion is reached which is 3.0 mm. There are a few factors that could affect test accuracy such as the rapid wear of steel balls, differences in age of concrete, insufficient number of wear readings.

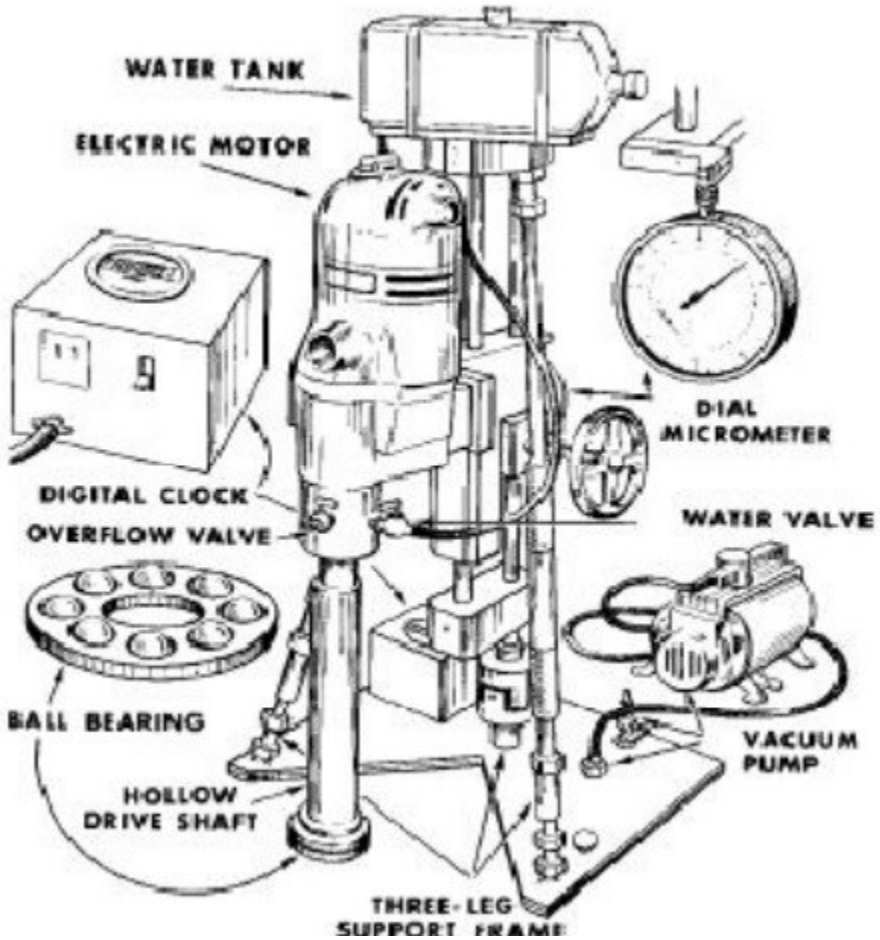

Figure 2-5: Ball-bearing abrasion test apparatus (ASTM C779, 2012)

2.3.3 Abrasion Resistance of Concrete by Rotating-Cutter Method (ASTM C 944)

The ASTM C944 test method is similar to procedure B of ASTM C779 (ASTM 2012). This method is used to determine the abrasion resistance of both concrete and mortar surfaces. It has been used successfully to control the quality of highway and bridge concrete subjected to traffic. It gives an indication of relative abrasion resistance of mortar and concrete based on testing of

cores of fabricated concrete specimen. The test machine contains a rotating cutter and drill press (Figure 2-6). Use of the lever, gear and spring system of a drill press is eliminated from this method to overcome the difficulty of maintaining a constant load on the cutter, instead of this a constant load of 98 N is placed directly on the spindle that turns the cutter.

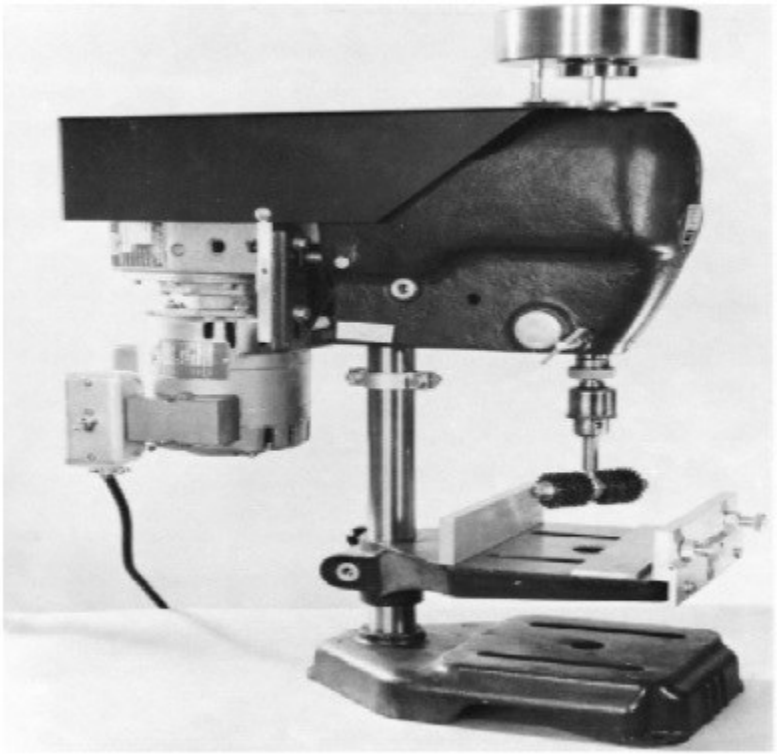

Figure 2-6: The Rotating cutter drill press (ASTM C944, 2012).

2.3.4 Test of Abrasion Resistance of Concrete - Under Water Method (ASTM C1138)

The ASTM C1138(ASTM 2012) test method was originally developed by Liu in 1980 for measuring the abrasion resistance of a concrete surface subjected to abrasion due to water borne particles such as sand and gravel on hydraulic structures like stilling basins, spillways and bridge piers. The test apparatus contains a drill press, an agitation paddle, a cylindrical steel container and 70 grinding balls made of steel of different sizes. Figure 2-7 shows the view of the test apparatus.

Water in the tank is circulated by the agitation paddle which is powered by the drill press rotating at a speed of 1200 rpm. Circulating water moves the grinding balls which create frictional forces on the concrete surface, producing abrasion effects. The duration of a standard test is six 12 hours test periods for a total of 72 hours.

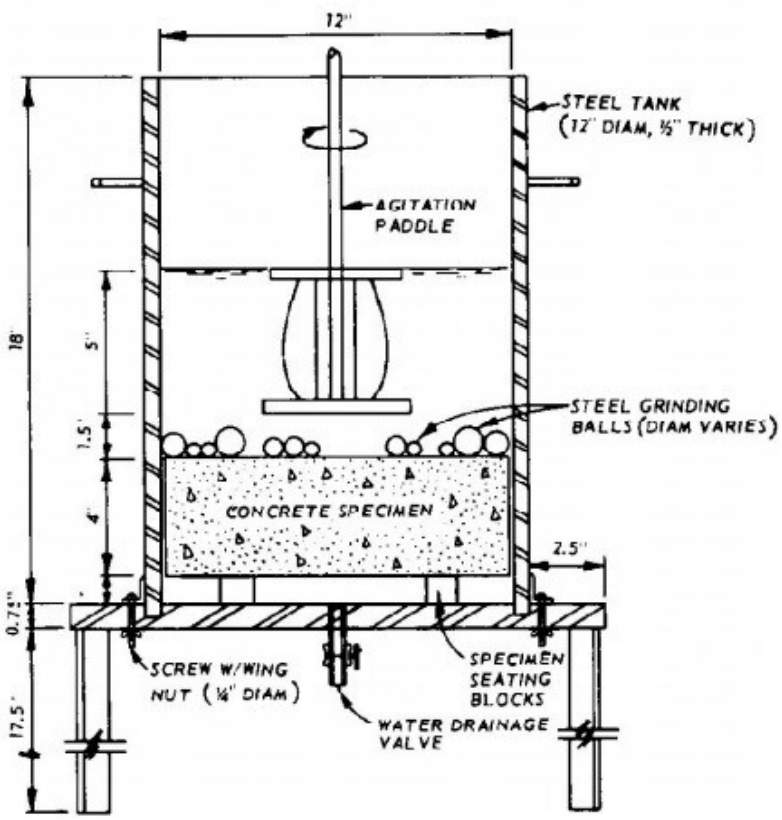

Figure 2-7: Abrasion test apparatus (under water method) (ASTM C1138, 2012).

Among four ASTM standard test method, only ASTM C1138 –Under water method is directly applicable for abrasion erosion in hydraulic structure as it can represents real abrasion scenario in nature. However, Li et al. 2006 says, this method is good for frictional abrasion but not good for abrasion due to impact and also, standard duration of abrasion test is 72hr which is very long.

2.4 Factors Affecting Abrasion Resistance of Concrete

There are several types of factors that affect concrete abrasion. All the factors can be categorized into two major groups. Factors in group one are related to concrete materials and mixture properties and factors in group two are related to the surrounding environment of hydraulic structures. Both types of factors are described below in detail.

Factors related to concrete materials and mixture properties are discussed below:

i. Effect of Water Cement Ratio

Water cement ratio is one of the basic criteria which defines the strength of concrete. Concrete with a low water cement has low porosity which leads to a higher strength and a stronger interfacial bond in hardened concrete, and thus enhances the overall abrasion erosion performance of concrete overall. Lower the water cement ratio lower is the workability. Concrete with a higher water cement ratio has higher workability but the extra amount of water in the concrete makes the hardened mortar porous which decreases the strength of concrete. Different researches has been done regarding the effect of the water cement ratio on abrasion strength of concrete. Liu, Yen and Hsu (2006) investigated Type I Portland cement concrete containing 30% Class F fly ash and used four w/cm ratios of 0.50, 0.36, 0.32 and 0.28. They developed a test method for specially designed to evaluate the abrasion resistance of concrete subjected to water-jet impact and sand impingement. A water jet, which contains sand with a concentration of 400 kg/m^3, directly hits the concrete surface with a speed of 8 m/s and creates a pressure of 0.17 MPa on the surface which causes the abrasion. The test result indicated that abrasion resistance is inversely proportional to the w/cm ratio used in the study. Figure 2-8 shows the relationship of w/cm and abrasion erosion rate. Figure 2-8, clearly shows that with an increase of w/cm the abrasion erosion rate of concrete is also increasing.

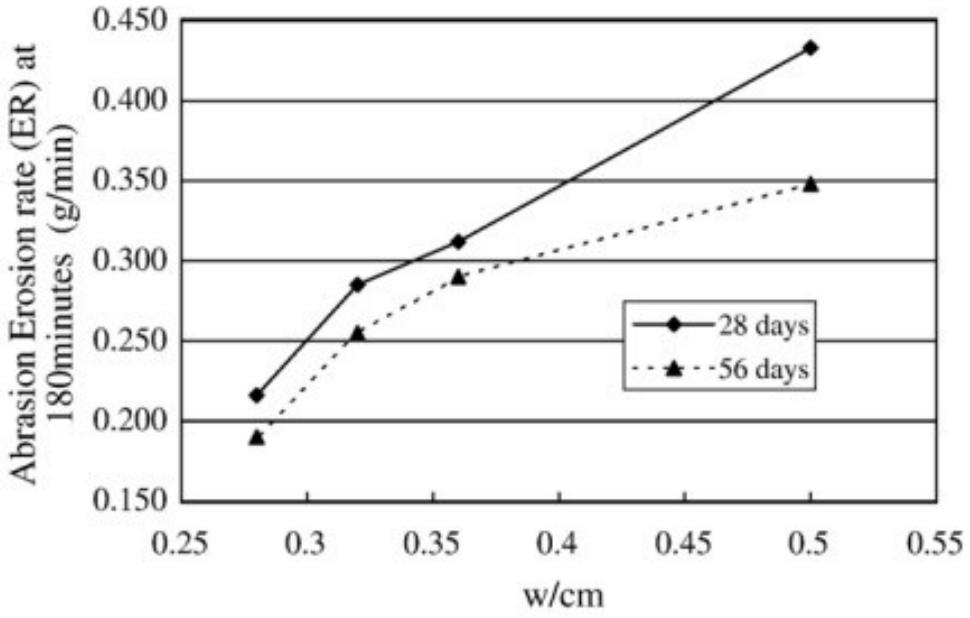

Figure 2-8: Relationship between w/cm and Abrasion erosion rate (Liu et al., 2006)

Shamsai et al. (2012) also evaluated the effect of water-cement ratio of abrasive strength of nano-silica concrete. They used Type I Portland cement in which 3% nano-powder was used to accompany by with 20 mm aggregates. The water-cement ratio varied and the range of the ratio was from 0.33 to 0.50. The experimental method used in this study is a wet-sand blast technique which reflects the abrasion due to water-borne particles in a real scenario.

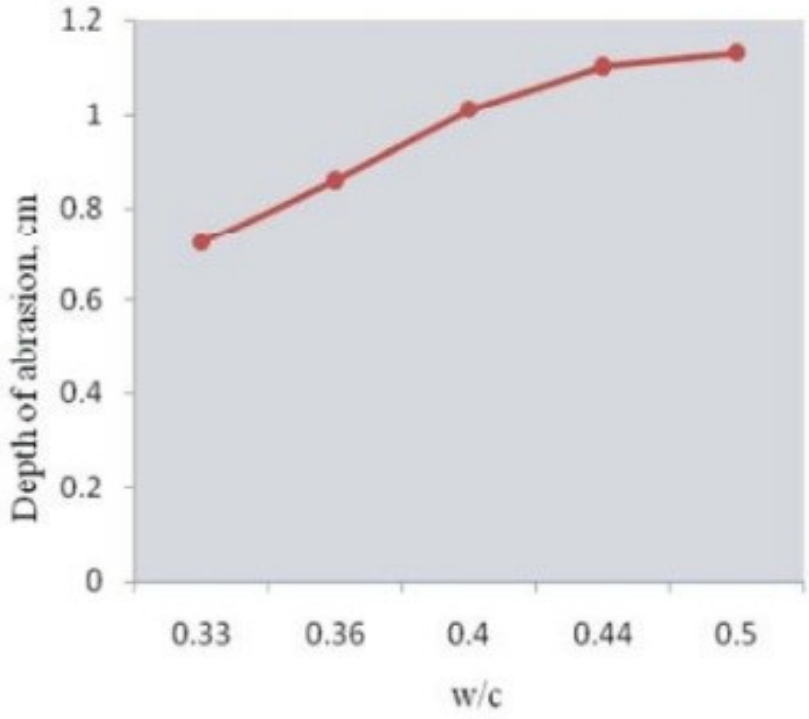

Figure 2-9: Relationship between depth of abrasion and w/cm (Shamsai et al., 2012).

Figure 2-9 shows a similar relation as Liu et al. (2006) between abrasion depth and water cement ratio. Abrasion depth gradually increased as the w/cm ratio increased from 0.33 to 0.50. Shamsai et al. (2012) stated that there are two phases in the nature of abrasion. As the water-cement ratio increases, the abrasion resistance of mortar decreases, but the abrasive resistance of concrete dominates by the resistance of aggregates.

Laplante (1991) used silica-fume concrete with four different w/cm ratios which are 0.27, 0.32, 0.33 and 0.41. All the concrete mixtures were super-plasticized non-air-entrained with a slump ranging from 90mm to 190mm. This study also depicts the same results as expected; lowering w/cm ratio resulted in higher compressive strengths and increased abrasion resistance in both concrete and its mortar.

ii. Effect of Compressive Strength

Compressive strength is one of the most significant factors responsible for the abrasion resistance of concrete stated by many researchers such as Witte and Backstrom (1951). For similar concrete mixtures which contain the same aggregates and finishing procedure, the abrasion resistance of concrete increases with an increment in compressive strength. Figure 2-10 shows an example; the average abrasion resistance of concrete containing limestone increases approximately 44% as compressive strength increases from 3 to 10 ksi (20.7 MPa to 62.1 MPa).

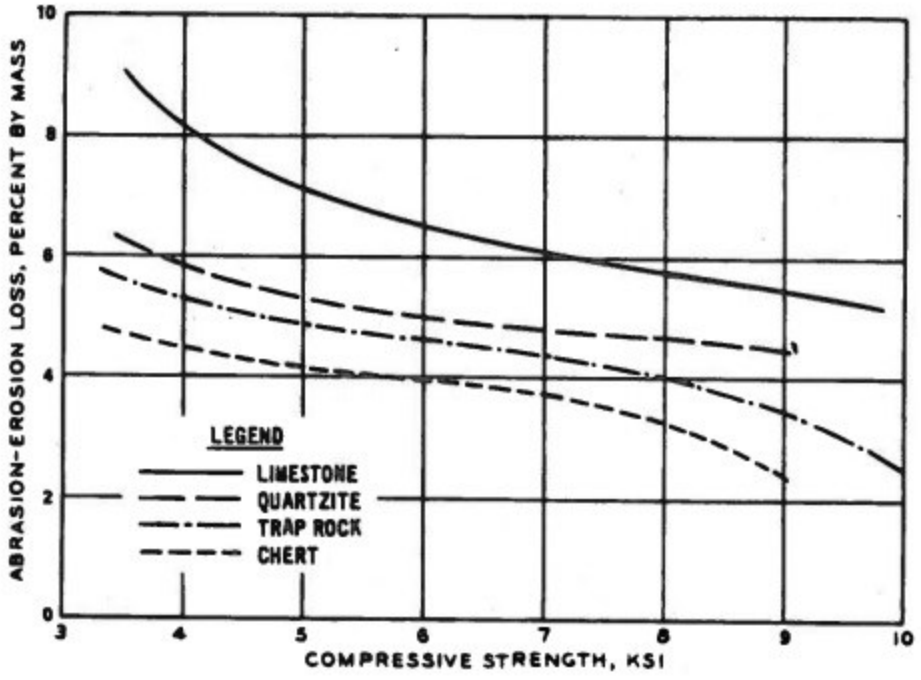

Figure 2-10: Relationship between abrasion resistance and compressive strength of concrete. (Witte and Backstrom 1951)

Liu et al. (2006) compared compressive and flexural strength with abrasion rate where a water-jet with sand was used for abrasion and abrasion was performed for 3 hours. It is clear that concrete strength has a profound impact on the abrasion resistance. Figures 2-11 and 2-12 show the

relationship between abrasion rate, compressive strength and flexural strength, respectively for 3-hour water-jet test.

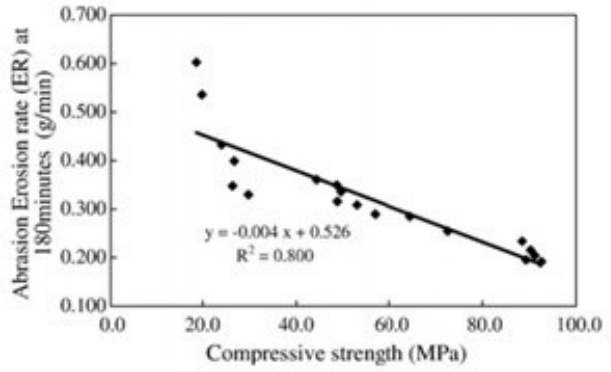

Figure 2-11: Relationship between compressive strength and abrasion erosion rate (Liu et al., 2006)

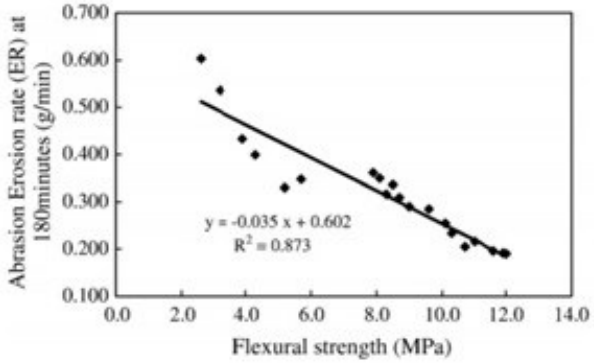

Figure 2-12: Relationship between flexural strength and abrasion erosion rate (Liu et al., 2006)

The computed R^2 for compressive strength and flexural strength are 0.80 and 0.873, respectively, which are reasonably high showing that the properties have good correlation between them. After observing the water jet test, it was revealed that the water jet with sand mix impinged the test slab which caused local tensile stresses on the top layer of the concrete. Intensities of tensile stress vary with the force of water-jet and concentration of sand particles in the jet. These tensile stresses are the main reason behind micro-cracks in the hardened mortar and fractures around the aggregates which eventually lead to abrasion erosion of the surface. The main way to slow down the abrasion erosion is to strengthen the mechanical properties of concrete like compressive strength and flexural strength (Liu et al., 2006).

iii. Effect of Aggregates

Aggregates occupy around 75% of the volume of concrete, which clearly denotes the importance of the properties of aggregates. Gencel et al. (2011) conducted a study on the effect of metallic aggregate on the abrasion resistance behavior of concrete. In this study, hematite was used as a replacement for limestone based aggregates in plain Portland cement concrete. Hematite is a natural bedrock which contains iron oxide and has a Mohs hardness between 5.5 to 6.5 and specific gravity between 4.9 to 5.5 $g \cdot cm^{-3}$; whereas Mohs hardness of limestone is between 3 to 4 and specific gravity is 2.5 to 2.7 $g \cdot cm^{-3.}$ Mixture samples were divided into four major groups A, B, C and D with 300, 350, 400 and 450 kg/m^3 of cement and five subgroups according to replacement percentage of hematite. A single w/cm ratio of 0.4 was used for all the mixture. In this study, 0, 15, 30, 45 and 60% aggregate replacement ratio was used to evaluate the effect of metallic aggregates in concrete (subgroups 1 to 5 respectively). The test method adopted in this study was TS699 which is a Turkish standard method used as an alternative of ASTM C779. The size of sample specimen is 70x70x70 which is used to determine the wear or abrasion resistance at the age of 28 days. According to TS699, the apparatus has a steel disc with a diameter of 750mm which rotates at a speed of 30 cycles/min. An abrasive dust used in this test was crystalline Al_20_3 which is also known as corundum and it gives better friction and causes wear. Three types of normal load (5, 10 and 15 kg) were applied to the specimen and the disc was rotated for four periods where each period was equal to 22 cycles, The normal and frictional forces due to rotation cause abrasion in the sample specimen. Figure 2-13 shows the test apparatus TS699.

Figure 2-13: Abrasion Test apparatus as specified in TS699 (Gencel et al., 2011)

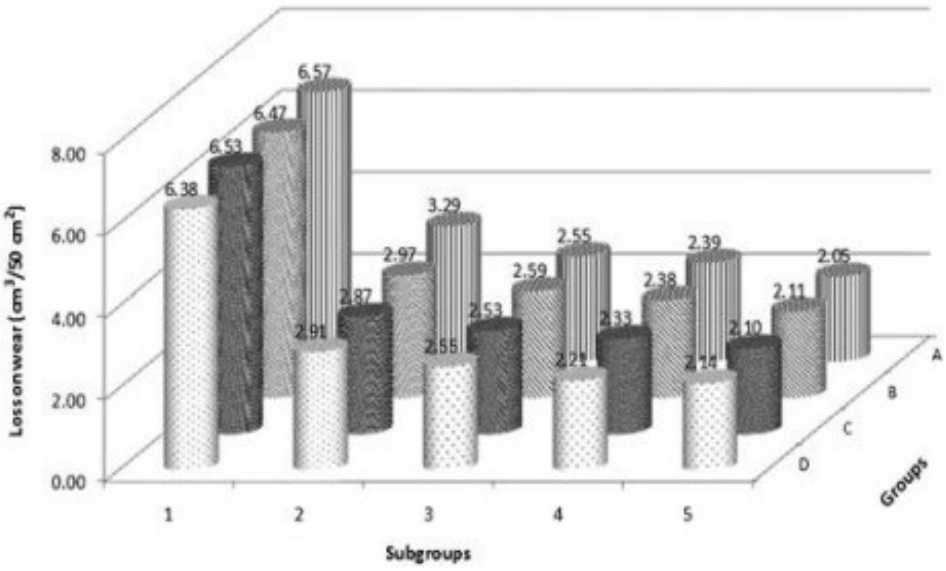

Figure 2-14: Mass loss of concrete under 5 kg load (Gencel et al., 2011)

The test results are illustrated in Figures 2-14, 2-15 and 2-16. Mass loss graphics can be explained in terms of cement content (Group A having the lowest and Group D the highest). Compressive strength increases with the increment of cement dosage with a low w/cm ratio. Mass loss increases with the increasing applied normal load. But when hematite percentage is 0%, an abrasion mass loss is the highest, and it drops at a great scale after adding 15% hematite. Beyond 15% hematite replacement the mass loss difference is not significant which proves that 15% hematite replacement gives optimum results. Abrasive particles produce shear forces due to rotation while normal load helps abrasive materials to penetrate into the specimen surface. The shear force helps to form scratches and grooves on the surface. The test results can be therefore summarized as, an increase in cement content with low w/cm and the replacement of limestone based aggregates in the mixture by hematite increases the compressive strength of concrete which improves the abrasion resistance of concrete.

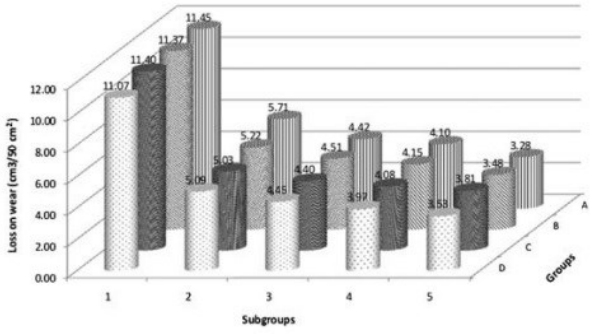

Figure 2-15: Mass loss of concrete under 10kg load (Gencel et al., 2011)

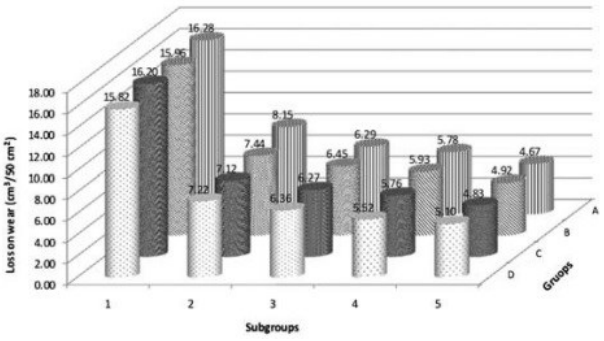

Figure 2-16: Mass loss of concrete under 15kg load (Gencel et al., 2011)

According to Liu et al. (2006), coarse aggregate size, quality, and bond between aggregates and mortar are the prime factors in concrete abrasion. Coarse aggregate near the top surface is often plucked away by the water-borne sand jet flow, which creates a void on the surface. Later, the wall

of the void is subsequently ruptured due to the swirling effect of sand and water pressure, which leads to a larger void and significant surface abrasion erosion. Figure 2-17 shows the void formation attributed to cracks and bleeding along the joint surface between mortar and coarse aggregate (in center of photo). If a high w/cm ratio is used in concrete, it will increase the amount of cementitious material and decrease the coarse aggregate content and will also increase the abrasion erosion rate. When *Dmax* is greater than 13mm it increases the abrasion resistance & when *Dmax* less than or equal to 5mm it decreases the abrasion resistance (Liu et al., 2006).

Figure 2-17: The cracks on the interface of the aggregate and cement paste with w/cm = 0.05 (Liu et al., 2006)

Laplante et al. (1991) tested four types of aggregate with similar composition in concrete with a w/cm ratio of 0.32 and silica fume. All aggregates were characterized in terms of compressive strength, modulus of elasticity, and Los Angeles abrasion resistance. Test results exhibited trap rock had the smallest wear loss which indicates the greatest abrasion resistance among the four. The trap rock and granite concretes exhibited high abrasion resistance where the soft limestone recorded much poorer results. Dolomite limestone is also a good abrasion resistant material, but

not as good as granite and trap rock. Figure 2-18 shows the relationship between abrasion depth and coarse aggregate.

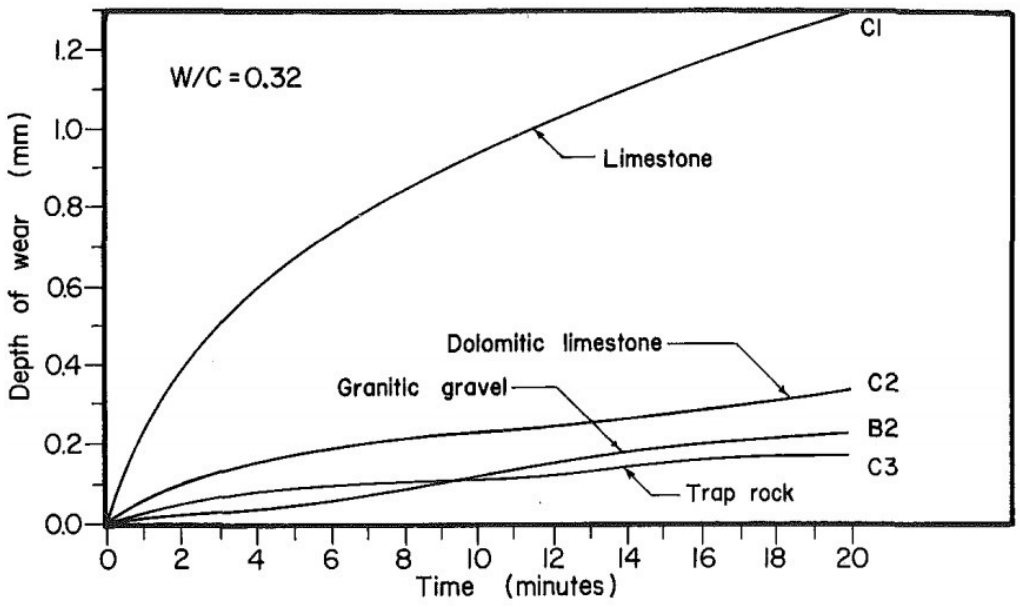

Figure 2-18: Influence of coarse aggregate nature on concrete abrasion resistance (Laplante et al., 1991)

iv. Effect of Silica Fume

Silica fume is a well-known concrete admixture which is primarily used for filling the micro voids of the concrete matrix and the interfacial zone between mortar and coarse aggregate. Silica fume is a pozzolan which reacts with calcium hydroxide and it produces more calcium silicate hydrate, hence reducing the porosity and increasing strength of concrete. Liu et al. (2006) studied the effect of silica fume on concrete abrasion. Two concrete mixtures were prepared by using 5% and 10% silica fume (by weight of cement replacement), with w/cm of 0.38 and 0.40, respectively. Both specimens were moist cured for 28 days. The test results showed that there is a decrease in the

abrasion rate of 10% and 16%, respectively compared to control concrete which contained 0% silica fume. Figure 2-19 shows the effect of silica fume on abrasion rate. Silica fume decreases the abrasion rate because it makes concrete denser and helps to develop good interfacial bond strength between mortar and aggregate.

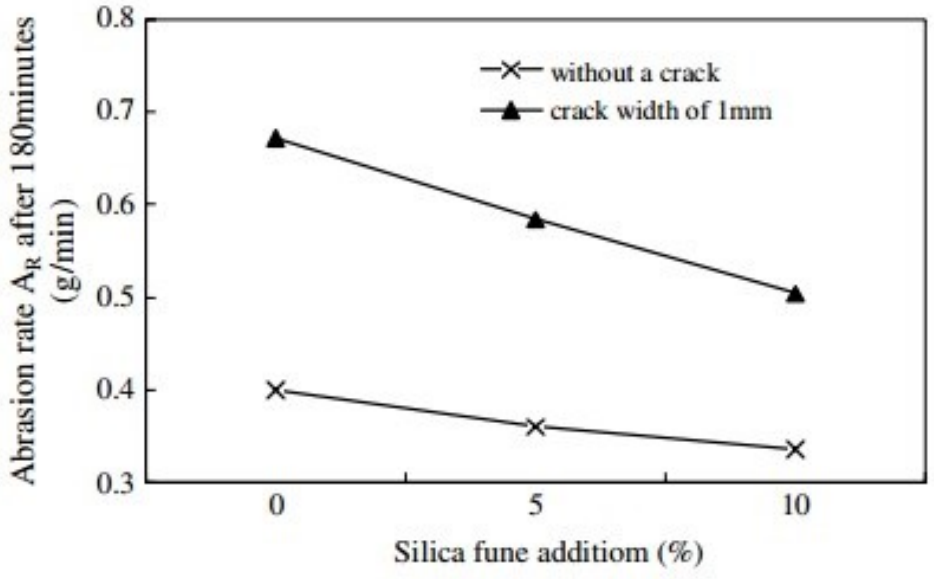

Figure 2-19: Effect of silica fume addition on abrasion rate. (Liu, 2006)

v. Effect of Blast Furnace Slag

Wu et al. (2006) investigated the impact of blast furnace slag on concrete abrasion. Five different w/cm ratios and four slag contents were chosen for the study and other parameters were kept the same. Type I Portland cement (used for general purpose with fairly high C_3S content for early strength development), coarse aggregate with a maximum size of 0.75" (19 mm), fine aggregates with FM 2.82 and super-plasticizer were the same for all concrete mixtures. The flow abrasion test method was used where quartz tic river sand was used to make a slurry mixture and the nozzle was held at 45°angle with respect to sample specimen. Figure 2-20 shows the abrasion loss due to

different slag contents at different ages of concrete. Concrete containing 45% slag with a w/cm ratio of 0.35 exhibited the best abrasion erosion resistance. A reduction in w/cm ratio from 0.42 to 0.28 reduced the abrasion loss.

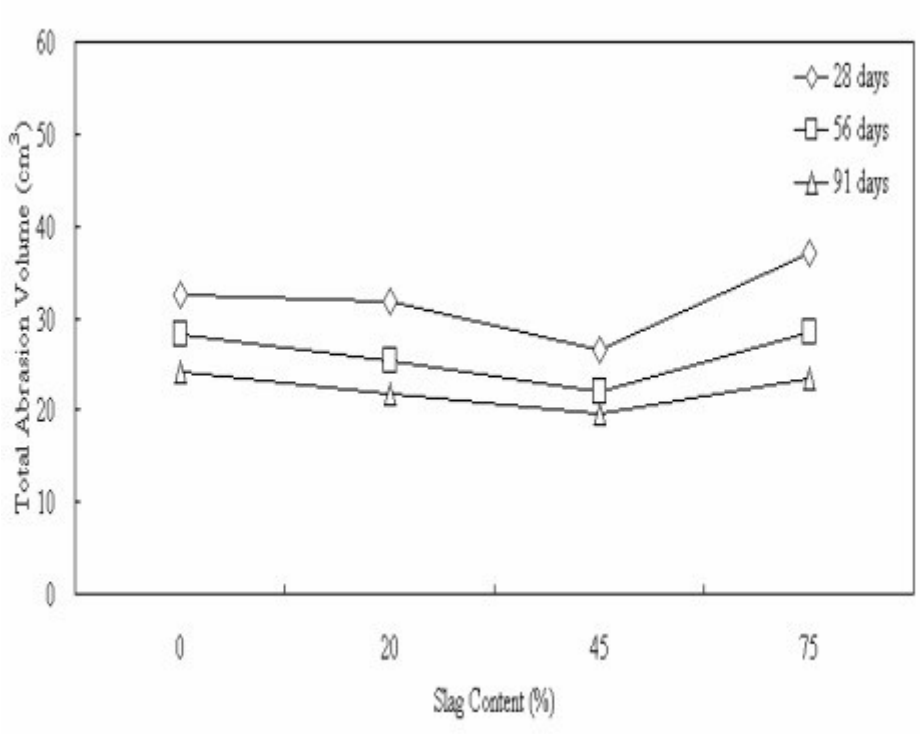

Figure 2-20: Relation of abrasion volume and slag content (Wu et al., 2008).

vi. Effect of Fly ash

Fly ash is one of the popular materials used as a partial replacement of Portland cement in concrete production. Fly ash also known as flue-ash, is one of the residues of coal combustion and it is made of silicon dioxide and calcium oxide. However the components of fly ash may vary considerably depending on the source & the way coal is being burnt. Naik et al. (1993) investigated the effect of Class C fly ash on the abrasion resistance of high-strength concrete. In that study, they used five

levels of cement replacement levels (15, 30, 40, 50, and 70%) of Class C fly ash. Their study says that abrasion resistance is very much related to compressive strength and up to 30% replacement of cement by class C fly ash exhibited similar abrasion resistance as cement without fly ash. However beyond 30%, the compressive strength of concrete decreased by a considerable amount and also abrasion resistance of concrete decreased significantly. Cement replacement of 70% with fly ash exhibits worst abrasion resistance as compressive strength decreases significantly. The conclusion of this study performs up to 30 % replacement of cement by Class C fly ash well, beyond that both compressive strength and abrasion resistance decreased with the increase of fly ash content in concrete.

However, Yen et al. (2007) stated that concrete mixtures up to 15% cement replacement by Class F fly ash had similar abrasion resistance to concrete without fly ash. Beyond 15%, abrasion resistance decreased with increasing amount of cement replacement, particularly at low w/c ratios. In this study, 15%, 20%, 25% and 30% cement replacement by Class F fly ash were used in high strength concrete (HSC) and the test was done in accordance with ASTM C 1138. Figures 2-21 and 2-22 show the relation of wear with cement replacement by mass with fly ash at the age of 28 and 91 days, respectively. It was found that when cement replacement by fly ash is beyond 15% and when the compressive strength of concrete samples are similar the abrasion resistance of the samples decreases with the increasing fly ash content.

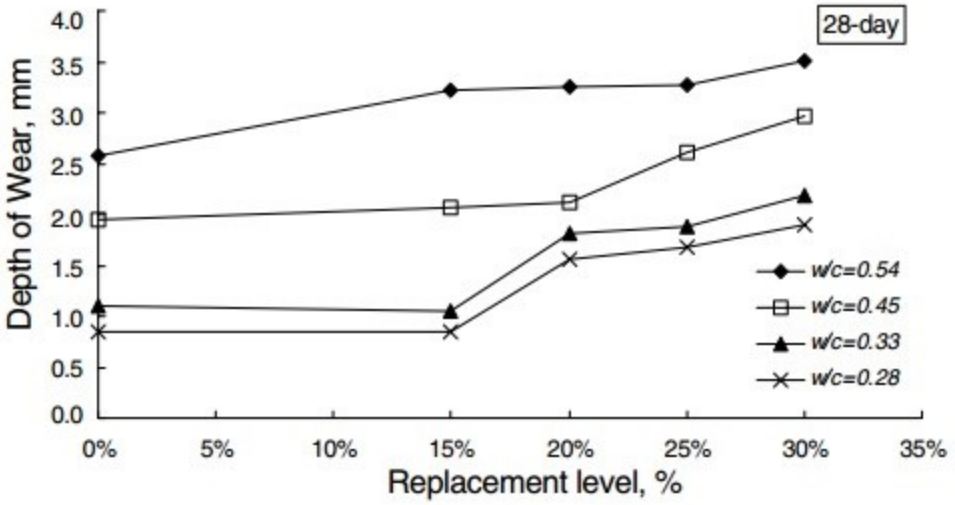

Figure 2-21: Effect of fly ash on the abrasion resistance of concrete at the age of 28 days (Yen et al., 2007).

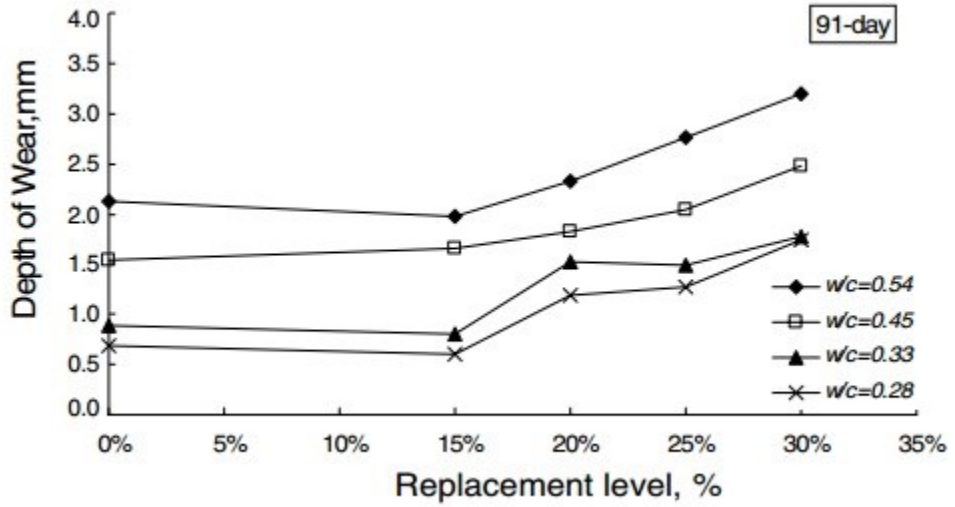

Figure 2-22: Effect of fly ash on the abrasion resistance of concrete at the age of 91 days. (Yen et al., 2007)

Siddique (2003) conducted similar research with 10, 20, 30, 40 % Class F fly ash as a replacement for fine aggregates in Portland cement concrete. Contrary to other researchers, the conclusion for this research was that abrasion resistance of concrete increased with the increasing fly ash content. Figure 2-23 shows that depth of wear decreased with the increment of fly ash percentage when it

is used as a replacement for fine aggregate and moreover abrasion decreases with the increasing age of concrete.

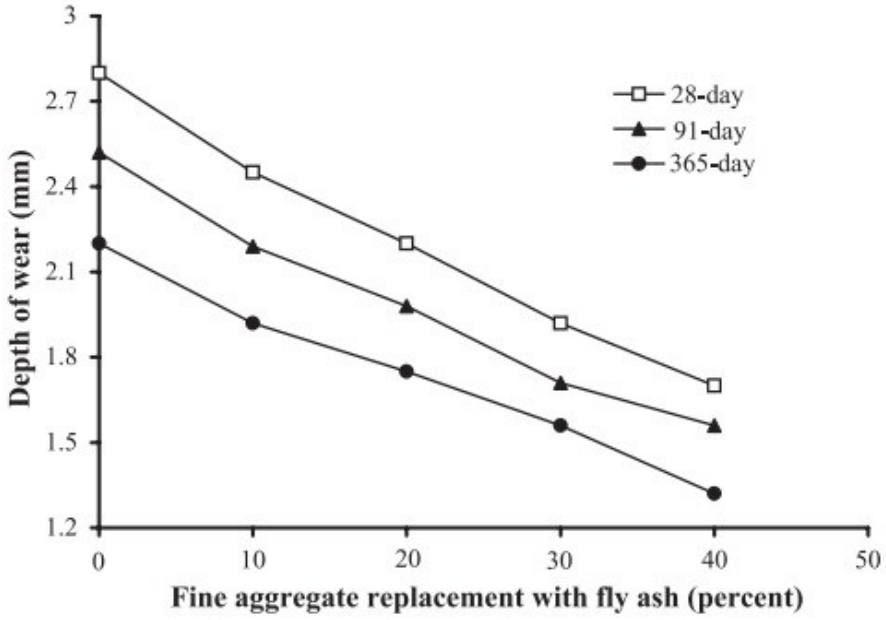

Figure 2-23: Depth of wear at 60 min of abrasion versus fine aggregate replacement with fly ash (Siddique, 2003).

However, in a later study, Siddique et al. (2007) used high volume fly ash (HVFA) concretes made with 35, 45, 55, and 65 % of cement replacement for their study. Test results indicated that concrete containing fly ash up to 35% as cement replacement exhibited similar abrasion resistance to control mixture at the ages of 28 and 365 days.

vii. Effect of Fibre on Concrete Abrasion

Horszczaruk (2009) investigated abrasion resistance of two types of concrete; high performance concrete (HPC) and high performance fibre-reinforced concrete (HPFRC). The three types of fibre used in this investigation are steel fibre of 30 and 50mm length and polypropylene fibres of 19mm length. Figure 2-24 shows an image of the three types of fibres used. The first steel fibre's length

is 30mm where the diameter is 0.5mm with an aspect ratio of λ=60 and tensile strength of above 1400 N/mm^2 and the second steel fibre's length is 50mm with a diameter of 1.0mm, aspect ratio of λ= 50 and tensile strength of above 1200 N/mm^2. High performance concrete used here had a compressive strength of 100 MPa and was made of Portland cement, natural river sand having a fineness modulus of 2.5. For aggregates, basalt was used with a nominal particle size of 16mm. Silica fume containing 92% SiO_2 with a specific surface area of 19,000 m^2/kg and a polycarboxylic ether was used as super-plasticizer. The test method used in this study was ASTM C 1138, "Underwater method''. All abrasion tests were performed for 120 hours.

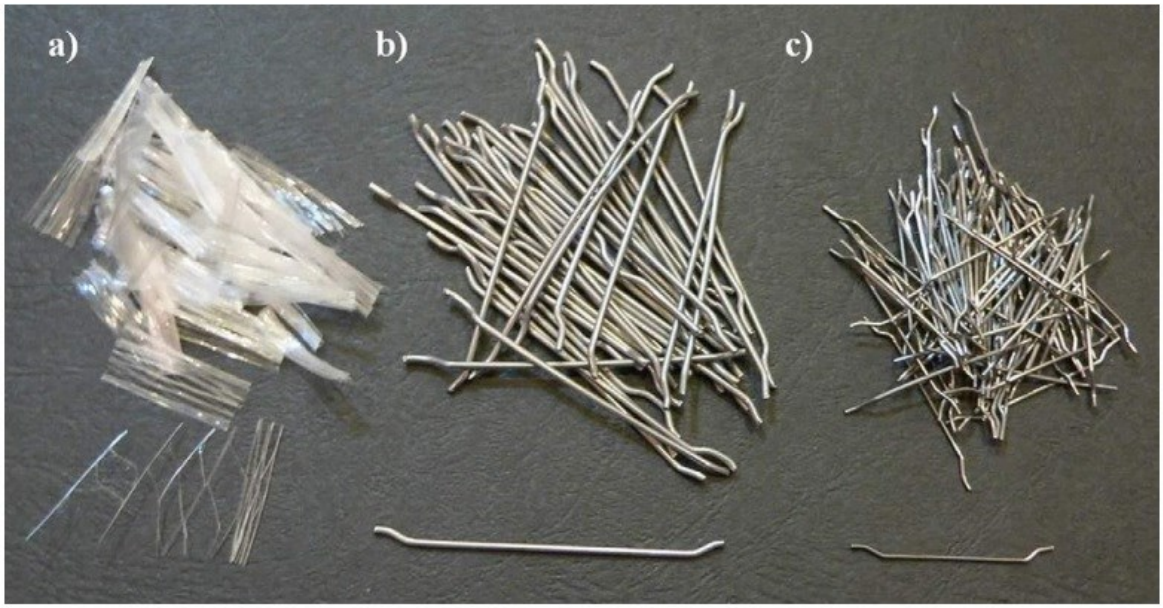

Figure 2-24: Fibre used for reinforcement: a) polypropylene fibres, (b) steel fibres (ME 50/10), (c) steel fibres (ME 30/50) (Horszczaruk, 2009)

The test results showed that the steel fibres do not increase abrasion resistance if the speed of flow is low. Abrasion erosion depends on the orientation of the fibres, especially on the upper surface of the concrete and the incident angle of abrasive particles on the fibres. It showed that the best abrasion resistance was observed for the steel fibre with an aspect ratio of 50 which has a low rigidity. Concrete with polypropylene fibre exhibited better abrasion resistance than HPC concrete

without fibres. Figure 2-25 (a & b) illustrates the mass loss and mean wear depth of different types of concrete with test duration.

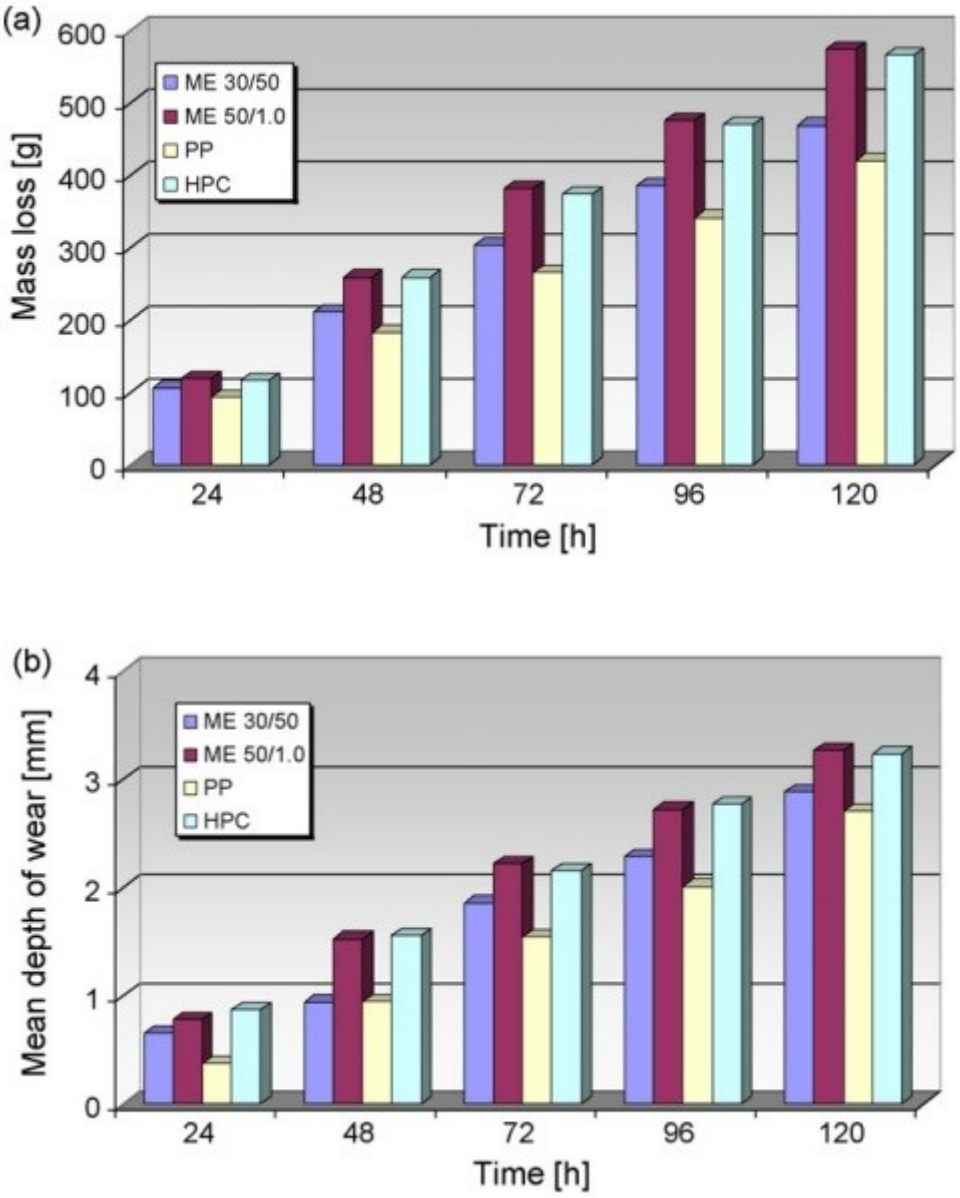

Figure 2-25: Abrasion test results of concrete specimens: (a) mass loss, (b) mean depth of wear, concretes with steel fibres: ME 30/50 and ME 50/1.0, PP- concrete with polypropylene fibres, HPC – concrete without fibres (Horszczaruk, 2009).

Wu et al. (2008) investigated the impact of three types of fibres on the abrasion resistance of concrete. Carbon fibre, glass fibre, and steel fibre were used with Type I Portland cement with a constant w/cm ratio of 0.28. Different percentages of fibre were used in the concrete mixtures; the content of carbon fibre was 1%, glass fibre 0.5%, 1.0%, 1.5% and steel fibre 0.5%, 1.0%, 1.5%. Two different types of test methods were adopted for the research; one was the flow abrasion test where a jet flow at 12m/s which also contained water borne sand was used to abrade concrete. The second method was ASTM C 1138 "Under water method" which is a standard method for abrasion of concrete. Figure 2-26 shows the test results from flow abrasion test for 1% fibre additions. Each test was conducted for 48 hours at the concrete age of 28 days and 56 days. In summary, the steel fibre concrete showed better abrasion resistance with compared to others. The authors also mentioned that fibre concrete with various fibre amounts of 0.5% to 1.5% at the age of 28 and 56 days show almost the same amount of abrasion loss from which it can be concluded that fibre contents have insignificant effects (using fibre reinforcement) on the abrasion resistance of fibre concrete. Results from underwater abrasion test exhibited a similar conclusion. Figures 2-27 and 2-28 show the relation of abrasion erosion volume with test duration of all three types of fibre. Abrasion volume is determined by evaluating mass loss of the concrete specimen. Based on both test results, steel fibre concrete gave better resistance when fibre content is 1%. In the underwater method (ASTM C1138), carbon and glass fibre performance were almost similar where steel fibre concrete showed the best results among the three. The volume of abrasion loss for steel fibre is 20% lower than carbon and glass fibre concretes.

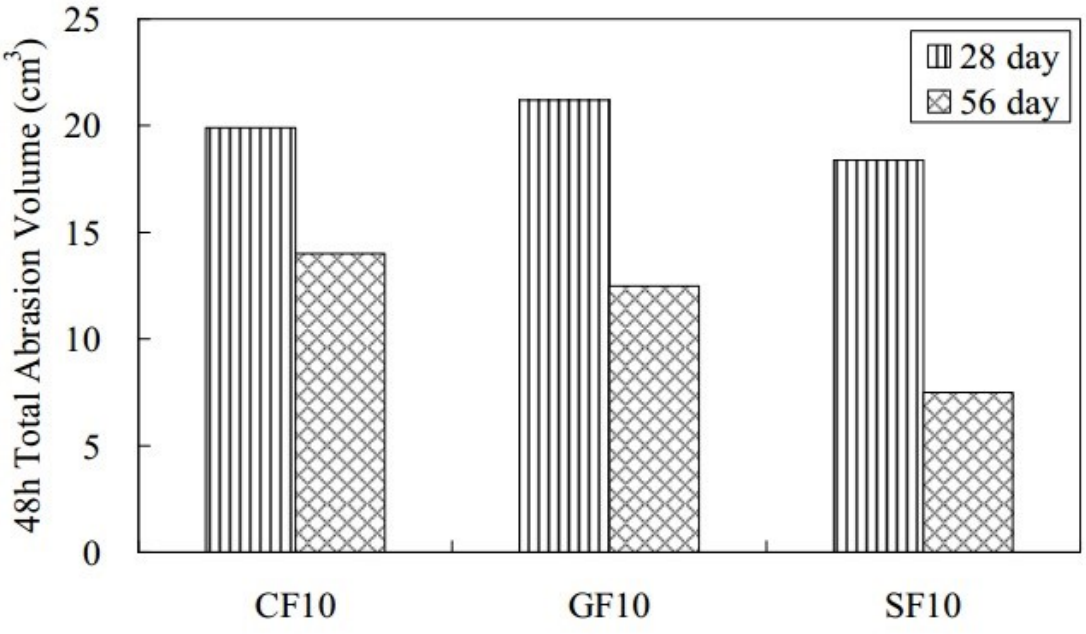

Figure 2-26: Abrasion volume of fibre concrete from flow abrasion test. (Wu et al., 2008)

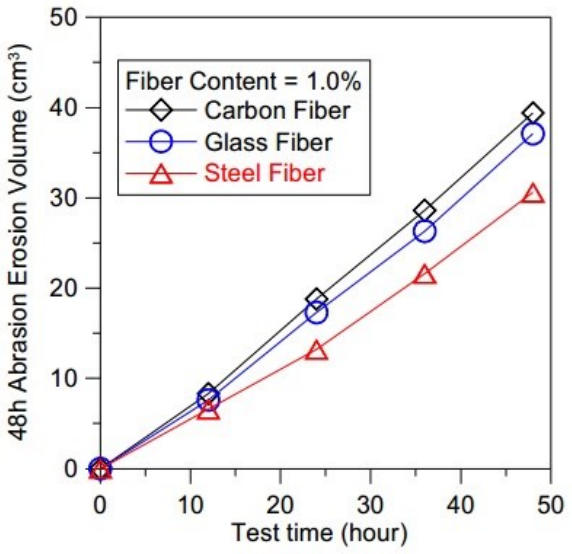

Figure 2-27: Abrasion volume of fibre concretes vs. Test time (28 days) (Wu et al., 2008)

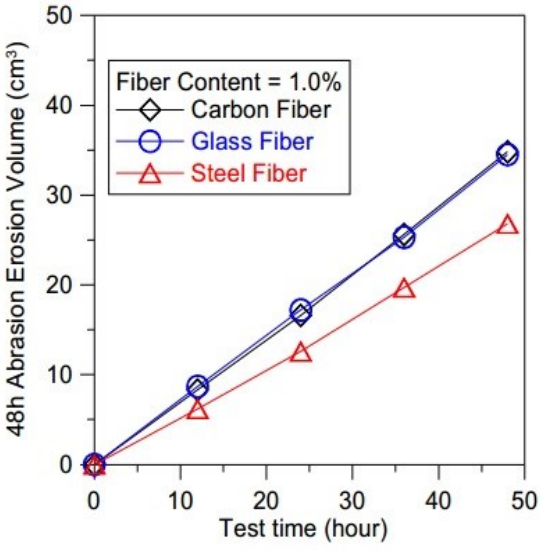

Figure 2-28: Abrasion volume of fibre concretes vs. Test time (56 days) (Wu et al., 2008)

viii. Effect of Polymer Fibre

Siddique et al. (2012) investigated the effect of polyester fibre on the abrasion resistance of high volume fly ash concrete (HVFA) where different percentage of class F fly ash was used along with different content of fibres. These monofilament fibres are alkaline resistant 100% virgin polyester with a length of 12mm with low thermal and electrical conductivity. The method adopted for this study was Indian Standard Specifications IS 1237-1980. Figure 2-29 shows the abrasion test machine which contains a grinding disk with some abrasive particles. In this study, a comparison was made between the content of fibres and compressive strength with same HVFA concrete of the same age.

Figure 2-29: IS 1237-1980 Abrasion test machine (Siddique et al., 2012)

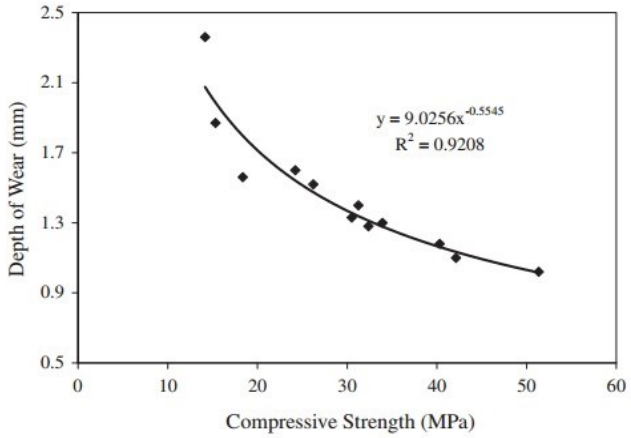

Figure 2-30: Relationships between compressive strength and depth of wear (without fibres) (Siddique et al., 2012)

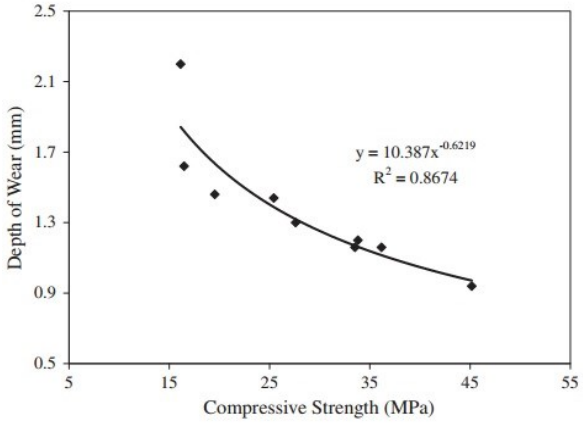

Figure 2-31: Relationships between compressive strength and depth of wear (with 0.05% fibres) (Siddique et al., 2012)

Test results showed that the abrasion resistance increased with the inclusion of fibres in the HVFA concrete matrix. The fibres are crack arresters which can improve the tensile strength and delay the abrasion but the maximum improvement in abrasion resistance is about 15% of these fibres. A possible reason for this is because these monofilament fibres are not as stiff as common plastic fibres. Figure 2-30 and 2-31 show the relationship between compressive strength and depth of wear. In Figure 2-31, the concrete mixtures had no fibres, whereas in the Figure 2-32, the concrete mixture had 0.05% fibre. Comparing both figures it clearly shows that there is a reduction in depth of wear when 0.05% fibre was used regardless of compressive strength.

In other research, Zoran et al. (2012) explored the impact of polypropylene fibres on the abrasion resistance of concrete (Figure 2-33). Two types of polypropylene fibres were used with Portland cement where 3 different w/cm ratios were used to evaluate the impact of the water cement ratio on abrasion resistance and compressive strength. Table 2-1 shows the properties of fibres used in the study.

Table 2-1 : Characteristics of fibres

Characteristic	FIBRILs F120 (fibrillated fibers)	FIBRILs S120 (monofilament fibers)
Fiber length	12 mm	12 mm
Tensile strength	274.0 ± 26.9 N/mm^2	300.7 ± 31.7 N/mm^2
Melting temperature	160.0 °C	163.1 °C

The flow abrasion test apparatus was used for conducting the experiment which is similar to the experiment done by Liu et al. (2006). Figure 2-32 shows the relationship between abrasion rate with compressive strength of three different concrete mixtures, where the first mixture is considered as the benchmark concrete containing Portland cement without any fibres. In the other two mixtures, F 120 and S 120 polypropylene fibre were used. The graph clearly shows that abrasion rate decreased with the increment of compressive strength. Also, it is clear that F 120 polypropylene fibre gave better abrasion protection than S 120 polypropylene fibre. At w/cm of 0.5 the addition of monofilament propylene fibres, FIBRILs S120, increased abrasion resistance by 7.08% where FIBRILs F 120 increased it by 13.74%.

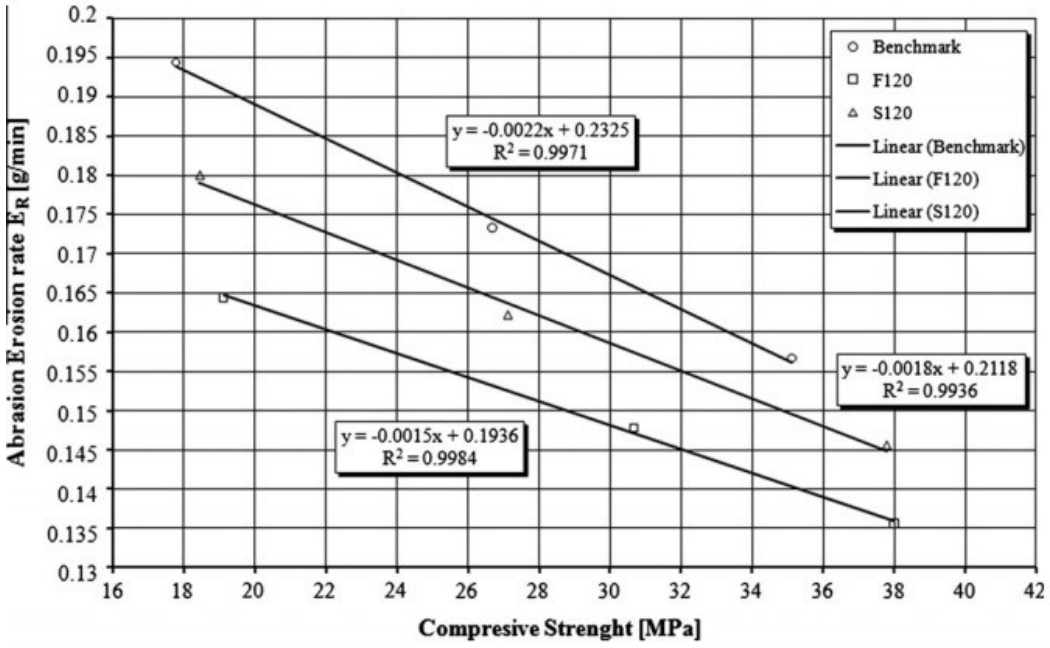

Figure 2-32: The relationship of compressive strength and abrasion erosion rate (Zoran et al., 2012).

ix. Effect of RCC, PCC and SC

Francis et al. (2002) studied several mixtures of Portland Cement Concrete (PCC), Roller Compacted Concrete (RCC) and Soil Cement (SC) to evaluate their abrasion resistance performance. For each type of concrete, similar kinds of aggregate were used to make an accurate comparison. For mixture design, ASTM standard procedure was followed for each material. Abrasion tests were conducted in accordance with ASTM C1138, which is the Under Water method. For RCC and PCC, the abrasion loss was obtained from the results between 24 and 72 hours testing whereas for SC the results were obtained from 12 to 36 hours because of its high erodibility.

Figure 2-34 shows the relationship between abrasion loss and time with three different concrete mixtures. RCC showed the least abrasion loss which means better performance against abrasion

where SC showed the least abrasion resistance. RCC exhibited better abrasion resistance than PCC, especially during the first 36 hours. The primary reasons are aggregates' hardness and strength of cement paste. (The compressive strength of each mixture is shown on the figure in the legend.) The graph indicates that SC is approximately 12 and 19.7 times more erodible than PCC and RCC, respectively at 36hours test.

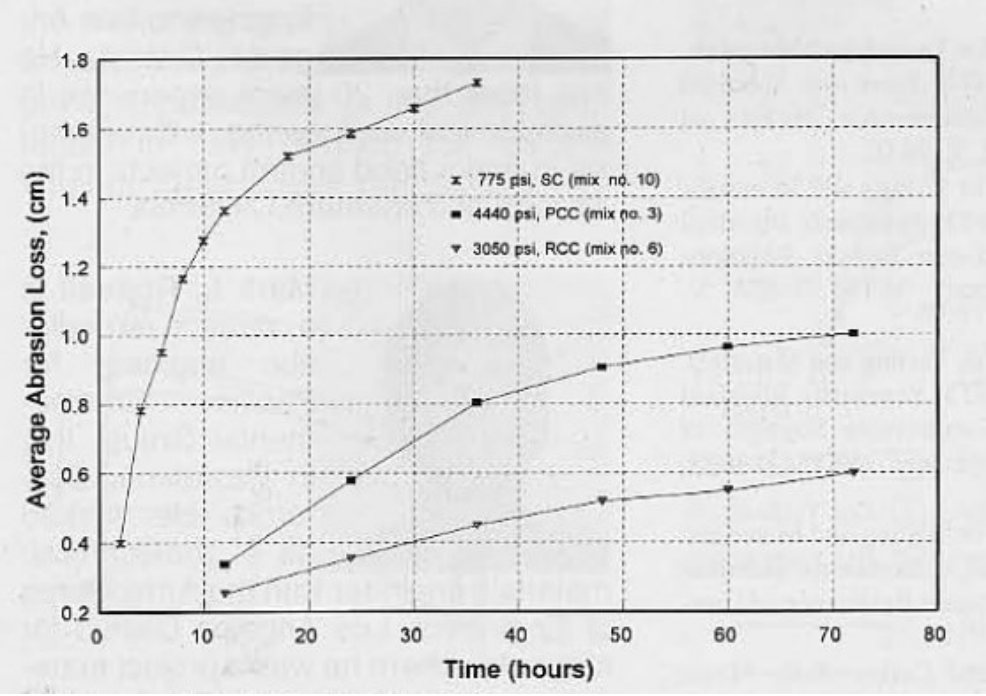

Figure 2-33: Abrasion erosion loss comparison between SC, PCC and RCC (Francis et al., 2002).

x. Performance by repairing materials on concrete abrasion

Korman et al. (2003) studied the performance of four repair materials as a function of a reference conventional concrete (RefC). The materials are polymer-modified cement mortar (PMor), steel fibre concrete (SFco), epoxy mortar (EMor) and silica fume mortar (SFmo). The test method was slightly modified from ASTM C1138 where a 20x5 cm void was left in the center of the concrete sample in order to place the repairing materials and to simulate a border effect which is typically produced when repairing concrete is used in water flow in spillway conditions. Figure 2-34 (a) shows an actual image of EMor sample and Figure 2-34(b) shows a schematic 3-D diagram of EMor sample after abrasion test. From Figure 2-35, it is clear that SFco was found as the best material, followed by EMor. Both of them presented a relative homogeneous surface and lower mass loss was than the RefC sample. The SFmo and PMor presented a visible border abrasion-erosion effect; also PMor presented the highest mass loss. Though SFco was good at abrasion it showed rigorous metal fibre corrosion which is usually followed by volume expansion and tends to crack the mortar or concrete in service which is considered a drawback to its use in hydraulic structures.

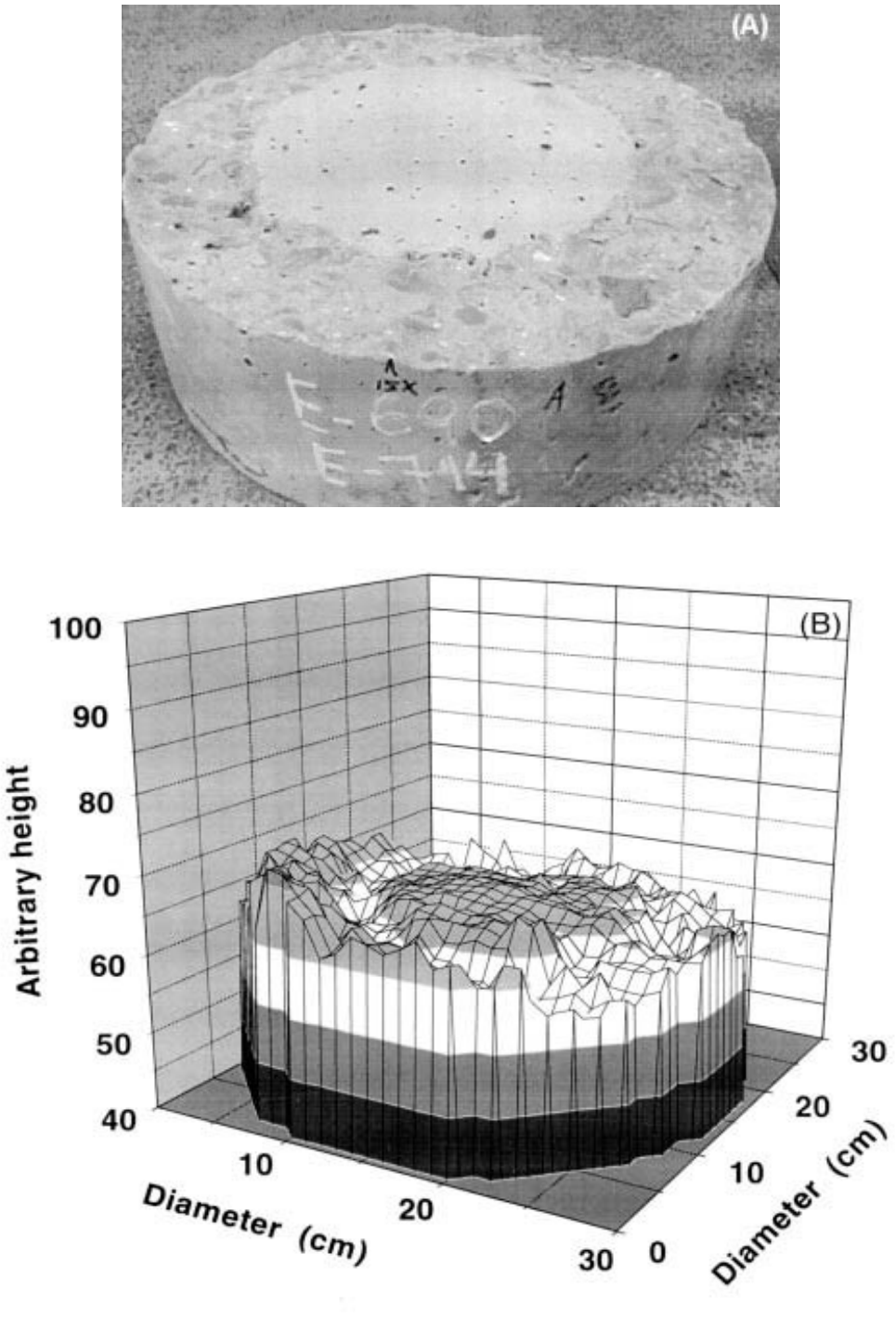

Figure 2-34: Abrasion-erosion underwater mass loss of the RefC|EMor system: (A) EMor sample photograph after abrasion-erosion; (B) EMor sample schematic 3-D abrasion-erosion mass loss (Korman et al., 2003).

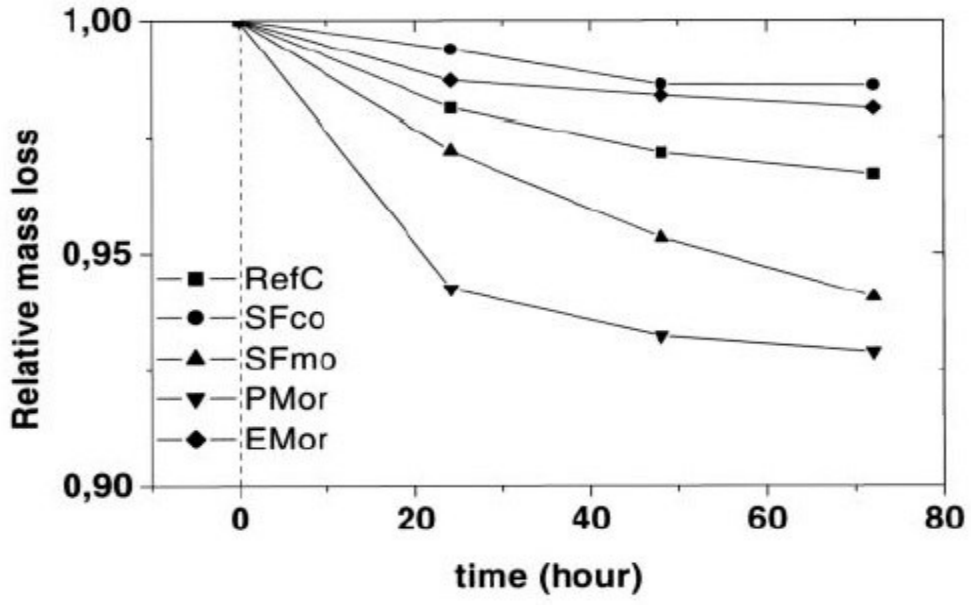

Figure 2-35: Relative abrasion-erosion underwater mass loss of the repairing material systems (Korman et al., 2003).

2.5 Factors Related to Environment

i. Effect of Flow velocity

Flow velocity is always an important parameter for the abrasion erosion process. According to Momber and Kovacevic (1994), a critical threshold velocity (w_o) is needed to initiate and continue the erosion process. Below this threshold velocity, no visible erosion will be observed, though invisible cracks will still be generated in the concrete matrix. In this research (Momber and Kovacevic, 1994), a 400 m/s water jet was used to erode concrete without using any abrasive material. It is observed from the test that concrete specimens were not destroyed completely at high flow velocities, but a continuous removal of materials was always found.

ii. Effect of Impact angle

The angle of impact of the water jet has a very high influence on abrasion erosion because the main culprits for abrasion erosion are the normal stress and tensile stress generated on the concrete surface. These stresses cause micro-cracks in hardened mortar and fractures around the aggregate particles which eventually leads to abrasion erosion. As both normal and tensile stress occurs simultaneously, the ratio of these two stresses depends on the incident angle of water jet on the concrete surface. Normal stress is maximum when the angle of impact is 90° and during this time shear stress is minimized. When the impact of an angle is 45°, both normal and tensile stresses have equal impact on the concrete surface. Figure 2-38 shows the relationship between impact angle and abrasion loss at various water cement ratios. It is obvious from the figure that abrasion is maximum when the impact angle is 90° as normal stress is maximum which has more power to abrade at any w/cm ratio. At 45°, concrete shows a minimum abrasion loss. It can be concluded that beyond 45°, abrasion rate increases with an increasing impact angle.

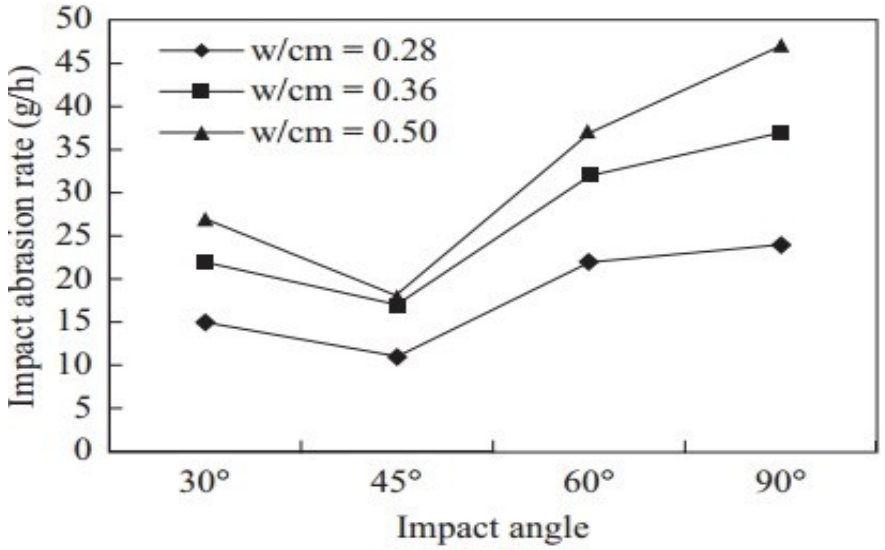

Figure 2-36: Relationship between impact angle and abrasion rate (Liu et al., 2012).

Concrete impacted at 90° exhibits a more rough and rugged surface than concrete impacted at 45°and 30°. Normal stress is maximum at 90°, whereas shear stress has a good contribution at 45° which is the reason for comparatively smooth abrasion erosion. Figure 2-39 (a) shows an image of a concrete surface impacted at an angle of 90°. It was observed that mortar was abraded easily and abrasion occurred by forming many small cracks rather than a few large cracks. The impacted surface is rougher and more rugged than concrete surface impacted at 45° (Figure 2-39(b)).

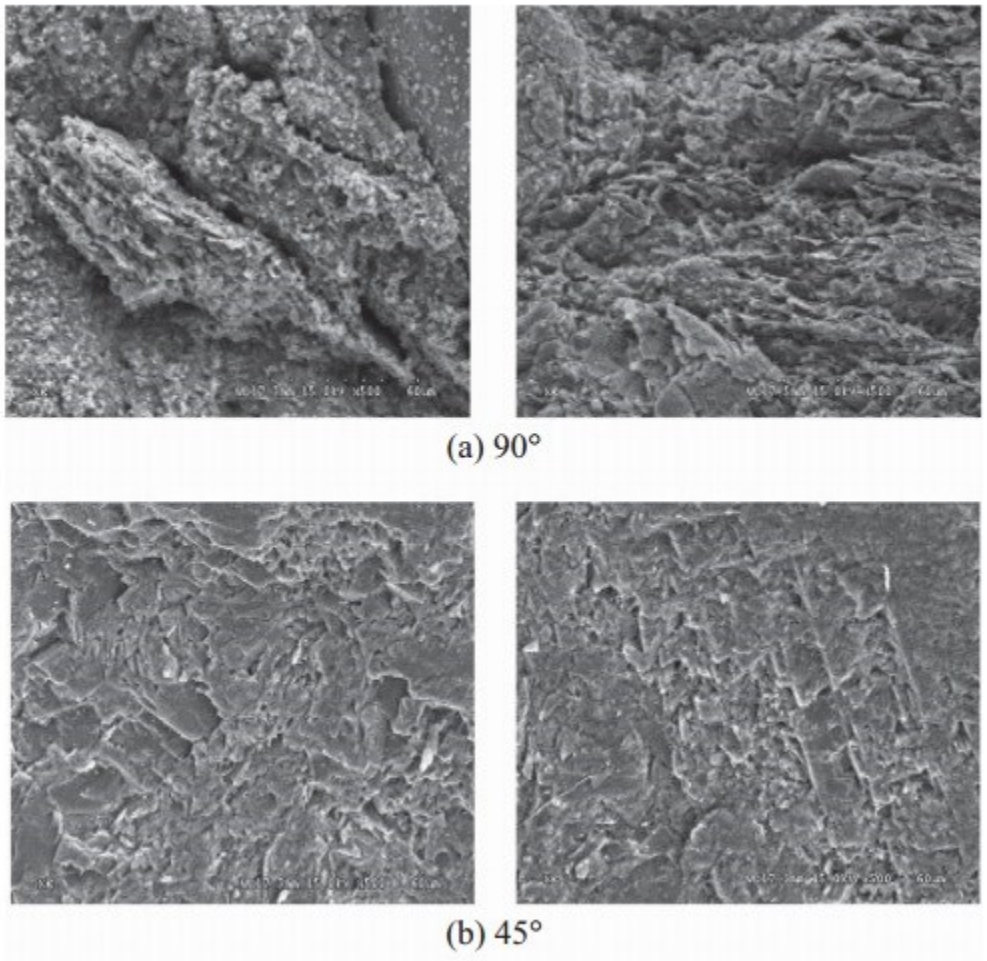

Figure 2-37: SEM-images of worn concrete surface (w/cm =0.36). Impacted at (a) 90°and (b) 45° (Liu et al., 2012)

iii. Effect of Erodent size

Size of erodent, shape, roughness, concentration and hardness have a significant influence on abrasion damage on concrete surface. Liu et al. (2012) investigated the impact of erodent size and concentration of erodent on concrete abrasion using waterborne sand flow impact abrasion method. Figure 2-40 shows the images of eroded concrete surfaces under various erodent sizes, where a fixed w/cm ratio of is 0.36 and angle of impact at 45° was used.

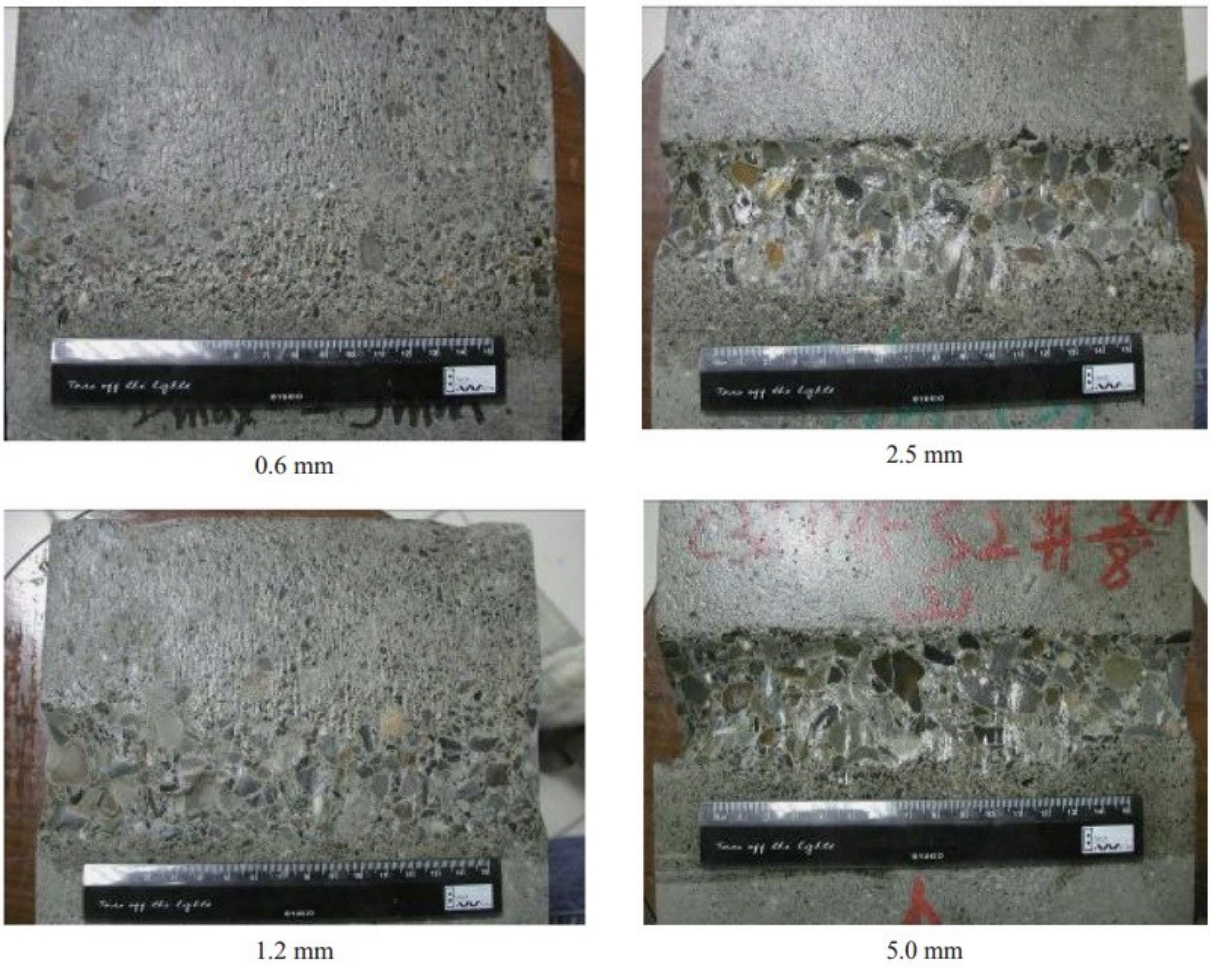

Figure 2-38: Worn concrete surfaces under various erodent size (w/cm = 0.36, angle of impact = 45°) (Liu et al., 2012).

Test results exhibited that when the size of the erodent increased, the rate of concrete abrasion increased from 100% to 217% and 367% respectively. The main factor is that when the erodent size is small, the small particles are not capable of initiating cracks on the surface; they could only plastically deform the surface.

iv. Effect of Sand Content in Water on abrasion

Concentration of sand has a great impact on abrasion. Water without sand or abrasive particles has much less abrasion damage than water with just sand (Liu et al., 2012). Figure 2-41 clearly shows that when sand concentration is zero, abrasion damage on concrete surface is nearly negligible. When sand content increases in the water flow, abrasion erosion increases. As the concentration of sand particle increases, impact energy of sand mixed with water also increases which causes more abrasion erosion. The test results exhibited that when sand content in water is 110, 230, and 340 kg/m^3, impact angle is at 45 °and 90 °and the abrasion rate is 10, 17 and 23 times, whereas the abrasion rate is 23, 37 and 57 times of when the water has no sand as illustrated in Figure 2-42.

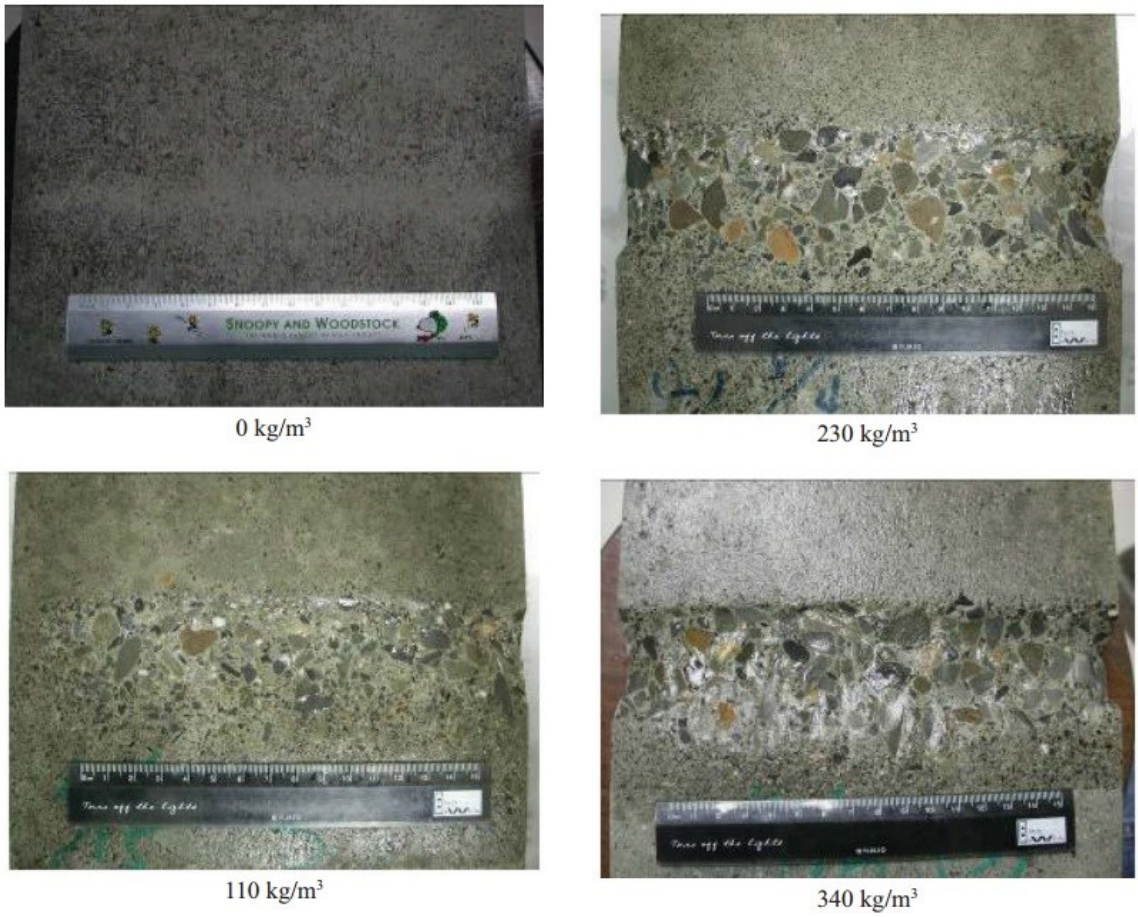

Figure 2-39: Effect of various sand content on abrasion erosion of concrete (Liu et al., 2012).

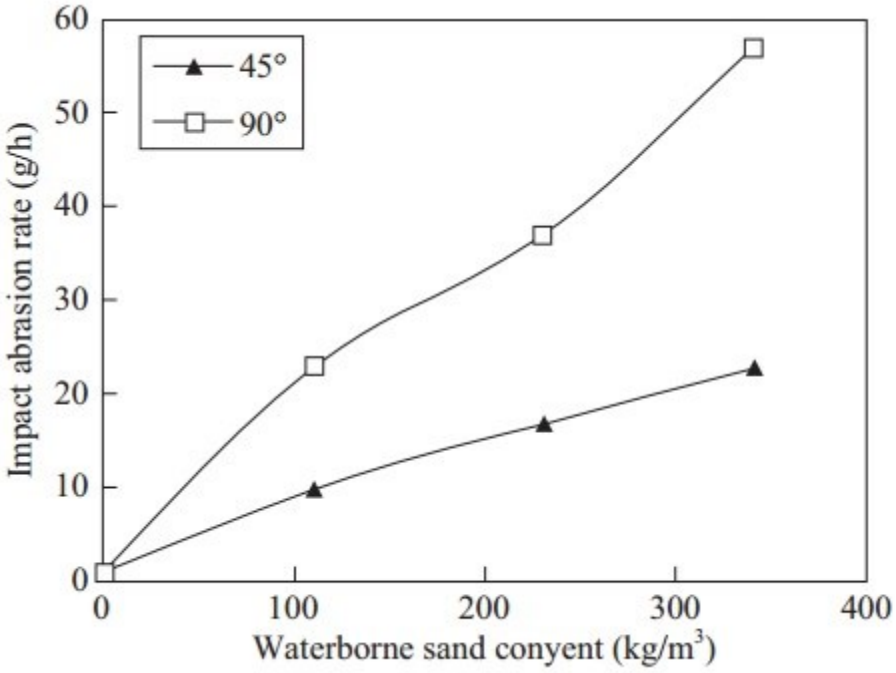

Figure 2-40: Relationship between abrasion rate and sand content in water for concrete made with w/cm= 0.36, angle of impact 45° (Liu et al., 2012).

v. Effect of Crack width and Flow direction

Microcracks are the starting point of abrasion erosion. Microcracks form in the concrete matrix due to impact and shear stresses originated by water flow and water-borne particles. These microcracks get widened gradually with time because of rubbing and swirling effects caused by water flow. Cement and other small aggregates get pulled out of the crack surface and cracks get bigger and bigger. Liu (2007) investigated how cracks increased abrasion and also what kind of difference the flow direction make on abrasion.

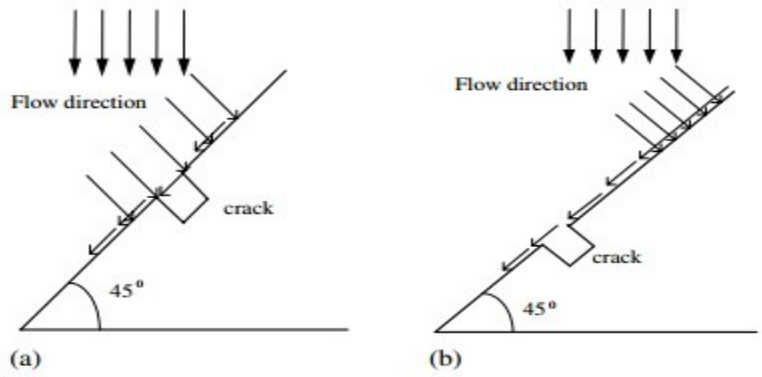

Figure 2-41: Water borne sand flow impinging site: (a) impinging site above crack site A and (b) impinging site on the crack site B (Liu, 2007).

Figure 2-43 shows two different impinging sites in the first figure the water flow impacted directly on the crack (site a) and it created vertical and shear stress at the crack. In the second figure b, it creates shear stress around the crack as water impact is above the crack. Figure 2-44 shows a typical abraded surface after test of the above two different impact conditions. In Figure 2-44 (a) water flow directly hit the crack from vertical direction and in Figure 2-44 (b), water flow hit the surface vertically above the crack.

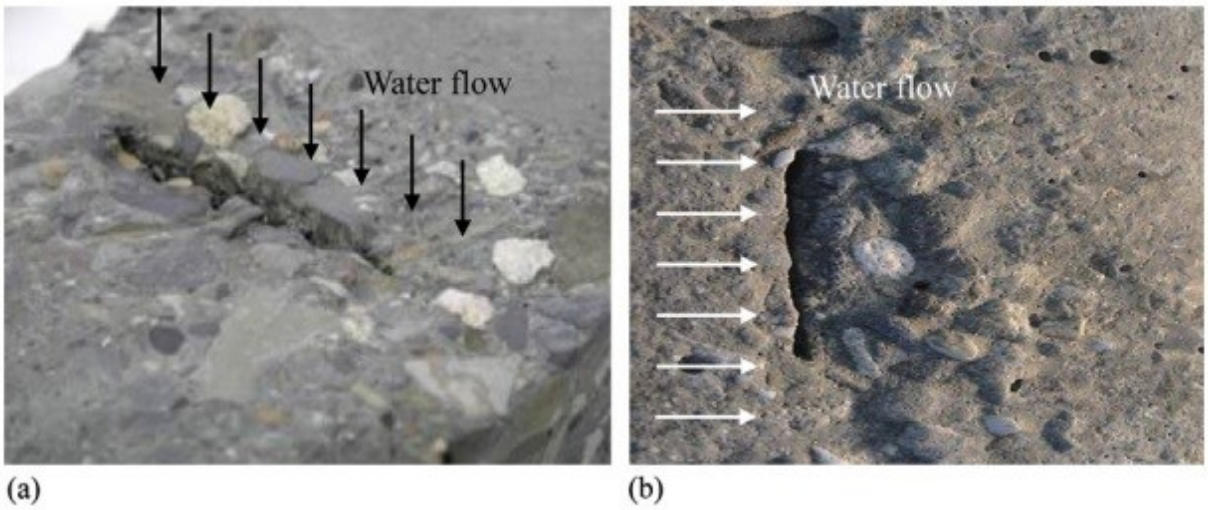

Figure 2-42: (a) water flow impingement directly on the crack (b) water flow impingement above the crack (Liu, 2007).

Figure 2-45 illustrates the relationship between the crack width and the abrasion rate for the two sites. The abrasion rate increases in the flow, which has a direct impinging effect on the crack. But, if there is an existing crack, abrasion increases with width for both sites.

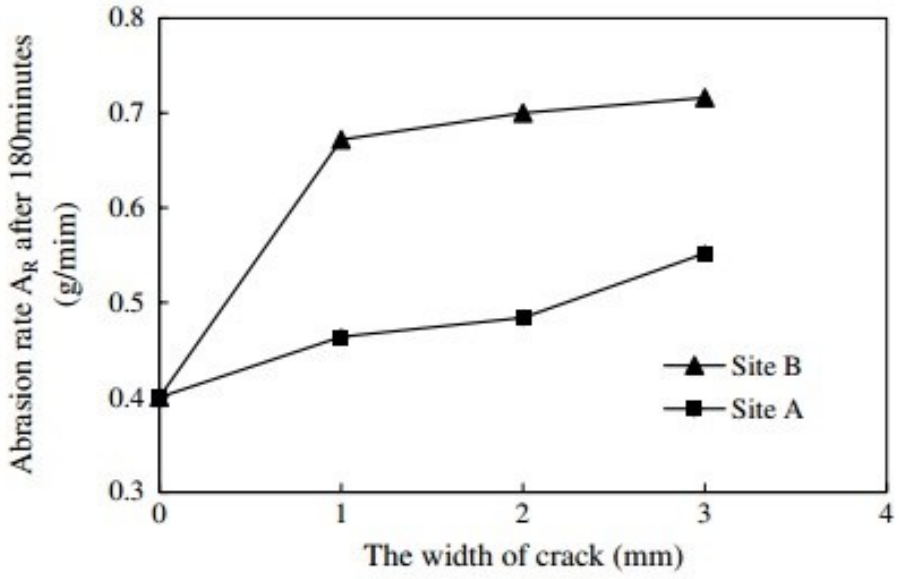

Figure 2-43: Relationship between crack width and abrasion rate (Liu, 2007).

In general, test results exhibited that abrasion rate increases with the increment of the width of the crack. If the crack width is larger than 1 mm, water can impinge directly into the crack and makes abrasion easier. Test results show a crack with a 3 mm width has the maximum abrasion rate. For the same concrete mixture made with 0.36 w/cm, the abrasion rate increases by 16%, 21% and 38% respectively, with respect to an increase of crack width from 1 to 3 mm.

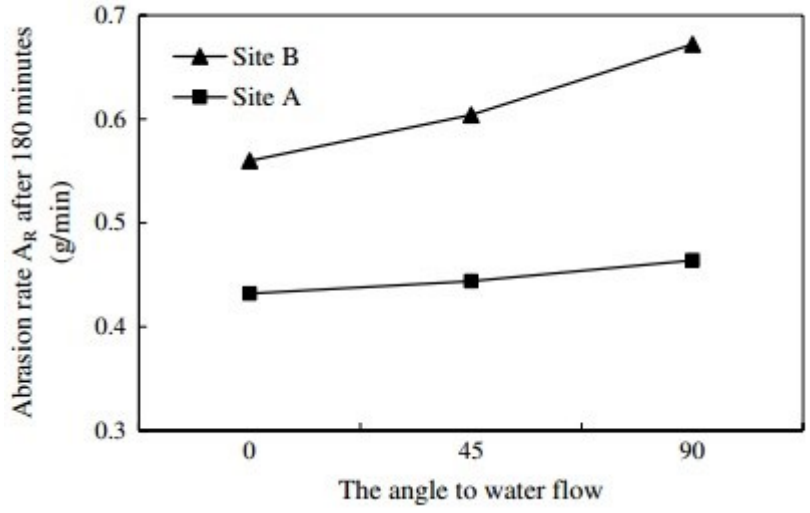

Figure 2-44: Effect of crack direction on the abrasion rate (Liu, 2007).

Liu (2007) tested the crack with three different flow angles on the crack surface and those angles are 0°, 45° and 90° (Figure 2-46). Test results showed that the abrasion rate increases significantly when flow impingement occurs directly on the surface crack (site a) and it was also found that a larger angle will give higher abrasion than a smaller angle. But, when impingement occurs above the crack surface (site b), the influence of the larger angle is not as significant. When water flow impinges directly on the crack surface with a large angle it creates more local stress and swirling and rubbing effect which causes more abrasion than when the impingement occurs above the crack surface.

2.6 Factors Related to Casting Procedure

vi. Effects of Curing

Bakke (2006) states that efficient curing increases the compressive strength of concrete simultaneously, it also increases the abrasion resistance of concrete. Sawyer (1957) investigated the effect of curing with a series of tests, including a wide range of cement contents, w/c and incremental curing. The study shows that a noticeable improvement in abrasion resistance can be expected with the extended curing time, especially for surfaces composed of leaner concrete. Another study by the California Division of Highways shows that greatest abrasion loss encountered were associated with less adequate curing procedure (Spellman et al., 1967).

vii. Effects of Vacuum Treatment

The vacuum treatment in which excess water is extracted from a concrete mixture by applying suction has been used for a number of years in numerous parts of the world to reduce water from the top surface of concrete as the top layer of the surface tends to have an extra amount of water (Mindess, 2003). It was found by investigating different types of concrete that the abrasion resistance was significantly higher for vacuum-treated concrete than for unprocessed concrete. Liu (1981) investigated two sets of concrete samples with two different w/cm ratios (0.54 and 0.72), one set of sample was vacuum treated where the other set was not. Abrasion tests were conducted with these samples in accordance with ASTM C1138. Test results showed that the average losses for 72 hours were reduced to 44% and 39% by vacuum treatment of concretes with water-cement ratio of 0.72 and 0.54 respectively. The improvement in abrasion resistance of vacuum-treated concrete was mainly due to reduction of water content in concrete mixtures. The U.S Army Corps of Engineers confirmed that vacuum-treated concrete surfaces are noticeably more resistant to

abrasion than surfaces with untreated concrete (Liu, 1980). The improvement in abrasion resistance of vacuum-treated concrete is due to the reduction of water content in the concrete mixture. This treatment is most effective on concrete with high w/c ratio.

viii. Effects of Surface Coating

Liu (2006) investigated the relative abrasion resistance of seven different types of concrete surface coatings: two types of polyurethane coating, acrylic mortar, high modulus and low modulus epoxy resin mortar, furan resin and iron aggregate topping. Generally, all surface coatings that were investigated had good resistance to abrasion and had significantly less abrasion resistance than the conventional concrete. The test results are shown in Figure 2-47. Among all the surface coatings, the iron aggregate topping had the largest amount of abrasion loss which is 1.16 percent for an average 72 hour abrasion.

Some specific chemicals such as magnesium and zinc flourosilicates, sodium silicate, gums and waxes increases the life of older floors and are considered an emergency measure for surface treatment (Bakke, 2006). Surface treatment with linseed oil can increase about 30% of abrasion resistance of poor or porous concrete surfaces. Paints and coatings are used for sealing concrete surfaces and to protect their concrete from the attack of toxic chemicals which possess only limited abrasion resistance. (Bakke, 2006)

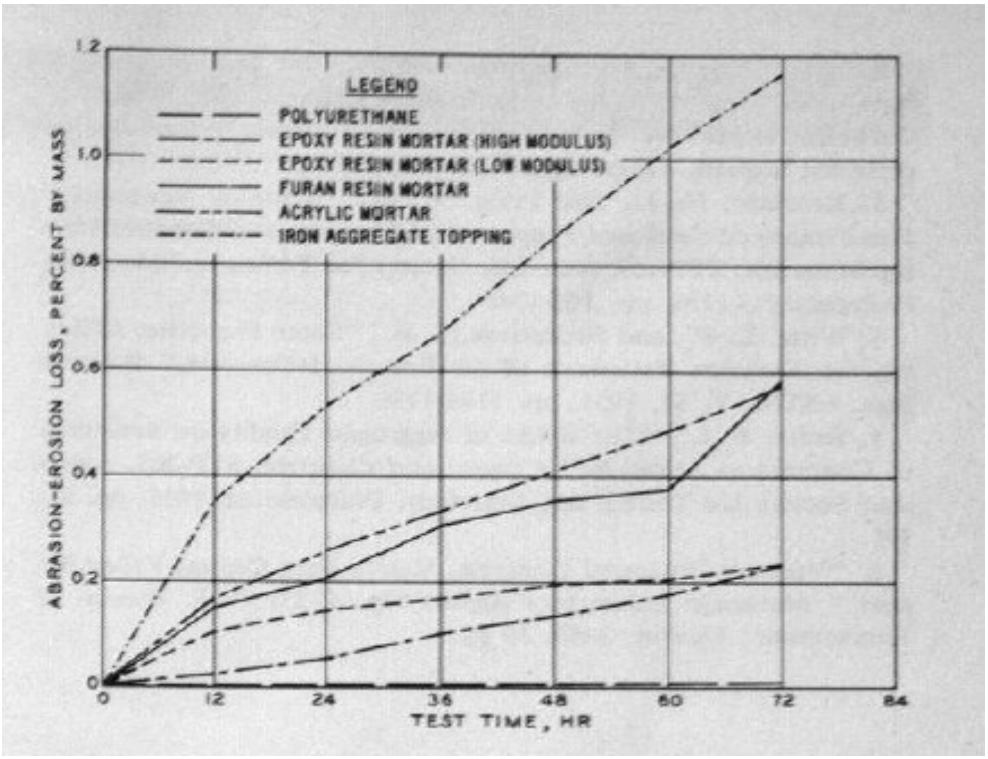

Figure 2-45: Abrasion resistance of various concrete surfaces (Mindess et al., 2003).

ix. Effects of Finishing Procedures

Bleeding is a problem of concrete; as bleeding occurs on the surface, w/cm ratio is higher at the concrete surface than other parts of concrete surface which makes concrete more porous and weak. Finishing procedures have a significant impact on concrete abrasion resistance. A study of Kettle and Sadegzadeh (1987) indicated that the abrasion resistance of concrete subjected to power finishing is significantly higher than that subjected to hand finishing. This is attributed to surface compaction and reduction of w/c of the surface matrix.

Wood float, magnesium float, steel trowel and hard-steel trowel finishes are some finishing techniques studied by Fentress (1973) in regards to the abrasion resistance of concrete. A wood

float tends to tear the surface and to displace the aggregate. The magnesium float, despite its ease of finishing, causes a rough-textured surface lowering in abrasion resistance. Both the steel trowel and hard-steel trowel produce smooth surfaces and provide excellent resistance to abrasion.

After going through all the research it has been realized that, there are numerous factors which contributes to the abrasion resistance concrete. Factors related to the properties of concrete have major impact on concrete abrasion such as a water cement ratio, strength of concrete, aggregates, etc. The contribution of water cement ratio, compressive strength, aggregates has already been analysed and no further analysis regarding these factors are not imperative. Now a day all the research regarding concrete abrasion are happening on supplementary materials and fibre reinforcement of concrete. There are lots of scope to analyse the impact of different supplementary materials along with the various types of fibre reinforcement with different content. Also factors related to environment such as flow velocity, waterborne particles and their concentration, impact angle etc. plays a great role in abrasion erosion. Such factors can also be a focus point in a research study about this topic. Among all factors, supplementary materials and fibre reinforcement, compressive strength and age of concrete were studied in this research, rest of the factors either kept constant or not considered in this study. Major factors considered in this study is flow velocity, sand concentration, water-borne particle and impact angle. In previous studies, abrasion resistance was compared mainly with abrasion mass loss, compressive strength or abrasion depth. Volume loss due to abrasion can also be a good way to compare the abrasion resistance of different concrete. However, quantifying volume loss of known density and mass will not be appropriate as accuracy of mass loss measurement has some error. For, volume loss measurement some new method can be developed.

3. Methodology

3.1 General Description

This chapter provides a description of the methodologies used in this study, including details about casting and curing of concrete specimens, experimental standards for testing the specimens, and procedures for the analysis of experimental data obtained from laboratory tests. Note that this study was intended to evaluate the abrasion resistance of different types of ready-made repair materials. Materials with high abrasion resistance presumably have the potential to be used for repairing ageing hydraulic structures in the aquatic environment.

3.2 Materials Used

Four types of ready-made prepackaged repair materials were used in this study. All materials were obtained from King Construction Products based in Ontario, Canada. The materials are listed below:

1) Concrete Material
2) Latex Modified Repair Material
3) Silica Fume Fibre-Reinforced Repair Material
4) Fly Ash Fibre-Reinforced Repair Material

The main reason to choose these materials were that all the materials used were pre-blended and pre-packaged and easily available on the market for surface repair. Only adding water was enough to cast the materials. Moreover, each type of material contains specific supplementary materials which gives some special properties to the concrete specimen.

3.2.1 Concrete Material

The first material is a concrete mixture designed for consistent strength and durability, which can be used for general purposes like slabs, sidewalk, footings, and poles. This pre-bagged material is marketed for the home improvement market; in this research it was used for comparison with other materials specifically designed for repair. The proprietary concrete mix contains Portland cement (30 to 60%), silica and total quartz (60 to 100%), and other ingredients. The specific gravity of the concrete mix is 2.5. Aggregates are well graded, ranging from 0 to 10 mm in size. The concrete mix is ready to use; adding water to the mix is the only requirement. The manufacturer's suggestion is that water addition at the ratio of 2.7 L water to 30 kg dry material gives an approximate water/cement ratio of 0.60. The height of slump ranges from 25 to 175 mm. Entrapped and/or entrained air volume range is 2% to 7%. The compressive strength of these materials is given as 41.9 MPa at 28 days and flexural strength is 5.3 MPa at 28 days.

3.2.2 Latex Modified Repair Material

The second material is a special type of concrete, which contains a re-dispersible polymer and other carefully selected compounds with Portland cement. Aggregates are well graded, their sizes being in the range of 0 to 6 mm. This concrete is very low in permeability and has excellent compatibility to parent concrete. It has good resistance to sulphate attack and bleeding. It contains 10% to 30% of Portland cement and 60% to 100% of silica and total quartz. The specific gravity of the material is 2.65. The manufacturer suggests water addition at the ratio of 2.5 L water to 30 kg dry material, giving an approximate water/cement ratio of 0.40. The height of slump ranges from 50 to 200 mm. Entrapped and/or entrained air volume range is 4% to 9%. The compressive

strength of this material is given as 45.4 MPa at 28 days and flexural strength is 7.5 MPa at 28 days

3.2.3 Silica Fume Fibre Reinforced Repair Material

The third material is a high performance concrete, which contains silica fume and polypropylene microfibres and other carefully selected ingredients with Portland cement. Aggregates are well graded; their sizes range from 0 to 6 mm. This concrete mix contains silica fume up to 5%, Portland cement (10 to 30%) and Silica, total quartz of 60% to100%. The specific gravity of the material is 2.5. The manufacturer's suggested water addition, which is 2.6L/30kg, gives an approximate water/cement ratio of 0.40. The height of slump ranges from 50 to 200 mm. Entrapped and/or entrained air volume range is 4% to 9%. The compressive strength of this material is 57.8 MPa at 28 days and flexural strength is 12 MPa at 28 days.

The fibre used in this material is a synthetic fibre that is hydrophobic. Thus, it does not absorb water and has no effect on water requirements of concrete. The length of this fibre ranges from 6.35 to 20mm. The tensile strength is about 550 to 750 kPa, where Young's modulus is 23769 to 33276ksi. Most of the research shows that fibre reinforcement has good impact on crack resistance and can improve impact and abrasion resistance (Horszczaruk 2009).

3.2.4 Fly Ash Fibre Reinforced Repair Material

The fourth material is a high performance pre-blended concrete with synthetic fibre similar to previously-mentioned material. The only difference is that fly ash is used in this material instead of silica fume. Aggregates are well graded; their sizes range from 0 to 6 mm. This concrete mixture contains fly ash of up to 5%, Portland cement (10 to 30%) and silica, total quartz of 60% to 100%.

The specific gravity of the material is 2.5. The manufacturer's suggested water addition which is 3.0L/30kg gives an approximate water/cement ratio of 0.40. The height of slump ranges from 50 to 200 mm. Entrapped and/or entrained air volume range is 4% to 9%. The compressive strength of this material is 48.15 MPa at 28 days and flexural strength is 11 MPa at 28 days. Polypropylene fibre used for this material is similar to the silica fume repair material. Relevant properties of the four types of concrete used in this study are summarized in Table 3.1.

Table 3-1 : A summary of the properties of all four types of materials used in this study

Properties	Concrete Materials	Latex Modified Repair Material	Silica Fume Fibre Reinforced Repair Material	Fly Ash Fibre Reinforced Repair Materials
w/cm (approximate)	0.60	0.40	0.40	0.40
Portland cement content (%)	30-60	10-30	10-30	10-30
Silica, total quartz (%)	60-100	60-100	60-100	60-100
Specific gravity	2.5	2.65	2.5	2.5
Aggregate sizes (mm)	0-10	0-6	0-6	0-6
Fibre Reinforcement	No	No	Yes	Yes
Entrapped/ Entrained Air (%)	2-7	4-9	4-9	4-9
Slump Range (mm)	25-175	50-200	50-200	50-200
Compressive Strength at 28 days (MPa)	41.9	45.4	57.8	48.15
Flexural Strength at 28days (MPa)	5.3	7.5	12	11

3.3 Procedures for Laboratory Tests and Data Analysis

The steps used in the methodology are described below with details.

3.3.1 Mixing, Casting and Curing

The following specimens were cast for each type of concrete mixture: (a) three cylindrical specimens (with a diameter of 100 mm and a height of 200 mm) for compressive strength; (b) three beams (with a length of 525 mm, a width of 150 mm and a thickness of 150 mm) for flexural strength; (c) five cylindrical specimens (with a diameter of 100 mm and a height of 50 mm) for abrasion test. Dimension of cylindrical specimens and beam are chosen in accordance with ASTM C39 and ASTM C78, respectively. As there was no specification regarding the dimension of abrasion test specimens, 100x50mm cylinders were selected. The size and mass of the specimen provided a sufficient surface area for abrasion while having a relatively small mass for precise measurement.

To mix all types of material, a mechanical pan mixer (Imer U.S.A Inc, Model: Workman II 350) was used where multiple bags of materials were mixed easily at once. Clean water was used as per manufacturer's recommendation. Mixing occurred for 10 minutes in the mechanical mixer. No super-plasticizer or admixture was used during casting. After casting, every specimen was kept in a moist environment in the moulds for one day, and then placed into saturated lime water until the day tested. The curing of sample specimens in lime water is shown in Figure 3-1. Cast beams, cylinders and samples for abrasion test are shown in Figure 3-2.

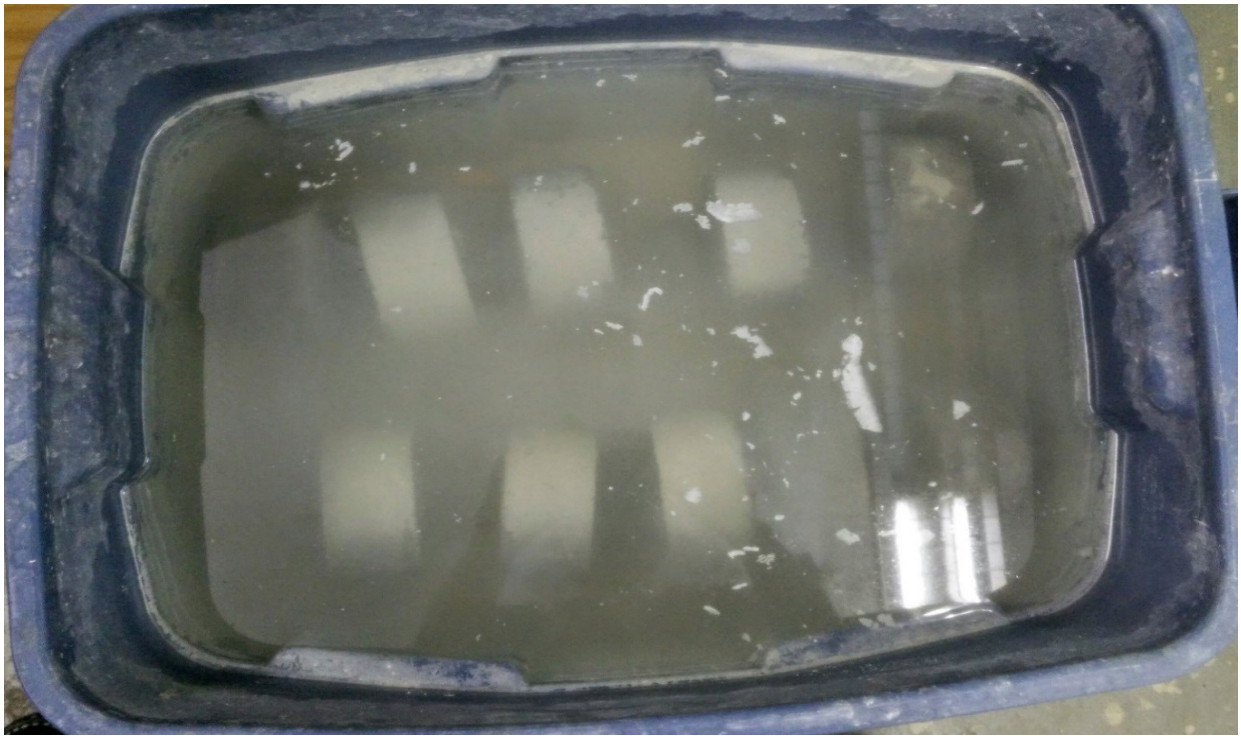

Figure 3-1: Curing of abrasion sample specimens in lime water.

Figure 3-2: Casting of beam, cylinder, and abrasion test samples.

3.3.2 Strength Testing

The compressive strength is the most commonly used parameter by engineers. Compressive strength is measured in a compression-testing machine by breaking a cylindrical specimen and is calculated from the failure load divided by the cross-sectional area of the cylinder. In this study, compressive strength test was performed at the age of 28 days for all types of materials in accordance with ASTM C39 [Standard Test Method for Compressive Strength of Cylindrical Concrete Specimens (ASTM 2015).

Another very important property of concrete used by designers is flexural strength, which is about 10 to 20 percent of the compressive strength of the same concrete, although it depends on the type, size and volume of coarse aggregates. Flexural strength represents the tensile strength of concrete where an unreinforced concrete beam or slab is tested to resist failure in bending. Flexural strength is expressed as Modulus of Rupture (MR). There are two ASTM standards: one is ASTM C78 (third point loading), and the other is ASTM C293 (center-point loading). In this study, flexural strength test was performed at the age of 28 days for all materials in accordance with ASTM C78. The dimensions of each beam were 525 mm × 150 mm × 150 mm, where 525 mm is the total beam length and 450 mm is the span length (Figure 3-3). The loading mechanism was third-point loading where the maximum stress occurs over the center 1/3 portion of the beam. The loading condition of beam in ASTM C78 is shown in Figure 3-3.

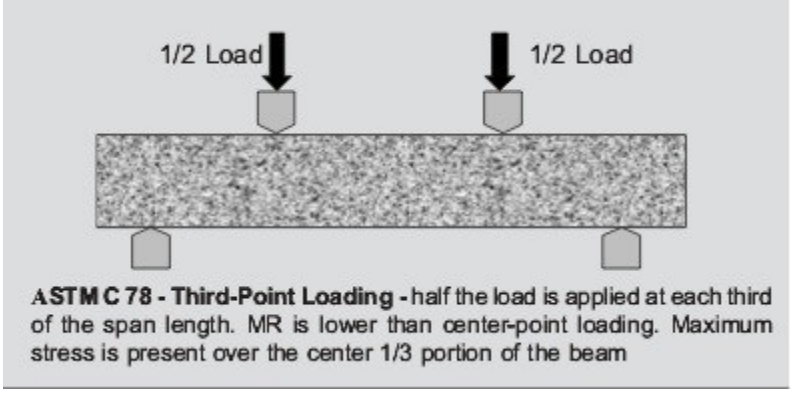

Figure 3-3: ASTM C78- Third-Point Loading- half of the load applied on each third of the span length (ASTM, 2015).

Flexural strength is calculated as

$$\text{Modulus of rupture: } R = \frac{PL}{bd^2} \tag{3.1}$$

where R = modulus of rupture (MPa), P = maximum applied load (N), L = span length (mm), b = average width of beam (mm), d = average depth of beam (mm).

3.3.3 Description of Abrasion Test Apparatus

The test method developed here in this study mainly focuses on the determination of the abrasion losses of concrete on hydraulic structures due to impact force and friction. The method is adapted from Liu et al. (2006). In this study, two types of sand were used with water to cause abrasion due to mixed particles, which reflects the real scenarios of abrasion in hydraulic structures. Aluminium oxide (Figure 3-4) with a Mohs hardness of 9 and 16 mesh size (average size of 0.6 to 1.18 mm and fineness modulus 3.85) and fine silica (average size of 0.15-0.30 mm and fineness modulus 1.36) (Figure 3-5) with a Mohs hardness of 7 have been used. The two types of sands were mixed in a ratio of 0.6 parts aluminium oxide to 0.4 parts silica. At 2, 4, 7 and 28 days of age the concentration of sand mix was 400 kg/m^3 whereas at 90 days of age the concentration of sand mix

was 500 kg/m^3 but the ratio of two types of sand was kept the same. Initially tests were performed using a sand and gravel mix. Although the pump can handle particles up to a size of 19.05 mm, during test larger particles became trapped between the impeller and casing which blocked the impeller and eventually stopped the pump. This can cause severe damage to the impeller, for this smaller particle size was used in this research. Figure 3-6 shows the probable area with red arrow the where large particle can become trapped. In Figure 3-7, it can be seen that the impeller was totally dislodged with a high amount of particles trapped in the space between the impeller and casing. . Images of the sands used in this study as abrasive materials are shown in Figures 3-4 and 3-5

Figure 3-4: Aluminum Oxide particle used in this study which is 60% of total abrasive material

Figure 3-5: Fine Silica used in this study which is 40% of total abrasive particle.

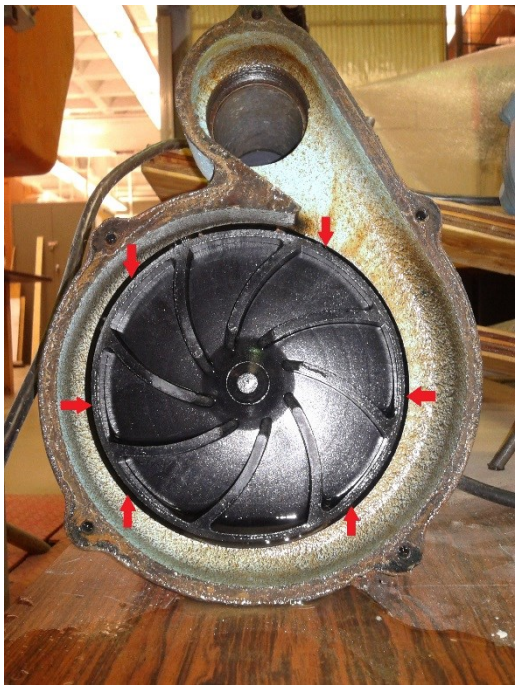

Figure 3-6: Impeller of the pump.

Figure 3-7: Blockage problem of the pump due to the usage of larger particles.

The dimensions of water tank (Figure 3-8) are 1219 mm x 914 mm x 914 mm (or 48'' x 36'' x 36''). Prior to the addition of sand, the height of the water is approximately 20 cm from the bottom of the tank when both pumps are submerged in water. The water level rises to some extent when the sands are mixed in water. The water tank is divided into two chambers: The first chamber contains the pumps as well as the water-sand mix, whereas the second chamber contains only water but no sand. Essentially, the sand remains in half of the floor area. Figure 3-8 shows the partition of water-sand zone and the water zone. There are two advantages: a) the concentration of sand remains consistently high in the water flow system, and b) the sands circulate well in the small area and near the pump. If the whole area were used for water-sand mixture, most of the sand would just settle far away from the pump. It would not circulate through the pump and would not participate in the abrasion process.

Moreover, the Al_2O_3 sand particles used in this study are very hard and heavy. Their average size is 1 to 1.5 mm. If they are not kept in small area, most of the sands would settle quickly far away from the pump and would remain unused for the whole duration of a test. To circulate the sand well, an air pressure nozzle was used during a test (Figure 3-9). The position of the air nozzle in the tank is such that it can push the maximum amount of sand towards the pump. When water-sand mixture comes back after hitting the specimen, it falls directly near or on the pump so that sand particles can circulate immediately through the pump.

Two submersible pumps of same congifuration were used to abrade concrete samples. Because concrete is a very hard material, it needs high water pressure to abrade concrete particles from its surface. Some details about the two pumps are listed in Table 3-2.

Table 3-2: Detail configuration of Pumps

Pump Type	Submersible Effluent Pump
Horsepower	4/10
Discharge rate at 5'' height	215 litres/minute
Size of Solids can handle	19.05 mm
Voltage	115V
Ampere	9 amps
Inner Diameter of pipe used	50.8 mm

The concentration of sand in the water is about 400kg/m$^{3.}$ To determine the sand concentration, the amount of clean water used in the tank was measured and then an adequate amount of sand was poured into the water to make the sand concentration 400kg/m^3. The two pumps (Figure 3-9) were used to create a high-velocity jet of water-sand mixture. The distance between the nozzle and the specimen is 30 cm. The diameter of the nozzle is 12.5 mm. As both pumps have constant discharge, the average velocity of the water jet is about 8.4 m/s. This creates a pressure of about 0.82 MPa. Equation (3.2) was used to determine the pressure created on the surface of the sample.

$$p = \rho . v^2 \tag{3.2}$$

where p = pressure of water jet on the sample surface (MPa); ρ= density of water-sand mix (kg/m^3); v = velocity of water jet (m/s). The density of the water sand mix was measured by collecting water-mix in a bucket for several times and measuring the mass and volume of water mix in the bucket. Dividing the average mass with average volume gives the density of water-sand mix; it was determined to be 1167 kg/m^3.

This high-velocity jet hits the sample specimen directly on its top surface, with an incident angle of 90°, and causes the impact and abrasion. Only 90° impact angle was used in this study. Note that previous studies (Liu, 2012) showed that abrasion due to impact is maximum when the incident angle is 90°. A schematic diagram of the abrasion test apparatus is shown in Figure 3-8. A photo of the actual experimental setup of abrasion test apparatus is shown in Figure 3-9.

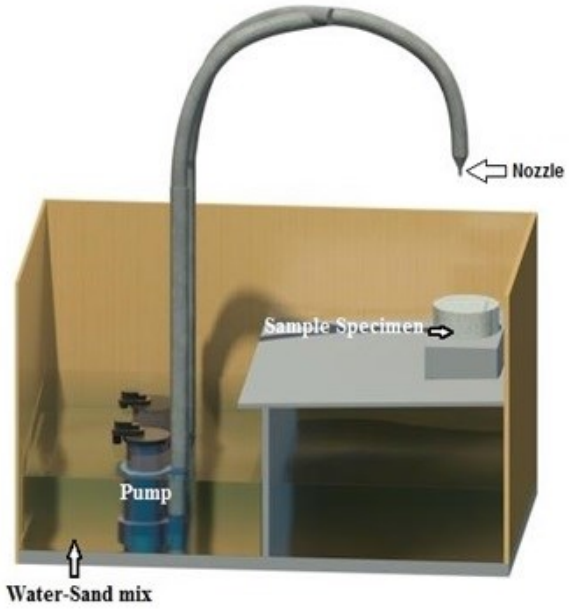

Figure 3-8: Schematic diagram of abrasion test apparatus.

Figure 3-9: Abrasion test apparatus used in this study.

3.3.4 Velocity of Water Jet Measurement

As mentioned in the previous section, the flow velocity used for the abrasion test is 8.4 m/s which was kept constant. The discharge rate of both pumps was the same and constant. For a specific pipe network, the flow velocity is always same as discharge is the same. In that condition, the best way to increase or decrease the flow velocity is by changing the diameter of the outlet pipe/nozzle. Three different nozzle diameters were used to find the best flow velocity which will give proper abrasion with a good amount of discharge. Table 3-3 contains all the data and results on velocity and discharge. The discharge rate was measured by collecting water in a bucket for a specific time period. The mass of water collected water mass was measured. From the weight of water, the volume was determined and from volume and time, discharge rate was measured. The results show that, when the nozzle radius is 9.5 mm (19 mm in diameter) the discharge is maximized, but the velocity is low and is not strong enough to abrade the concrete surface. When the radius is 7.9 mm (15.8 mm in diameter) which is the smallest among the three nozzles gives highest velocity, which is 13.22 m/s, but the discharge is too low and also as the radius is small; therefore, it is not convenient for sand particles to pass smoothly through this small hole . Also there is a possibility of jam/ blockage by the sand particle as the average size of particles is 1 to 1.5 mm. The optimum results were obtained when the nozzle radius was 9.5 mm (19 mm in diameter) which exhibited sufficient flow velocity to initiate and abrade the concrete surface and also the discharge rate is adequate to carry sand particles smoothly. For these reasons, flow velocity of 8.4 m/s was chosen for this research; from previous studies, the most common flow velocity was used is 8 to 12 m/s.

Table 3-3 : Flow velocity and discharge

Nominal nozzle radius (mm)	Area of nozzle opening (m^2)	Discharge (m^3/s)	Velocity (m/s)
9.5	0.00028502	0.001966	6.9
7.937	0.00019793	0.001662	8.4
3.9687	0.00004950	0.000654	13.2

3.3.5 Abrasion Test Procedures

The duration of each abrasion test was 3 hours. Prior to a test, each sample was removed from the curing and was made saturated surface dry (SSD), then the mass of the sample (w_1) was determined to an accuracy of 0.01 grams. After the completion of the test, the saturated surface of the sample was made SSD again, then the mass of the sample (w_2) was determined. The difference between w_1 and w_2 gives the abrasion-induced mass loss, Δw:

$$\Delta w = w_1 - w_2 \tag{3.3}$$

The abrasion rate (Ar) is determined as

$$Ar = \frac{\Delta w}{at} \tag{3.4}$$

where a = affected surface area (m^2); t = test duration (minute).

During a test, the sand flow through the pump was consistently monitored. Typical conditions as observed in the laboratory were as follows. In the first 2 to 3 minutes, sand flow through the pump was maximized as a high amount of sand near the pump goes into the pump very quickly. Subsequently, the sand flow maintains at a steady rate. The test apparatus was covered with a thin plastic sheet to prevent water splashing outside the tank. The water flow velocity was estimated using the volume-time method. It was measured several times by catching water in a bucket for a fixed period of time and then calculating the discharge from it. As discharge was known as well as the cross section of the outlet nozzle, it was easy to measure the velocity of water-jet. The

velocity of the water jet was sufficient enough to initiate and continue abrasion on concrete surface. Also, it was important to check the velocity of a water-jet to maintain a constant pressure on the sample surface. As the nozzle is circular, the cross sectional surface area of the concrete surface area affected by the water-jet is also a circular and the approximate area covered by the water-jet was $0.0045m^2$ (0.076m dia) which was used in Eqn 3.4 as affected surface area. Maximum abrasion occurs in the centre of the circular area as force was maximum in the centre of water jet. Table 3-4 contains all the test variables of each mixture used in this study. In the case where 3 tests are indicated, they are subsequent tests on the same sample.

Table 3-4: Casting & test date of abrasion test of each sample

Sample Name	Number of Sample tested	Number of tests	Age (days)	Casting Date	Test Date
Concrete	1	1	2	14-01-2015	16-01-2015
	1	1	4		18-01-2015
	1	3	7		21-01-2015
	1	3	28		11-02-2015
	1	3	90		23-04-2015
Latex Modified	1	1	2	21-01-2015	23-01-2015
	1	1	4		25-01-2015
	1	3	7		28-01-2015
	1	3	28		18-02-2015
	1	3	90		30-04-2015
Silica Fume Modified	1	1	2	28-01-2015	30-01-2015
	1	1	4		02-02-2015
	1	3	7		05-02-2015
	1	3	28		25-02-2015
	1	3	90		07-04-2015
Fly ash Modified	1	1	2	24-02-2015	26-02-2015
	1	1	4		28-02-2015
	1	3	7		02-03-2015
	1	3	28		23-03-2015
	1	3	90		25-05-2015

3.3.6 Scanning in 3D Scanner and Data Processing using MATLAB

In addition to the mass loss [equation (3.3)], changes to the concrete surface due to abrasion (Figure 3-10) are obtained by three-dimensional scan. The abraded concrete specimens were scanned using a Nextengine 3D Scanner HD. The scanner can be set to a number of resolutions, ranging from 700 points per square inch to 40,000 points per square inch. The finer the scan resolution, the larger the size of output data files. These output files are object files whose file names have the extension '*obj*'. In this study, a constant resolution of 4400 points per square inch was used. This resolution was a compromise between file size and surface details. The maximum accuracy of the scanner is ±0.127 mm. At 4400 ppi, it is ±0.381mm.

In the Cartesian coordinate system (*X*, *Y*, *Z*), the *Z*-axis is taken to point positively upward (Figure 3-10). Prior to jet-induced abrasion, a cylindrical concrete specimen has its top surface located at $Z = Z_0$. Let Δz denote the abrasion depth at a given point of (*X*, *Y*) in the *X*-*Y* plane. Δz is given by

$$\Delta z = Z_0 - Z(X,Y) \tag{3.5}$$

In equation (3.5), *Z* presents the elevation of the abraded top surface S_a.

The 3D scan gives output data of coordinates (*X*, *Y*, *Z*) for the abraded top surface S_a. All the data files were post processed in MATLAB. The *obj* format is a common visualization format readable by many computer graphics software such as Maya (2015) and Meshlab (2015). An 'obj' data file contains various types of geometric data, which includes geometric vertices of an object, texture coordinates, and vertex normals. In this study, only vertices were required on the sample surface.

The '*obj*' text file was opened in Microsoft Notepad, and only vertices data were extracted from the file and saved in a new data file (whose name has the extension 'txt') for processing using MATLAB scripts.

There are several steps in MATLAB data processing, as discussed below:

1) Read the (*X*, *Y*, *Z*) coordinates from a txt file. The MATLAB script for this purpose is given in Appendix A.
2) While scanning a concrete specimen, the scanner's front plate and the specimen were more or less aligned to be parallel, but the scanner's laser diodes were not necessarily perpendicular to the specimen. Thus, the output data has an 'arbitrary' orientation in space.

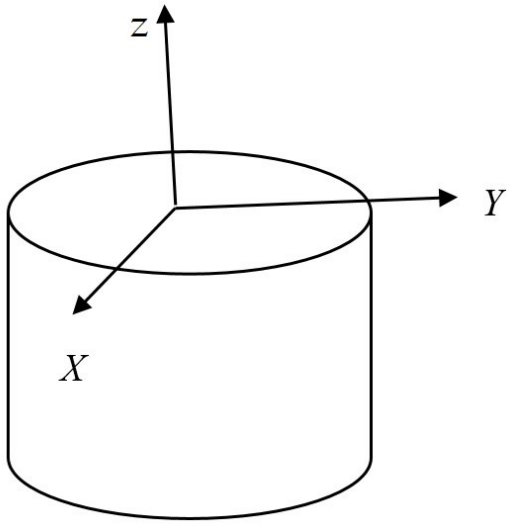

Figure 3-10: The Cartesian coordinates system

The arbitrary orientation is rectified in a MATLAB script which rotates the dataset such that the disk is in the *X*-*Y* plane (Figure 3-10) and the depth of the concrete surface is in the z-direction. In this MATLAB script, the center of the dataset is identified by averaging each coordinate component using the 'bsxfun' function. This function deducts the mean of each axis from each corresponding (*X*, *Y*, *Z*).

After that, the direction of most variance or the direction of the principal component (PC) of the variance of the dataset was determined through singular value decomposition (SVD). Details about SVD will be discussed later. As illustrated in Figure 3-11, the (*X*, *Y*, *Z*) data were plotted as blue dots. The two dimensions (X, Z) are moderately correlated to each other, by taking the SVD of the data. The two principal components (PC) were obtained, shown as the yellow and red arrows. The first PC points in the direction along which the data tend to lie. In Figure 3-12, the data was projected onto the PC's and re-plotted. The result is that the space has been rotated, and the data points are correlated and aligned with the coordinate axes. In other words, the new (*X*, *Y*) coordinates become parallel to a horizontal plane, and the *Z*-axis becomes in the vertical. The average of the *Z* values is very small (close to zero). The difference in *Z* coordinates between before and after an abrasion test gives the depth of abrasion (equation 3.5). The MATLAB script for SVD is given in Appendix B.

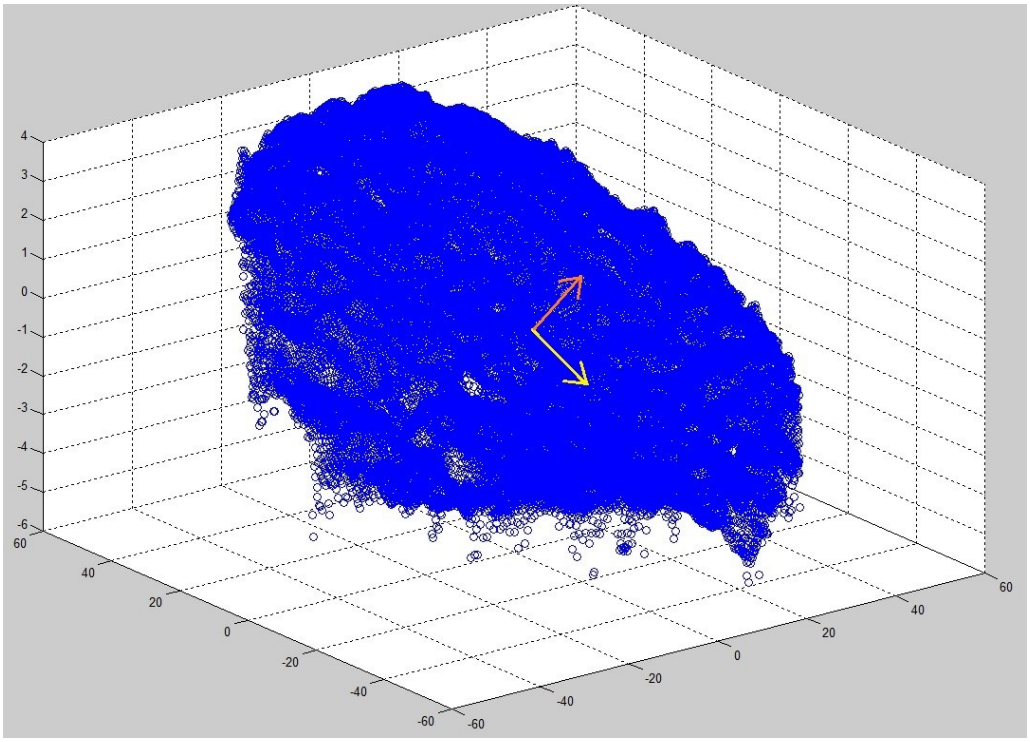

Figure 3-11: (*X*, *Y*, *Z*) coordinates from three-dimensional scanning, shown as blue circles. The two arrows are the directions of most variance or PC's.

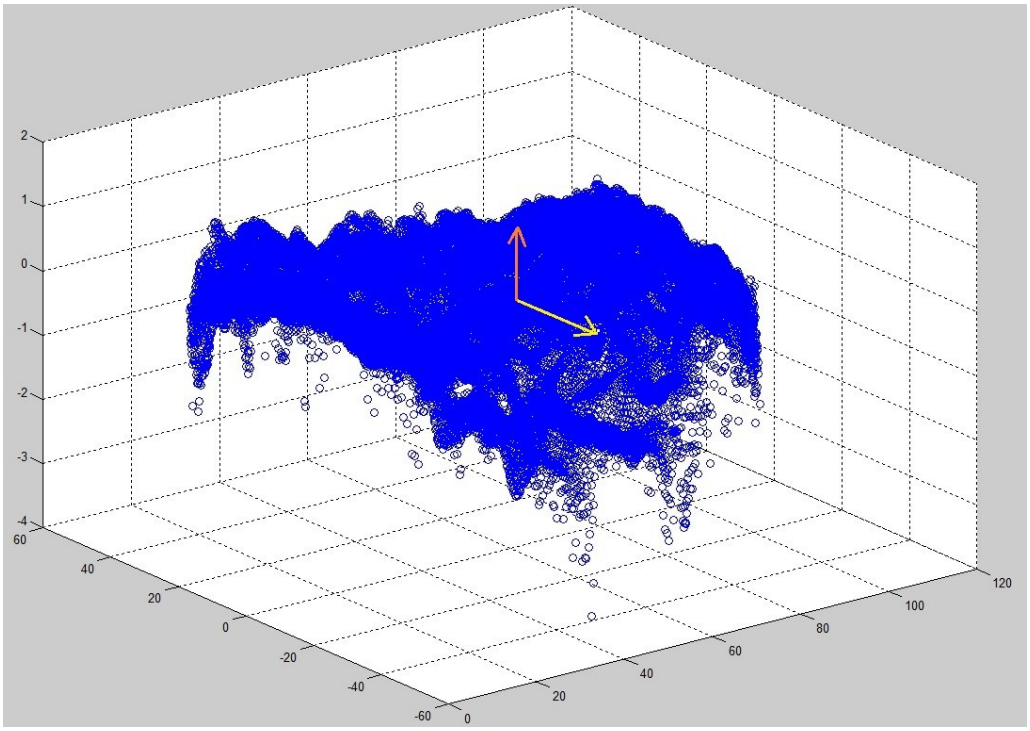

Figure 3-12: (*X*, *Y*, *Z*) coordinates (blue circles) after SVD or after rotation. The two arrows or the directions of most variance or PC's after rotation become parallel to the axes.

The mathematical analysis behind the Singular Value Decomposition or SVD function is discussed below. SVD is a method for identifying and ordering the dimensions along which data points exhibit the most variation. SVD is based on a theorem of linear algebra which says that a rectangular matrix **A** can be broken down into the product of three matrices. The theorem can be presented as

$$\mathbf{A}_{m\times n} = \mathbf{U}_{m\times n}\mathbf{S}_{m\times m}\mathbf{V}^{T}_{n\times n} \tag{3.6}$$

where **U** = an orthogonal matrix, its columns being orthogonal eigenvectors of $\mathbf{AA}^{\mathrm{T}}$; **V** = the transpose of an orthogonal matrix, its columns being orthogonal eigenvectors of $\mathbf{A}^{\mathrm{T}}\mathbf{A}$; **S** = a diagonal matrix containing square roots of the eigenvalues from **U** or **V** in descending order.

The matrix **A** can contain any number of column and rows. In this study, **A** is the original data set of the abraded surface which needs to be rotated. Typically a raw scan data file of a sample concrete surface contains around 46000 ± 1000 (*X*, *Y*, *Z*) coordinate points. Thus, a raw data file has 3 columns (*X*, *Y*, *Z*) and around 46000 rows. For the purpose of demonstration, take 46000 as the number of rows. In other words, the dimensions of the *A* matrix are 46000 × 3. In order to find **U**, first, the transpose of **A** (or $\mathbf{A}^{T}$) was determined. As the dimensions of **A** matrix are 46000 × 3, the dimensions of $\mathbf{A}^{\mathrm{T}}$ are 3 × 46000. Then, $\mathbf{AA}^{\mathrm{T}}$ was determined by multiplying **A** with $\mathbf{A}^{T}$. The dimensions of $\mathbf{AA}^{\mathrm{T}}$ are 46000 × 3. Next, the eigenvalues and corresponding eigenvectors of $\mathbf{AA}^{\mathrm{T}}$ are evaluated by solving the equation given below

$$\mathbf{B}\vec{v} = \lambda\vec{v} \tag{3.7}$$

where $\mathbf{B} = \mathbf{A}\mathbf{A}^T$, its dimensions being 3 × 3; $\vec{v}$ = non-zero eigenvector of *v*, its dimension being 3 × 1; λ = eigenvalue of **B**, which is a scalar.

Equation (3-7) can be rewritten as

$$\mathbf{B}\vec{v} - \lambda \cdot \mathbf{I} \cdot \vec{v} = 0 \tag{3.8}$$

$$(\mathbf{B} - \lambda \cdot \mathbf{I})\vec{v} = 0 \tag{3.9}$$

The first step is to solve equation (3.9) for λ, from $(\mathbf{B} - \lambda \cdot \mathbf{I}) = 0$. The second step is to substitute values of λ into equation (3.7), to determine the vector $\vec{v}$. The eigenvector $\vec{v}$ forms the column vector in a matrix ordered by the size of the corresponding eigenvalue. The third step is to convert the vector $\vec{v}$ into an orthogonal matrix by applying the Gram-Schmidt orthonormalisation process of column vectors. This process produces **U**, its dimensions being 46000 × 3.

The calculation of **V** is similar to that of **U**. **V** is based on the matrix $\mathbf{A}^T\mathbf{A}$. In order to determine **V**, the first and second steps mentioned above need to be repeated. Once **V** is obtained, **V** needs to be transposed to find $\mathbf{V}^T$. The dimensions of both **V** and $\mathbf{V}^T$ are 3 × 3.

In order to find the matrix **S** in equation (3.6), the square roots of non-zero eigenvalues was taken and populated the eigenvalues diagonally in a way that s_{11} is the largest among all eigenvalues, s_{22} is the next largest and so on until the smallest value. The non-zero eigenvalues of **U** and **V** are always same. Thus, it does not matter from which one eigenvalues are to be taken. The dimensions of the matrix **S** are 3 × 3. An example of calculations in the SVD analysis is provided in Appendix C.

The main purpose of computing the SVD is to determine **V**, because the columns are the principal components (PCs) of **A**, and these columns are mutually orthogonal unit-length vectors. The few characteristics of PCs are that PCs define an orthogonal coordinate system such that in this system the data are uncorrelated and PCs maximize the variance explained in the data.

The last step is to multiply the original data set by **V** to project all the data points onto each of the PCs. This yields the coordinates of the points with respect to the space defined by the PCs. Since the PCs forms an orthogonal basis, what is really happening is the rotation of space, as given below

$$\mathbf{A} = \mathbf{U}\mathbf{S}\mathbf{V}^T \tag{3.10}$$

$$\mathbf{A}\mathbf{V} = \mathbf{U}\mathbf{S}\mathbf{V}^T\mathbf{V} = \mathbf{U}\mathbf{S} \tag{3.11}$$

The result of **US** has the property that the columns are uncorrelated with one another. Since the matrix **S** is a diagonal matrix, multiplication with *S* simply rescales the columns of the matrix **U**, which does not change the condition of the mutual orthogonality.

In summary, the purpose of these calculations is to rotate the data set of an abraded surface such that the horizontal surface becomes parallel to the *X*-axis and *Y*-axis of the coordinates system, whereas *Z*-axis gives the depth of the surface abrasion. This rotation is done by calculating the Principal component axis of the original data set and projecting the data set onto the PCs.

3) Abrasion loss only occurred in the middle or centre of the circular concrete surface. There was no significant abrasion near the edge. For this reason, a 10 mm length from the edge was not considered for further calculation. Accordingly, the actual radius is 50 mm, whereas the effective radius is 40 mm (Figure 3-13). This 40 radius is larger than the 38 mm radius of the water jet. Figure 3-13 shows the plot where the red circle indicates the 40 mm radius area. Using the 40mm radius surface a 3D surface profile was plotted to see how much abrasion has occurred, and in which position abrasion has occurred, using a mesh function (Figure 4-10). The script of MATLAB is given in the appendix.

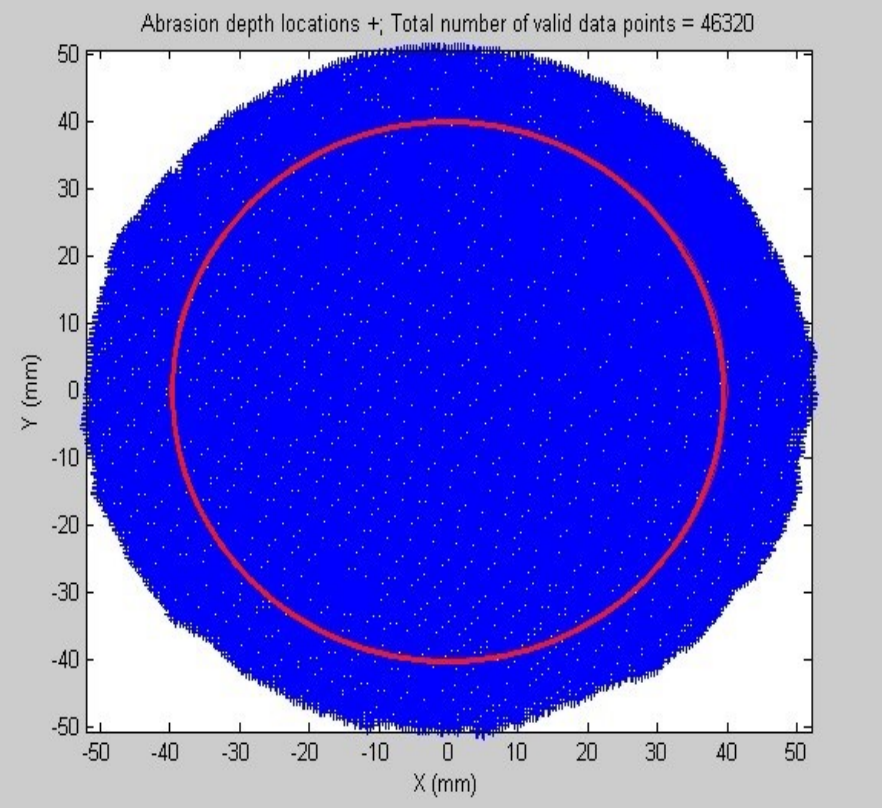

Figure 3-13: Effective surface area of the concrete surface. The area inside the red circle (40 mm in radius) denotes the effective area.

3.3.7 Calculation of Abraded Volume using ArcMap

Calculations of the abraded volume (V_a) use the following equation

$$V_a = \iint_{S_a} [Z_0 - Z(X,Y)]ds = \iint_{S_a} \Delta z ds = \sum_{n=1}^{N} \Delta z(X_n, Y_n)\Delta s_n \tag{3.12}$$

where N is the total number of data points (or surface elements) from 3D scan of an abraded concrete surface. The depth of abrasion Δz, given in equation (3.12), differs from point to point. Δs_n represents the horizontal area of the n'th surface element.

ArcMap (2015) is a program for processing geospatial data, which is the main component of Esri's ArcGIS suite. The version ArcMap 10.1 was very convenient to use to find the abraded volume (V_a) from concrete surface. The steps about how to determine the abraded volume from concrete surface are given below:

1) The data of (X, Y, Z) coordinates of a sample specimen are imported to ArcMap using "Add XY data" from the file menu. The data are saved in a shape file. By right clicking on the current data layer at "table of contents", one will find the "Export Data'' option which will export all the data in a specified directory.

   For volume calculation, the whole sample surface was not considered as it was not affected by the water jet impact. The concrete surface area affected by the water jet is about a circle of 20 mm radius. But the position of the abraded surface on all samples is not fixed, it varies a little from sample to sample, for this reason, a 40mm radius circle from the surface center was chosen from which volume loss will be measured for all sample specimens. It was observed that the abraded surface occurred within the 40 mm circle for all sample

specimens. As was mentioned earlier, data 10 mm from the edge was excluded, but this area was used to determine Z_0.

2) Data were clipped into two files. All the data outside the 40mm radius were excluded using "Clip' tool in ArcMap for abrasion. Data between 40 and 48 mm radius were used to determine the average initial datum height. To perform the clipping accurately, a polygon shapefile was created in the same directory. In that polygon shape file, a circle was drawn with a radius of 40 mm and the center of the circle is the center of the concrete surface. After that, using the ''Clip'' tool data outside the circle were excluded and new file was saved as shapefile using "Export data" like step one.

3) In this study, average depth of an annular surface of which the inner diameter is 40 mm and the outer diameter is 48 mm was taken as a reference height for each individual sample. It was observed that there were some data points at the edges (between 48 and 50 mm radius) that were not consistent and belong to the side surface of the sample (Figure 3-12 clearly shows this). For this reason, points within 2 mm distance towards the center from the edge were excluded from the data set. Figure 3-14 shows the ring surface from which average depth was determined.

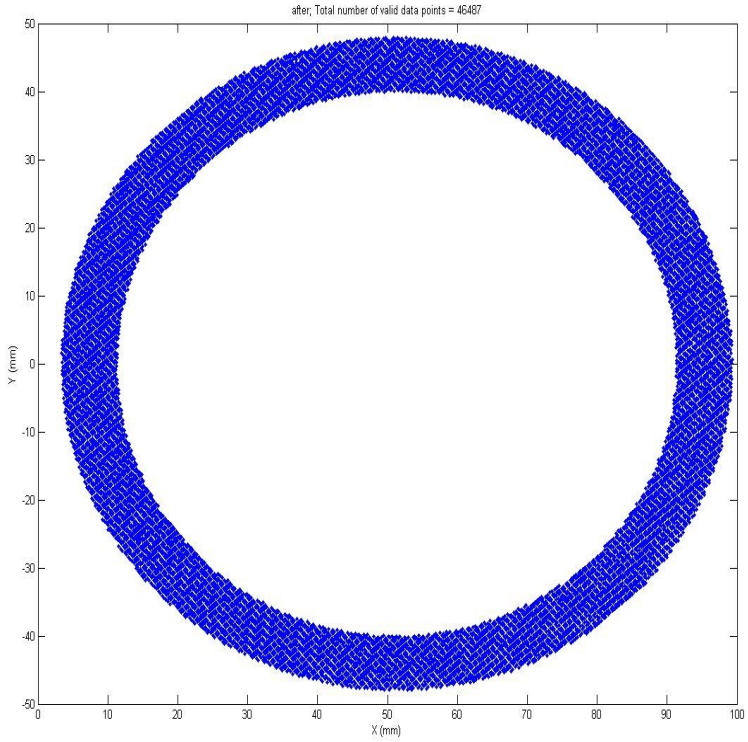

Figure 3-14: Surface area considered for calculating average depth of the specimen, which was used as a reference height in abraded volume calculation.

4) It was necessary to convert the latest shapefile into TIN (triangulated irregular network). The TIN is a vector data structure which represents a surface in a geographic information system. TIN consists of a non-overlapping triangular network of vertices associated with the coordinates in three dimensions. In “3D Analyst toolbox” of ArcMap there is an option called “Data Management toolset’’. In “Data Management toolset there is an option called “TIN’’ under this option, one can find “Create TIN’’ option. Using “Create TIN’’ current shapefile was converted to TIN. Figure 3-15 shows a TIN surface of a Fly ash modified materials with an age of 90days. The different colours showthe range of abrasion depth..

As the non-abraded portion does contain small irregularities, some points are higher than the calculated datum.

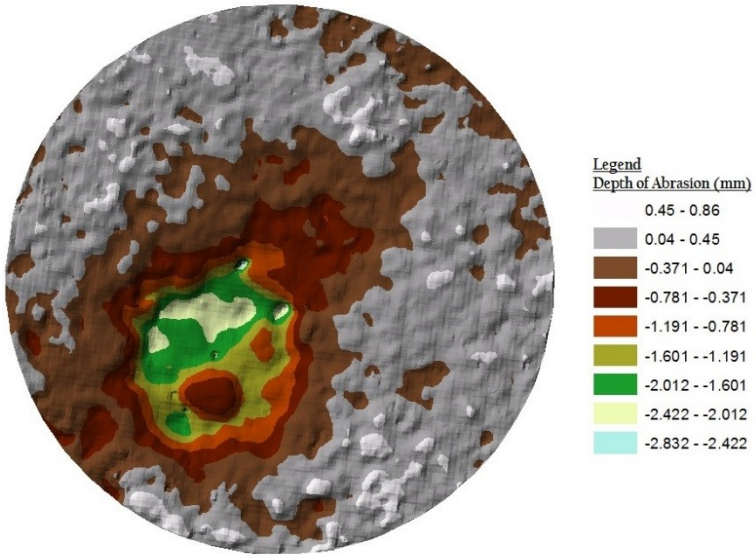

Figure 3-15: TIN surface of Fly ash Modified Repair Materials sample at the age of 90 days.

Note that in the integral (equation 3.11) for determining the volume of abrasion, the reference value Z_0 is taken as the average elevation of 40-48 mm ring (Figure 3-15) in this study. Appendix C shows the MATLAB script for evaluating the average elevation of a concrete specimen.

Using the "Surface Volume'' tool, setting the reference plane height as the average depth and selecting the "Below" option in the "Reference plane", the surface volume was measured. An output text file was generated from the "Surface Volume" analysis, which contains some results, including projected area, surface area and volume. Figure 3-16 visualizes how 'surface volume' tool works. Surface volume tool calculates the area of

each triangle on the surface and use integration to method to calculate the volume from the reference plane to the bottom/top point the surface.

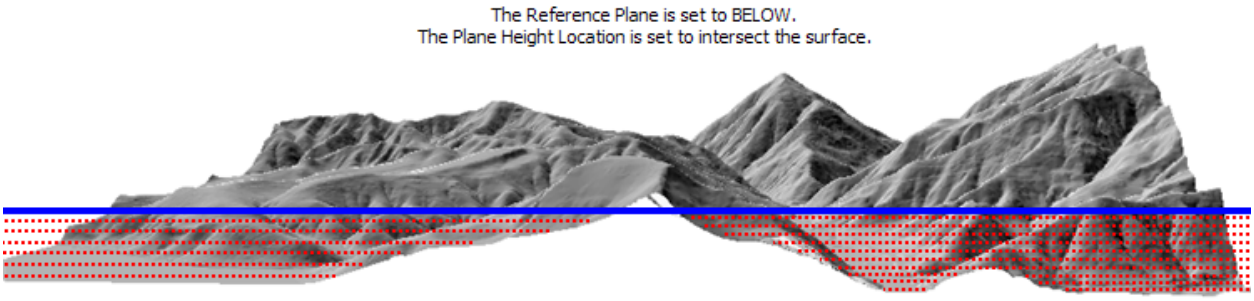

Figure 3-16: Measurement of volume using "Surface Volume" tool from a reference plane (http://resources.arcgis.com, accessed on 15/06/2015).

4. Test Results and Discussion

4.1 Introduction

This chapter contains the results obtained from all the experiments. The results are analyzed and discussed in detail in regards to relevant published research findings. For determining compressive and flexural strength of concrete specimens, the average observation of three samples tested at same condition was considered. Both compressive and flexural strength test was performed at the age of 28 days in accordance with ASTM methods. For abrasion resistance measurements, single tests were performed at concrete ages of 2, 4, 7, 28 and 90 days. At early ages, 2 and 4 days, one sample was tested for 3 hours. For 7, 28 and 90 days, 3 cycles of abrasion testing was performed on a single sample. The density of sand mix with water was maintained same which is 400 kg/m^3 at the age of 2, 4, 7 and 28 days and during the experiment; at the age of 90 days sand density was increased to 500kg/m^3 to observe that effect of density variation of the sand-water mixture. Another reason to increase the sand density was that the expected abrasion mass loss at 90 days age for a few types of material such as silica fume modified material would be very negligible.

The main parameters used to compare the results are type of material, age of concrete, duration of exposure and sand/water density. All the results are discussed and graphically represented in this chapter.

4.1.1 Effect of Age of Concrete on Abrasion Resistance

Four types of materials were used to observe the effect of age on the abrasion resistance of concrete. Figure 4-1 shows the relationship between ages of concrete with the abrasion resistance

at different ages of concrete. The test duration at 2 & 4days of age was 3hours and at 7, 28 & 90days it was 9hours. The abrasion test was performed at ages of 2, 4, 7 and 28 days and the sand mix concentration was 400 kg/m^3 water. However, for the better observation another set of experiments was performed at the age of 90 days with a sand concentration of 500kg/m^3 to evaluate the impact of higher sand concentration. In general, it is observed that, for each type of concrete mixtures, abrasion rate decreases with the increasing age. It is clearly observed that the standard concrete material is more vulnerable to abrasion then other repair materials. The silica fume repair material shows the best abrasion resistance among the three materials. The silica fume and the randomly distributed micro polymeric fibres give increased resistance. After silica fume, latex modified repair exhibits the next best abrasion resistance. The abrasion rate of concrete material was reduced by 19.6% within a duration period of 2 to 4 age with respect to 4days abrasion rate, by 25.6% at 7 days age with respect to 4days abrasion rate and by 47.7% at 28days age with respect to 7days abrasion rate.

Table 4-1 shows the average abrasion rate at different ages for all four types of concrete for a 3hour abrasion test. The abrasion rate of Concrete material at 28 days of age was reduced by 69% comparing to 2days of age. Though the reduction is very high the abrasion rate is still high in comparison to other materials. At 28days of age, Latest modified showed a reduction of 63.4%, Silica fume modified material showed a reduction of 69.5% and Fly ash modified material showed a reduction of 28.9% within compared of 2days of age abrasion rate.

Table 4-1: Abrasion rate of concrete materials at different age for a 3hour abrasion test

Age of concrete (days)	2	4	7	28	90
	Abrasion rate ($g/m^2/min$)				
Concrete material	21.66	17.41	12.95	6.72	9.99
Latex modified material	13.04	12.51	11.98	4.77	10.65
Silica fume modified repair material	8.66	8.00	6.72	2.64	3.57
Fly ash modified repair material	10.30	6.57	7.53	7.32	8.34

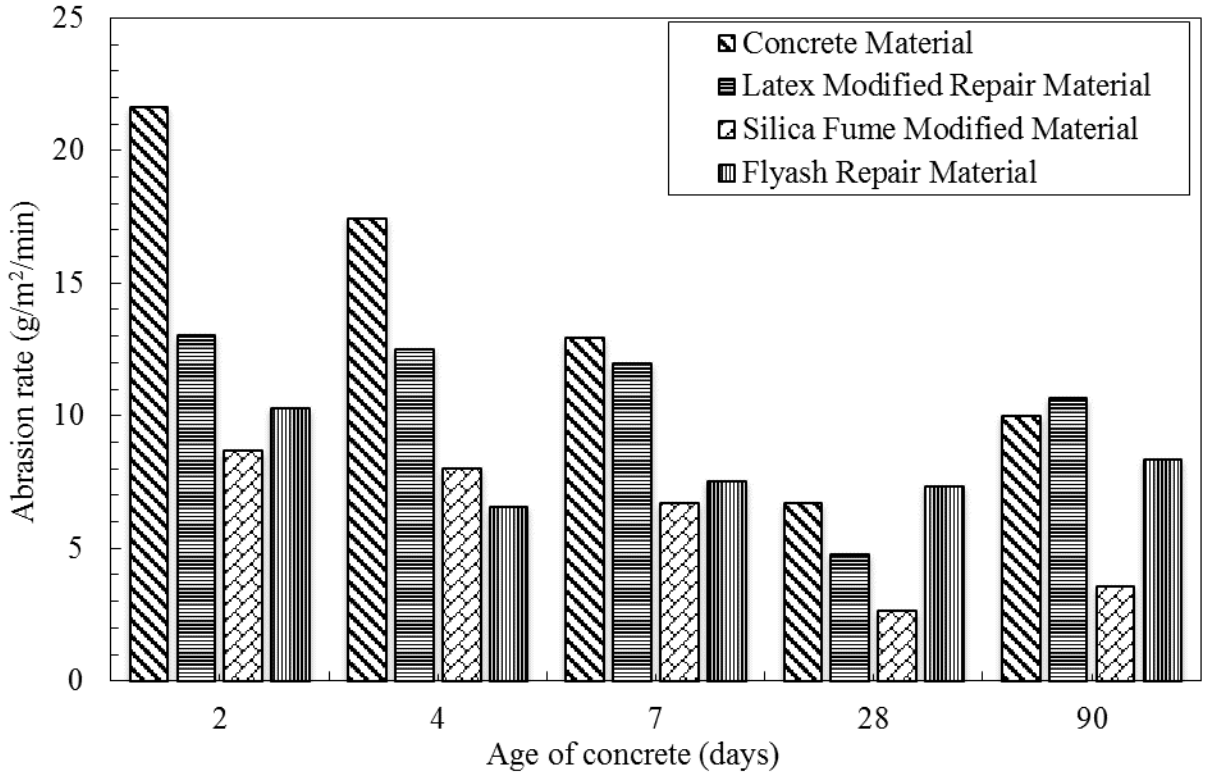

Figure 4-1: The relationship between abrasion erosion rate and age of concrete at different ages.

As it was observed that for silica fume material the abrasion rate is very low which denotes its high abrasion resistance. At 28 days, the abrasion mass loss for silica fume material is below 1 g. It was expected that at the age of 90days abrasion rate will decrease as concrete's strength will increase compared to 28 days. For this reason, the density of sand in water was increased to 500 kg/m^3. The results show that at higher concentrations of sand mix it was observed that the abrasion

rate was higher than it was during 28 days; clearly indicating that the density of sand has an influence on abrasion. But the overall ranking is similar to 28 days results. Again, silica fume exhibits best abrasion resistance as expected. Latex modified and concrete materials exhibited an almost similar kind of abrasion whereas fly ash repair material exhibited a little less abrasion than both of them. Through all the experiments, the fly ash material's abrasion rate was not reduced as much with its increasing age in comparison to other types of materials, Figure 4-2 shows the image of all types of sample after abrasion test.

Figure 4-2: Image of sample specimens used in abrasion test. From left: a) Latex modified material, b) Fly ash modified material c) Concrete material d) Silica fume modified material

.

4.1.2 Effect of Exposure Duration

All four types of materials were tested for 9 hours at intervals of 3 hours at 7, 28 and 90 days of age. Overall, the test results showed that the amount of abrasion increased with the increment of exposure time and the relation is linear. At the top layer of the surface, the water cement ratio is higher which made the top surface of the concrete weaker and caused higher abrasion. Abrasion erosion reduced when aggregates became visible and the relationship became nonlinear as they became dislodged. In this research, non-linearity relationship was not observed. It was observed that the abrasion depth was just a couple of millimeter, which was not sufficient to dislodge the larger aggregates.

At 7 and 28 days age, the abrasion test was performed with a sand mix concentration of 400kg/m^3 and at 90 days age sand density was 500kg/m^3 as the abrasion mass loss for silica fume material during an age of 28 days was below 1g. This will reduce more at the age of 90 days thereby making it negligible to compare. Figure 4-2 shows the relationship between abrasion loss and duration of test at the age of 7 days when sand density was 400 kg/m^3. Again, the silica fume material exhibited the best abrasion resistance among the other three types. The concrete material showed a maximum abrasion loss followed by latex modified material and fly ash material. For all the four types of materials, the relationship is linear between abrasion loss, exposure time and slopes.

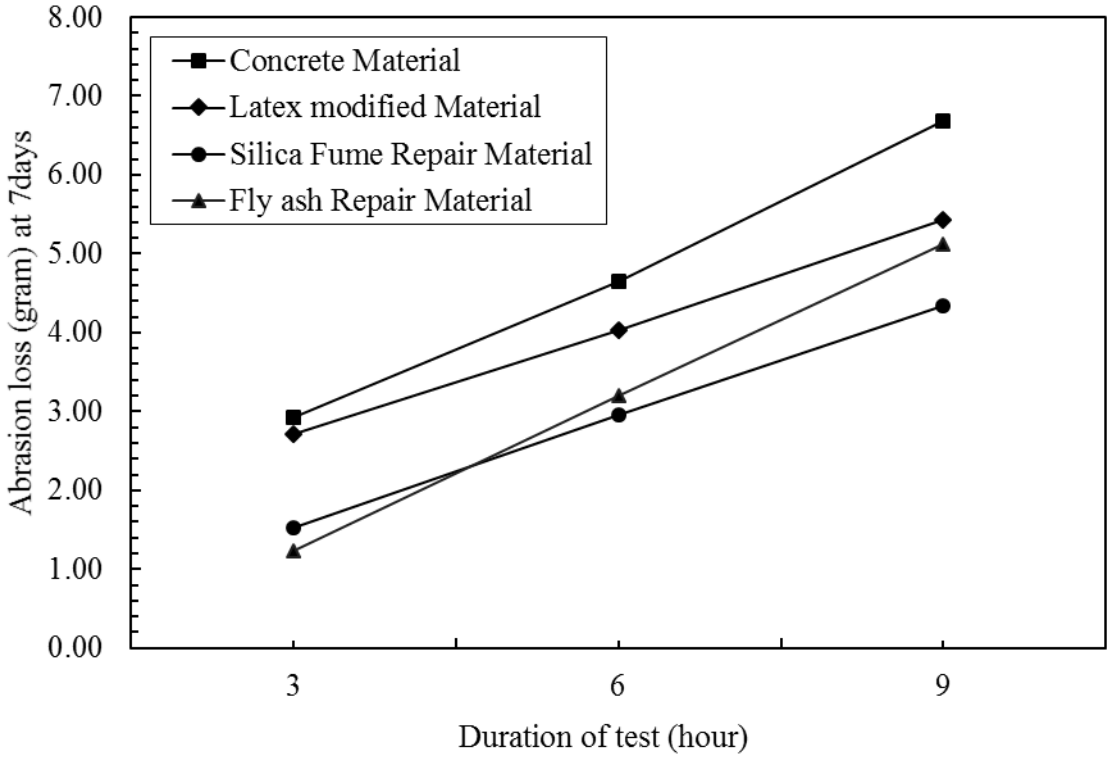

Figure 4-2: The relationship between abrasion loss and duration of exposure at the age of 7 days with a sand density of 400 kg/m^3 in water.

Figure 4-3 shows the same relationship at the age of 28 days. This time, the latex modified material exhibited higher abrasion than others. The slope of the concrete material was quite high compared to the other materials. At the beginning, concrete material showed less abrasion than fly ash, but at the end of 9 hours abrasion, it exhibited higher abrasion than fly ash but lower than latex modified material. The overall results of all ages' concrete showed that abrasion loss increased linearly with an increasing exposure time and reduced with an increasing age and increasing sand density. There was no significant change in the rate of abrasion as all the three tests were conducted on the same day, which denoted the same age of concrete for each individual sample. There was a reduction of about 58.8% in abrasion loss of silica fume material at the age of 28 days compared to 7 days abrasion test results. For latex modified materials, it was about 40.2% and for concrete

materials it was about 31.5%. Fly ash concrete showed the highest abrasion loss with a reduction in abrasion loss which is only 3% in comparison with a 7 days abrasion loss.

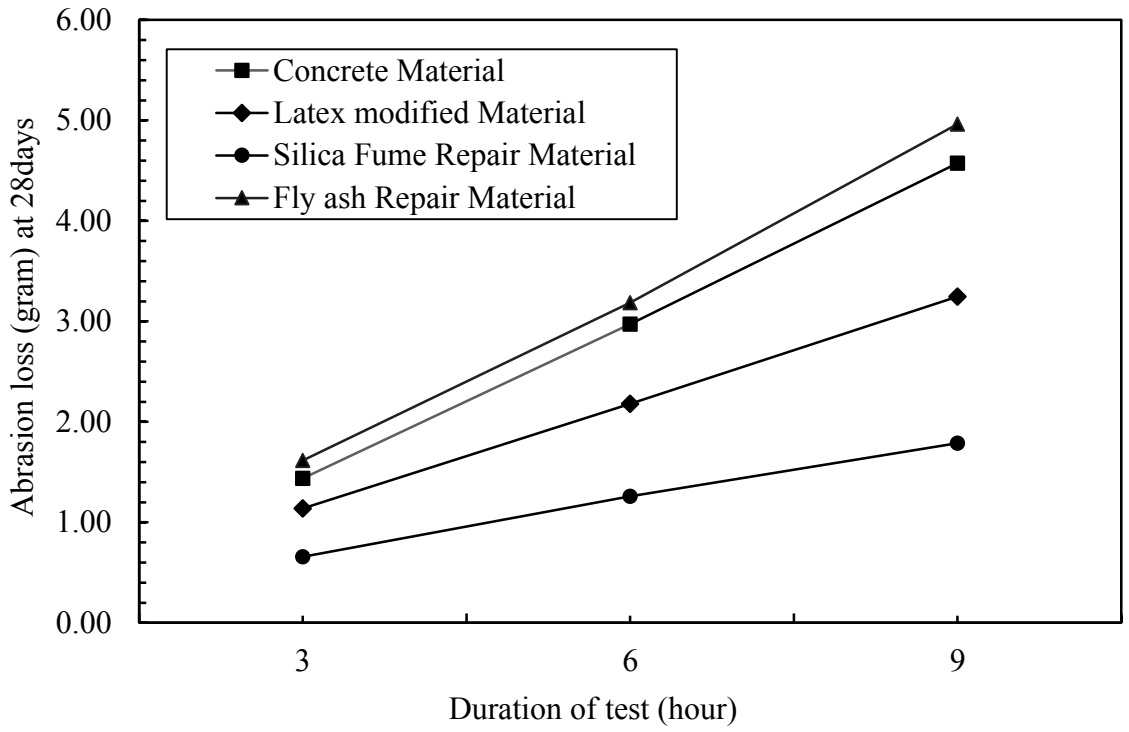

Figure 4-3: The relationship between abrasion loss and duration of exposure at the age of 28 days with a sand density of 400kg/m^3 in water.

At 90 days, abrasion loss was higher for all types of concrete with respect to 28 days as sand density was increased to 500kg/m^3 (Figure 4-4). Even though the test results were similar, again silica fume exhibited minimum abrasion loss. It also exhibited the same kind of results as that during 28 days, but fly ash concrete exhibited a bit higher abrasion loss than the concrete material. Silica fume material showed a minimum abrasion loss which was less than 2 g in 9 hours. On the other hand, latex modified concrete showed moderate abrasion loss.

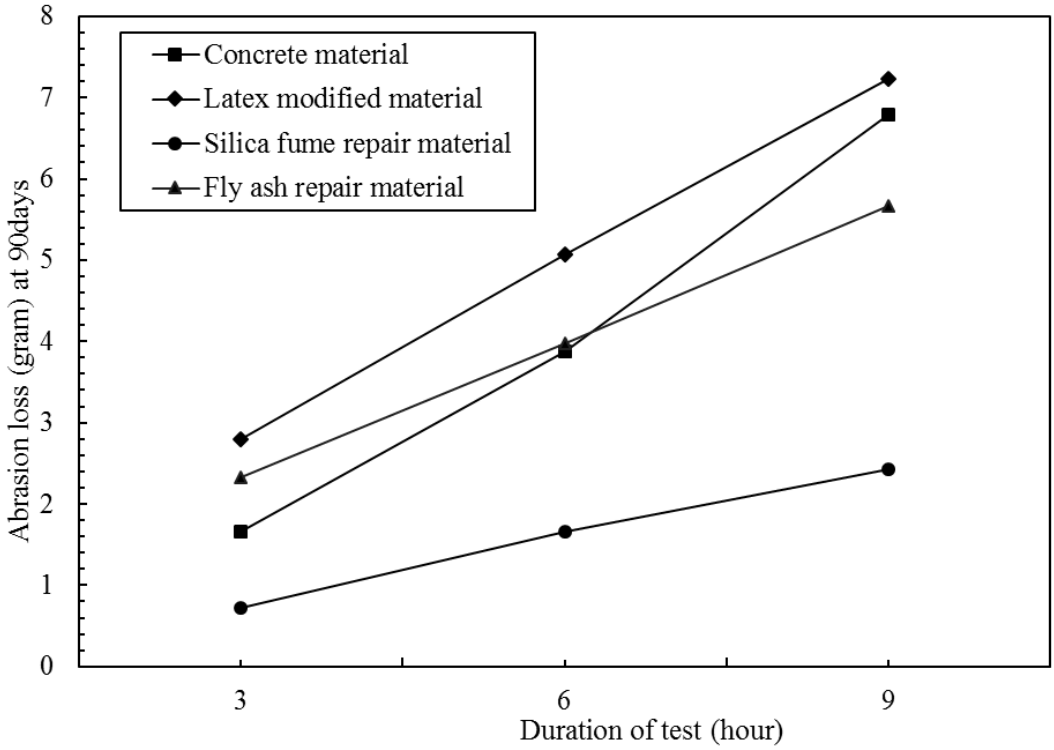

Figure 4-4: The relationship between abrasion loss and duration of exposure at the age of 90 days with a sand density of 500 kg/m^3 in water.

4.1.3 Effects of Strength

When a sample specimen is subjected to the abrasion test according to the method used in this study the specimen faces compressive, tensile and shear stresses near the top surface of the specimen due to the impact induced by the water-jet. From literature, it has been already established that the strength of concrete has a profound impact on the abrasion resistance of concrete. Table 4-2 shows the values of compressive strength and flexural strength at 28 days and the abrasion rate at various ages of all types of concrete materials used in this study. It can be seen that the compressive strength generally exceeded the manufacturer's values. This is expected as these represent minimum results.

Table 4-2: Compressive strength, flexural strength and abrasion rate of concrete at 28 days

	Compressive Strength MPa	Flexural Strength MPa	Abrasion rate ($g/m^2/min$)
Concrete Material	41.9	5.3	6.36
Latex modified Repair Material	45.4	7.5	5.04
Silica Fume Repair Material	57.8	12	2.91
Fly Ash Repair Material	48.15	11	7.15

Figures 4-5 and 4-6 illustrate the relationship between abrasion rate, compressive strength and tensile strength, respectively, for the 3 hour jet test at the age of 28 days. In a nutshell, the abrasion rate decreases when the concrete strength increases. Coefficients of determination (R^2) are often useful to correlate the concrete strength with the abrasion rate. The figures show that excluding the fly ash material, the R^2 for compressive and flexural strengths are very high, 0.9685 and 0.9962, respectively. Both the figures and table clearly show that if compressive and flexural strength increase, the abrasion rate decrease which coincides with the previous research. However, the abrasion rate of fly ash modified materials were quite high despite of its high compressive and flexural strength. The triangular point on both Figure 4-5 and Figure 4-6 denotes the data of fly ash modified material.

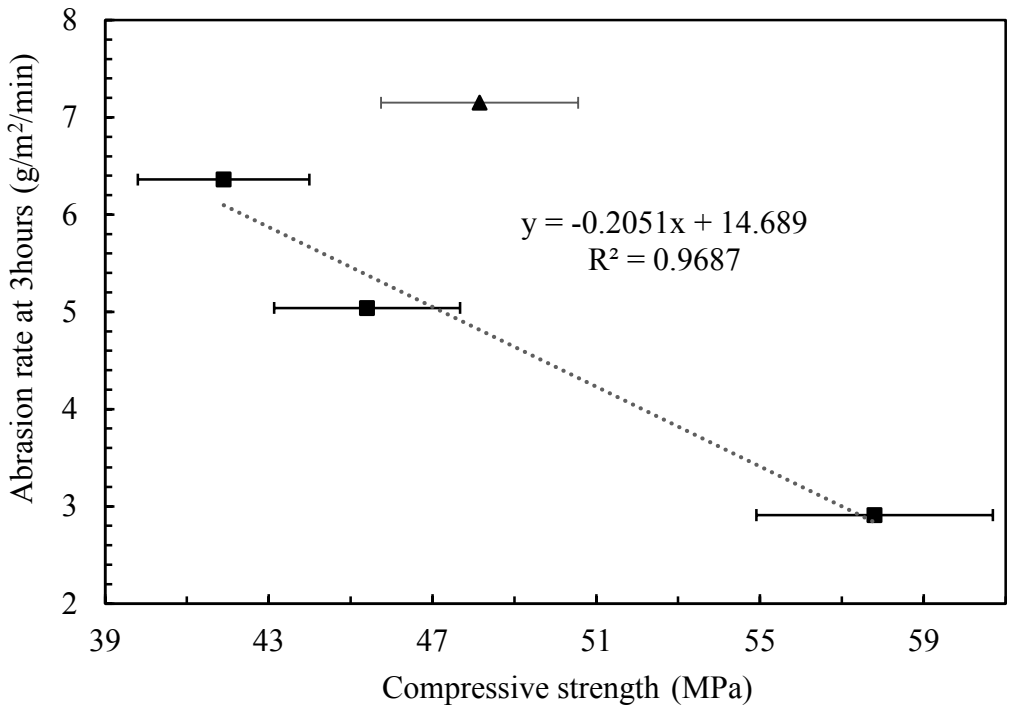

Figure 4-5: The relationship between compressive strength and 28 day abrasion rate.

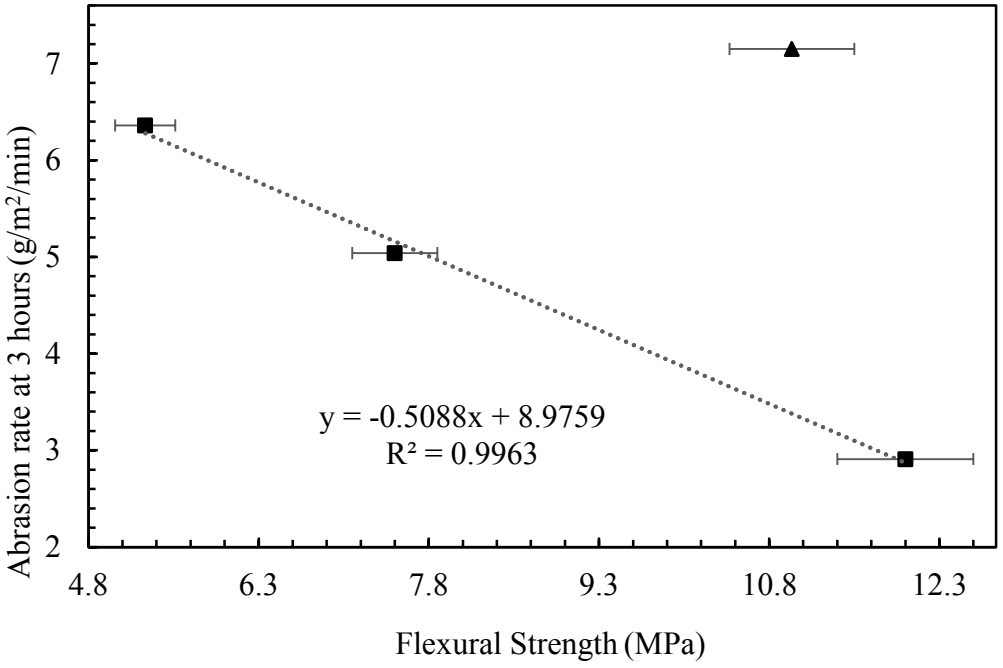

Figure 4-6: The relationship between Flexural strength and 28 day abrasion rate.

4.1.4 3D Scanner Results

To measure the abrasion depth and abraded volume, the Nextengine 3D scanner was used. A total of sixteen sample specimens were scanned. Data files obtained from the 3D scanner contained vertices with XYZ coordinates which formed the triangular mesh surface. The scanner was capable of scanning any sample with different resolution ranging from 700 to 44,000 points per square inch. If a higher resolution is used, the accuracy of the analysis will be high as it will take more data point into account in the same area. If the resolution is high, the file size is also becoming high which needs more time and a powerful computer to analyze the data. Table 4-3 shows the volume loss and the average abrasion depth due to abrasion. The volume loss is obtained from the circular area with a radius of 40mm from the center of the surface and the abrasion depth is obtained from the area between 40mm to 48mm radius where abrasion did not occur.It is clearly visible that, volume loss and abrasion depth is not constant with a changing resolution. The higher the resolution, the higher is the volume loss even though the difference is not that big, however higher resolution provide more accurate results. Among 5 different resolutions, 4400 points per square inch provided the optimum volume loss and also the volume loss difference between the 10000per square inch and 4400 per square inch was very negligible, the number of vertices was very high in the second one for which data file was very high. That is why 4400 per square inch resolution was used for the analysis which provided optimum results with good accuracy and moderate file size.

Table 4-3: Comparing different resolution with abrasion depth of same sample specimen

Resolution of Scanner (per square inch)	Volume loss (mm^3)	Ave. Abrasion Depth	Number of Vertices	File size (Mb)
700	116.8503	-0.1823	16241	1.93
1100	121.8208	-0.1784	25514	3.11
2000	138.2612	-0.1677	45150	5.62
4400	138.7712	-0.1698	45342	5.64
10000	136.1226	-0.1688	101908	12.8

Two different types of graph were plotted in MATLAB to visualize the abrasion depth and abrasion surface. One is a surface profile of each sample in three dimensional space and another one is abrasion depth from one edge to another in a 2D plot. A TIN (triangular irregular network) surface was also obtained from analysis in ArcMap, which also represented the surface topography in two dimensional space. Figure 4-7 shows a real image of the 7 day latex-modified sample after the 9 hour test. Figure 4-8 shows the TIN surface of the same sample specimen from which abraded area on the surface was easily distinguishable. The legend besides the TIN surface in Figure 4-8 shows the abrasion depth with respect to their color. In Figure 4-9, shows a ring shaped surface of which inner radius is 40mm and outer radius is 48mm. It is observed that there was no abrasion erosion in this zone for all sample specimens, that is why this average depth of this area was considered as zero and abrasion depth in 40mm circle was measured with respect to this zero depth.

Figure 4-10 illustrates the surface profile of the Concrete Material sample after a 9 hour test at the age of 7 days. The orientation of Figure 4-10 with respect to Figure 4-9 is *X*-*Y* plane 45° anti-clockwise, *Z*-axis 36° clockwise. The yellow and blue colour areas represent the abraded surface of that specific sample.

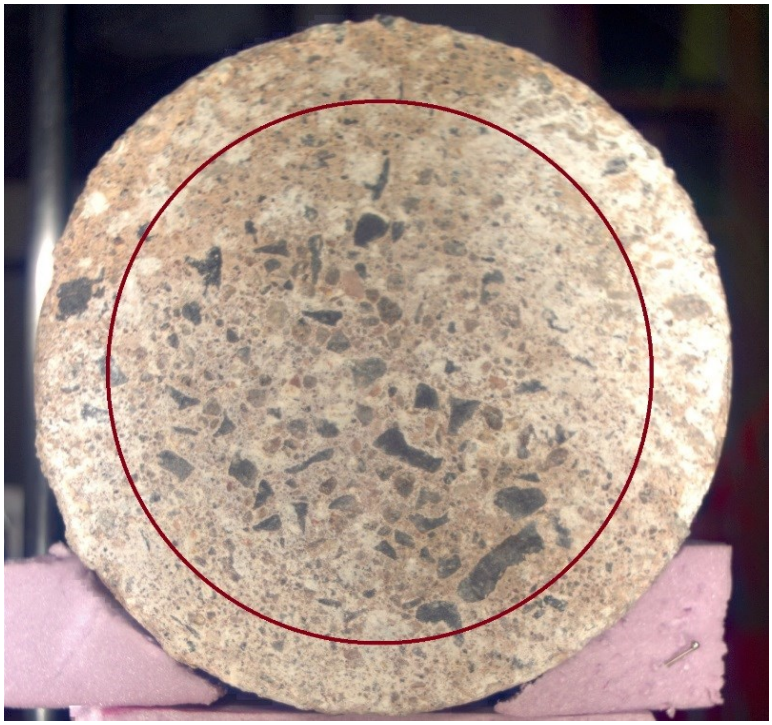

Figure 4-7: Concrete material sample after 9 hour abrasion test at the age of 7 days (surface radius 50mm) The dark red circle on the image shows the 40mm radius circle.

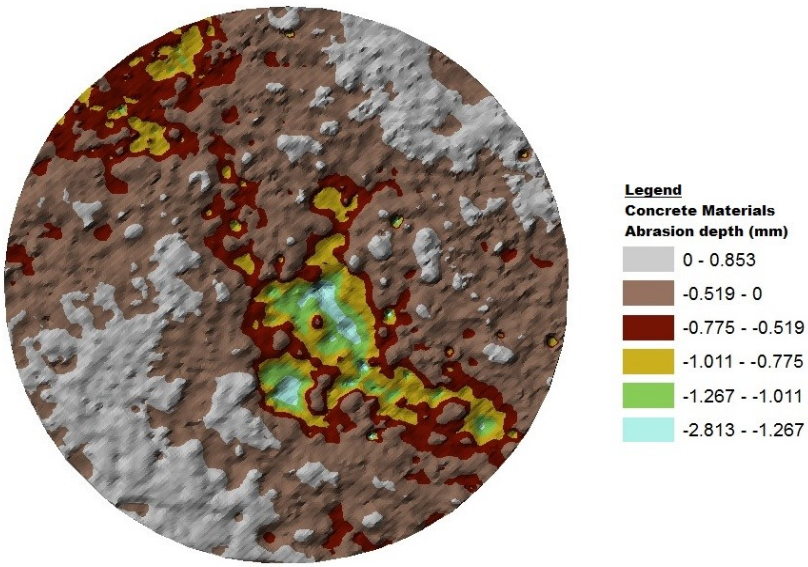

Figure 4-8:TIN surface of a Concrete Material sample after 9 hour abrasion test at the age of 7 days (surface radius 40mm) .

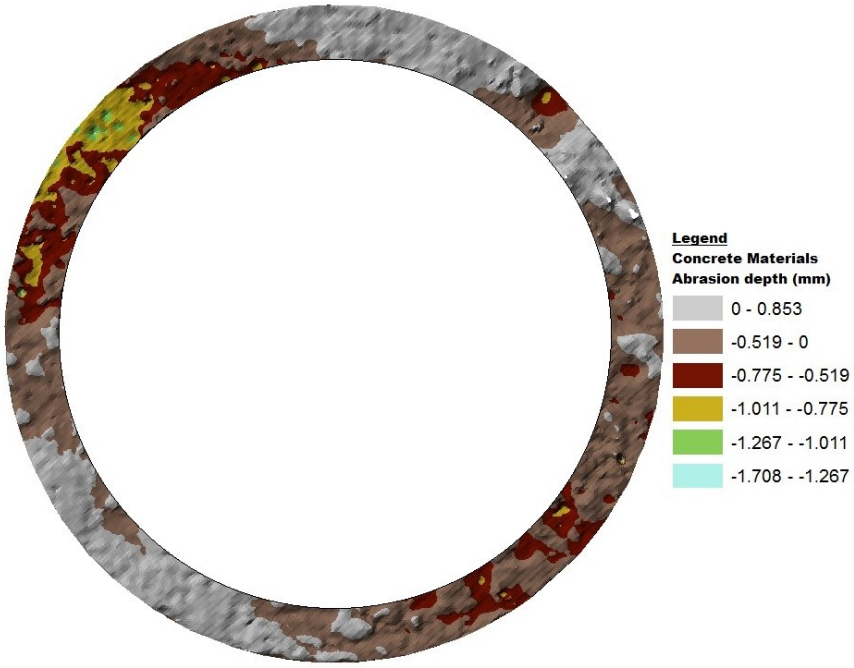

Figure 4-9: Ringshape TIN surface of a Concrete Material sample after 9 hour abrasion test at the age of 7 days of which average depth is zero mm. (inner radius 40mm, outer radius 48mm).

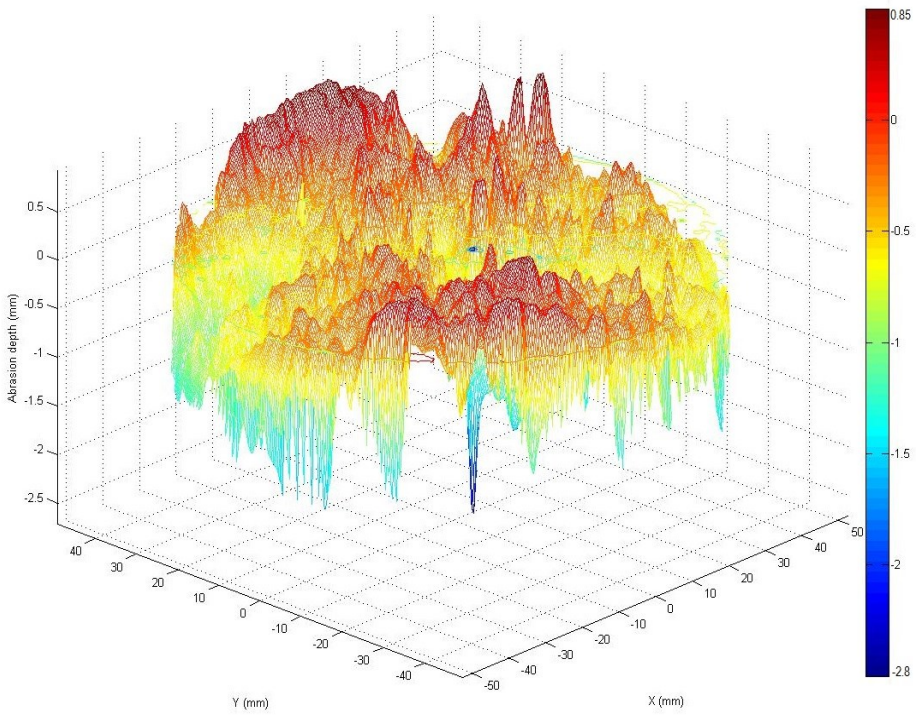

Figure 4-10: Surface profile of a concrete material sample after a 3 hour at the age of 7 days (surface radius 50mm).

4.1.5 Relationship between Abrasion Volume Loss and Age

Calculation of abrasion depth and volume was performed in MATLAB and ArcGIS from data obtained from the 3D scanner. Previously, the relation between the abrasion mass loss and age of concrete was discussed. As weight and volume are closely related to each other it was expected that the analysis in ArcGIS would show similar kind of relation. Figure 4-11 shows the total volume loss results of the analysis in ArcGIS for all concrete types at the age of 2, 4, 7 and 28 days. The duration of the test was only 3hours at the age of 2 and 4 days and the sand concentration was 400kg/m^3 throughout. The data for the volume loss of latex modified material at 2 days of age was not available. The results showed a similar trend as the graph of abrasion rate vs. age of concrete at the age of 2 & 4 days. At both 2 &4 days of age, volume loss was least for silica fume

modified repair materials whereas it was the highest for the concrete material. Fly Ash material showed a similar volume loss at the age of 2 & 4 days as silica fume.

The duration of the abrasion test was 9 hours at the age of 7 and 28 days. It was also observed that volume loss decreased with an increment in age for tests for the same duration. For concrete materials, volume loss was reduced by 15.37% from 7 days to 28 days where as for latex modified materials volume loss was reduced by 44.20%. For silica fume modified materials and for fly ash modified materials the reduction was 11.64% and 9.19%, respectively.

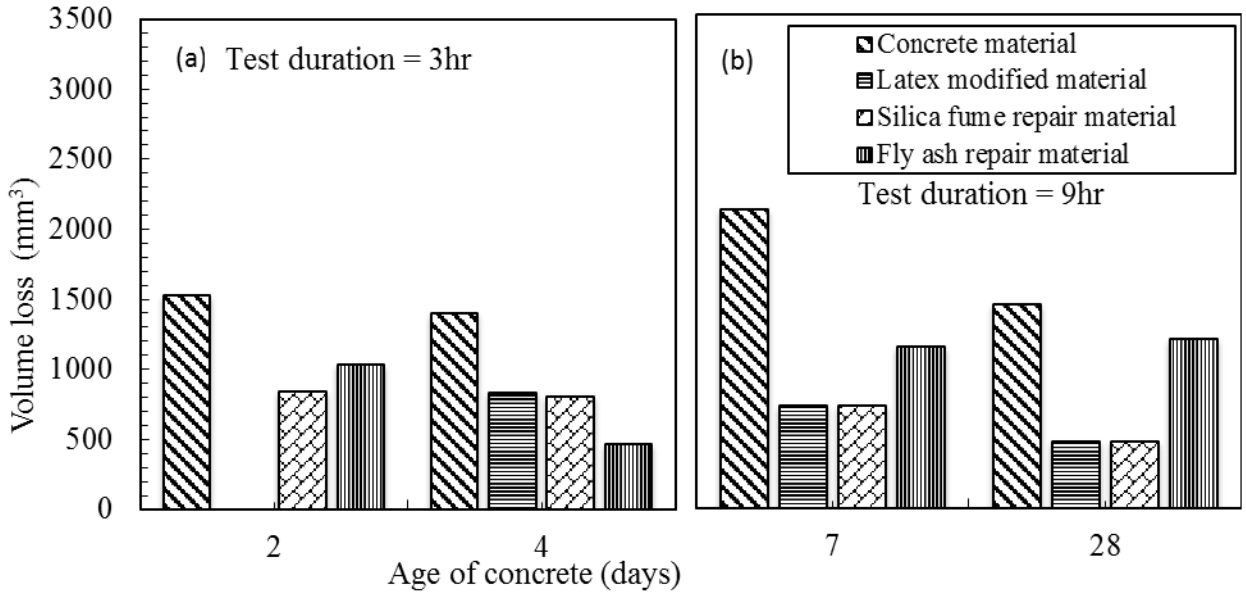

Figure 4-11: The relationship between total abrasion volume loss and age of concrete at 2, 4, 7 and 28 days age.

At the age of 90 days, sand concentration was increased to 500kg/m^3 to see the effect of sand concentration on abrasion resistance. Figure 4-12 shows the volume loss at the age of 90 days for all the four types of materials. As the mass loss in 90 days was higher than the mass loss at the age of 28 days because of the increased sand concentration; volume loss also showed similar results. Again, among the four materials, silica fume modified materials showed less abrasion loss and

concrete materials showed the highest volume loss. From the relation between mass and volume, the mass loss and volume loss should be proportional to each other.

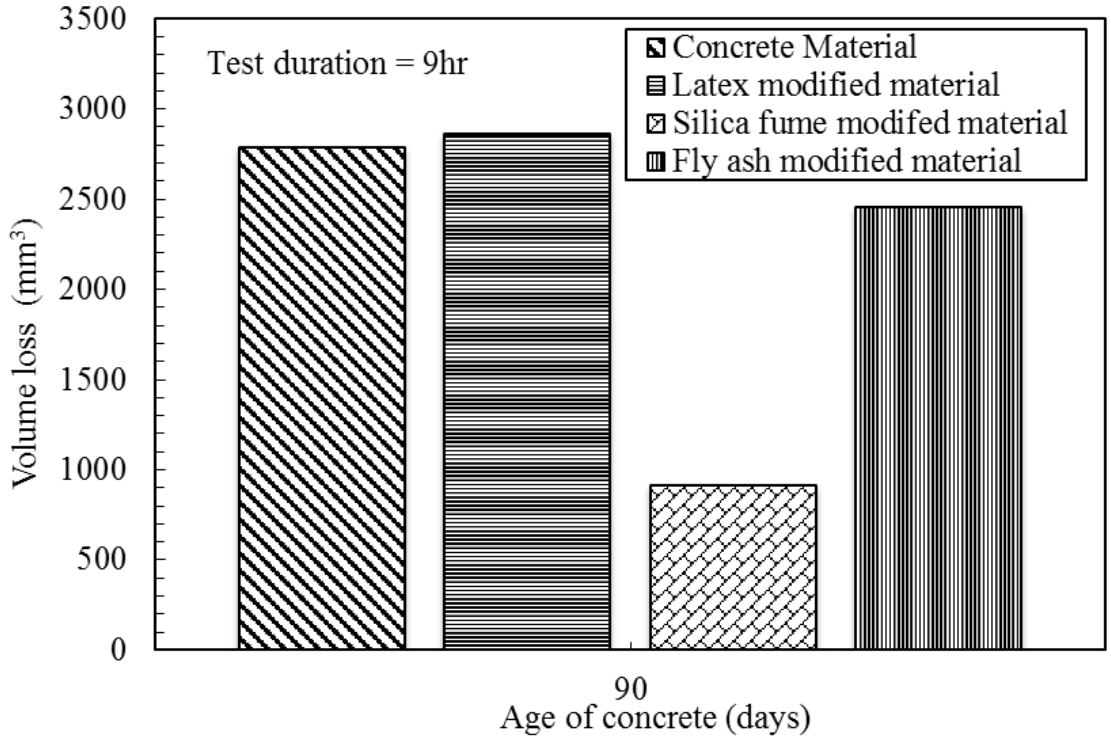

Figure 4-12: The relationship between abrasion volume loss and age of concrete at 90 days age.

Figure 4-13 shows the relationship between volume loss and mass loss at different age. As, density is almost same for all specimens (2500-2650kg/m^3), the ratio between mass and volume should be constant at all ages. But, in this analysis it was observed that the ratio was not constant at all ages. Figure 4-13 was plotted with all mass loss and respective volume loss data at different ages. The dotted line in the graph shows the trend line for all data points and the solid line shows the expected line. The slope of the trend line provides density of the concrete sample as density is the ratio of mass to volume. It is clear that, expected trend line does not coincide with obtained trend line from data. It is due to this uncertainty in the abrasion test procedure for which mass volume ratios varied

and the probable reasons could be the human error in measuring weight, improper saturated surface dry of the specimen before starting and after the test and non-uniform flow of sand through pumps during abrasion test.

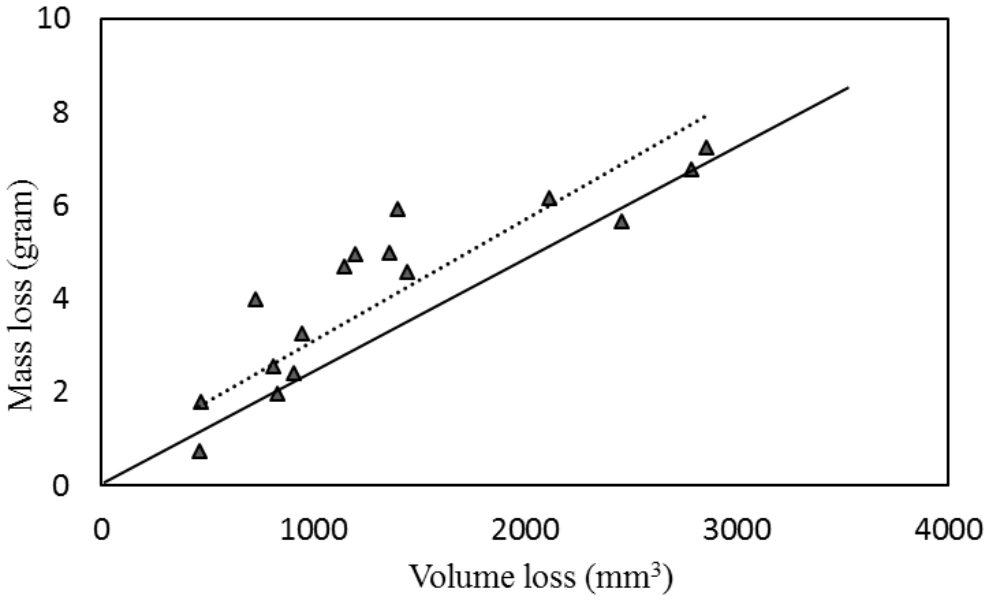

Figure 4-13: The relationship between volume loss and mass loss of concrete surface.

4.1.6 Depth of Abrasion

The depth of abrasion is also a measure which can correlate abrasion resistance of different types of concrete. Depth of abrasion was evaluated in MATLAB using data from the 3D scanner. The test results showed that the higher the abrasion volume, the higher the abrasion depth as shown in Table 4-4. But the depth of abrasion depends on the abraded surface area. For the same abraded volume if the area is small, depth of abrasion will be higher than where the abraded area is large. Also, maximum abrasion depth can be locally higher for a small abrasion mass loss due to an aggregate particle loss as it make a hole on the surface of the concrete. There are some other discrepancies with depth measurements as the water-jet does not cover the entire surface of the

specimen. As well as, the pressure is higher in the center of the water-jet, so if the center moves a bit in each 3 hour test for the same sample, the maximum abrasion depth location also changes. So, only considering the depth of abrasion does not provide the whole scenario, as the position of the water jet impact area were not kept constant for the whole test duration. One must consider the depth along with the abrasion mass loss and affected surface area. Table 4-4 shows all the data obtained from analysis regarding average abrasion depth and maximum abrasion depth.

For better observation and accurate volume loss calculation, average abrasion depth was measured in three different ways. Firstly, average abrasion depth was measured in a ring shape, surface area whose inner radius was 40mm and outer radius was 48mm and this ring shape was not affected by the water jet and volume loss was calculated taking this depth as the reference depth. Secondly, abrasion depth was calculated at the center part of the surface where abrasion occurred and the radius of the area was 40mm from the center. Thirdly, the whole surface area was considered for determining average depth. Average depth in Table 4-4 show the depth in a 0-40mm radius circle in relation to the depth in a 40-48mm radius circle. The overall results showed that, average abrasion depth was lower in the circle in the center with a radius of 40mm as all abrasion occurred in that area, as compared to the average depth in the ring shaped surface area since there was no abrasion loss. When the whole surface was considered the average abrasion depth value fall in between the circular area in the center with 40mm radius and the ring shaped area outside the a 40mm circle.

Table 4-4: Average depth of abrasion and maximum depth of abrasion

Age of Specimen (days)	Abrasion Depth (mm)	Test duration (hour)	Mass (g)	Volume (mm^3)	Maximum Depth (mm)
4	Concrete Material	3	5.92	1400.58	-2.59
	Latex Modified Repair Material	3	1.98	833.84	-1.47
	Silica Fume Modified Material	3	2.56	809.4	-1.05
	Fly Ash Modified Material	3	0.74	462.57	-1.19
7	Concrete Material	9	6.15	2115.87	-3.03
	Latex Modified Repair Material	9	4.99	1362.88	-1.13
	Silica Fume Modified Material	9	3.99	728.23	-2.17
	Fly Ash Modified Material	9	4.71	1147.09	-1.82
28	Concrete Material	9	4.57	1445.77	-2.35
	Latex Modified Repair Material	9	3.25	946.4	-1.77
	Silica Fume Modified Material	9	1.79	470.73	-1.40
	Fly Ash Modified Material	9	4.96	1200.56	-2.08
90	Concrete Material	9	6.79	2788.5	-2.85
	Latex Modified Repair Material	9	7.24	2860	-2.60
	Silica Fume Modified Material	9	2.42	910.278	-1.33
	Fly Ash Modified Material	9	5.66	2457.11	-3.07

It is useful to consider the maximum abrasion depth of concrete to compare the abrasion resistance of concrete. Figure 4-14 shows the results of abrasion depth at the age of 4,7,28 and 90 days for all four types of concrete with respect to age. Comparing the results with the abrasion loss at 4 days age, it is observed that, though abrasion mass loss of silica fume modified material was higher than fly ash modified material the abrasion depth is higher for fly ash modified materials. The probable reason is the movement of the specimen during an abrasion test for which impacted area of water jet was changed a bit.

At 7 days age, maximum abrasion depth for silica fume modified materials are higher than fly ash modified materials which should be opposite according the abrasion mass loss results. Despite of some of these individual discrepancies, the test results for abrasion depth shows similar trends as that of abrasion mass loss and volume. Maximum abrasion depth reduces as age of concrete decreases. The maximum depth of abrasion was higher at 90 days age compared with 28 days age as sand concentration was increased from 400 kg/m^3 to 500 kg/m^3. Ultimately, at 28 days age and 90 days age, silica fume modified materials showed the less abrasion depth compared to with others and fly ash modified and concrete material showed higher abrasion depths.

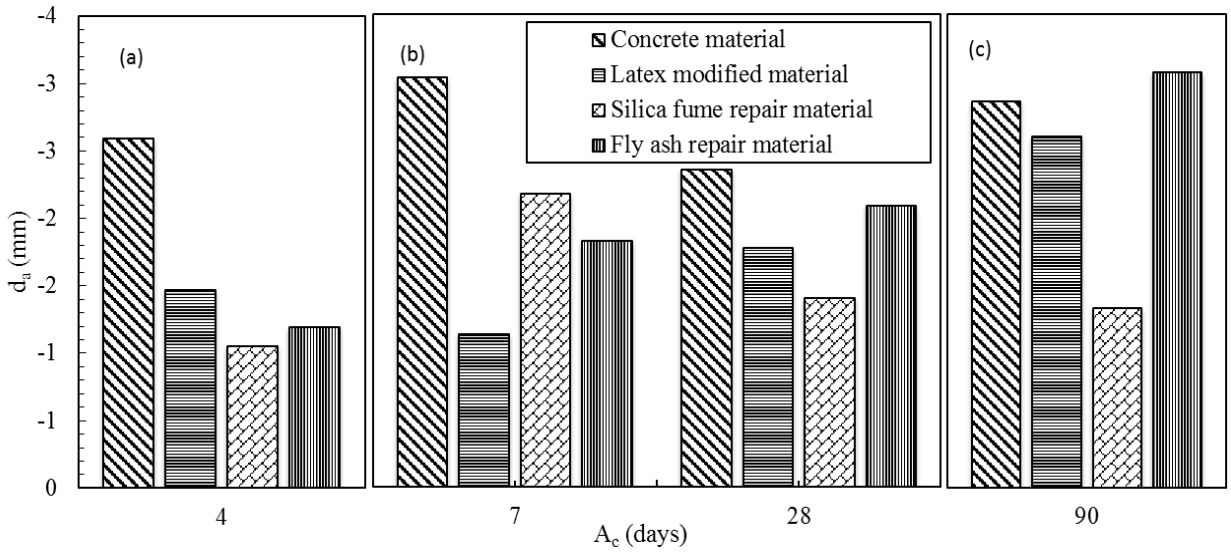

Figure 4-14: The relationship between abrasion depth and age of concrete at 4, 7, 28 and 90 days age for all four types of concrete.

Figure 4-15 shows the relationship between maximum abrasion and mass loss of a concrete specimen at different ages. It clearly shows that, if the maximum depth increases the mass loss

also increases linearly. However, there are some data points which go against the linear relationship due to the accuracy of abrasion test.

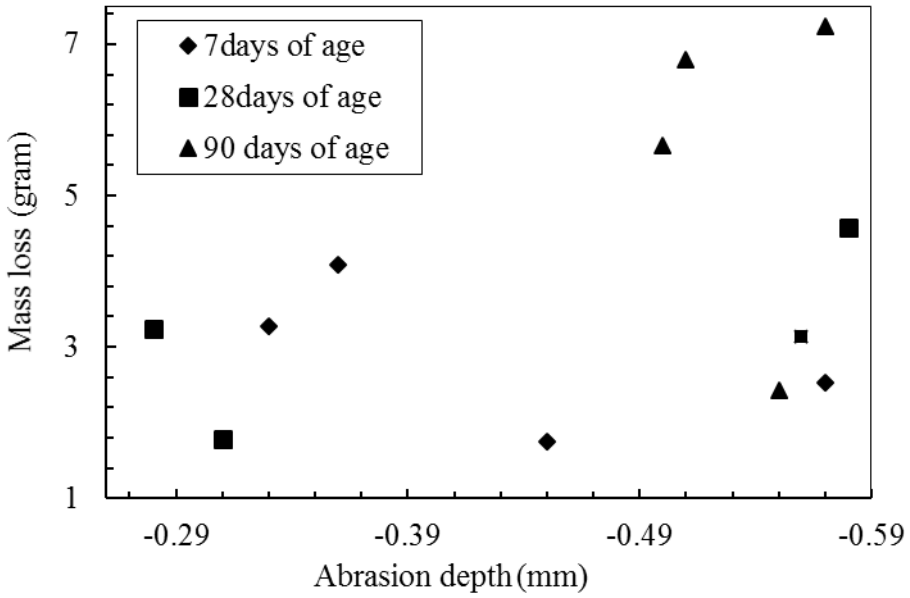

Figure 4-15: Relationship between mass loss and maximum abrasion depth

5. Conclusions and Recommendations

5.1 Conclusions

The aim of the study was to evaluate the abrasion resistance of different concrete repair materials due to the impact of water-borne particles. The experimental study was helpful to understand the influence of physical properties of different concrete repair materials regarding the abrasion erosion problem in hydraulic structures and will help to achieve a viable engineering solution for this particular problem. The conclusions drawn from the results of this study can be summarized as follows:

1) The experimental procedure used in the study is appropriate to perform experimental evaluation of abrasion resistance of concrete due to impact as this test method can replicate the real scenario occurred in hydraulic structures. The abrasive materials and velocity of flow was sufficient to initiate the disintegration of particles from the sample surface. Hardness of aluminum oxide played a major role in the observed abrasion erosion. There is some variability in the test procedure such as uniform sand flow into the pumps, concrete specimen's moisture content before and after test for which experimental results may vary but proper care and attention can eliminate that variability easily. One probable improvement is to design the water tank in a way that it will supply the same amount of sand flow into the pumps during the test and measuring the moisture content of concrete sample before and after the test.
2) Four types of materials were used in the study. Among all four materials, silica fume modified fibre reinforced repair material exhibited better abrasion than others. Latex modified material comes after silica fume modified material in terms of abrasion resistance. The worst abrasion resistance was exhibited by the concrete material, which is a

conventional concrete. Test results proved that supplementary materials can improve the abrasion resistance of concrete to a good extent. Fly ash modified repair material, exhibits lower abrasion than concrete repair material, but it's more than latex modified concrete. The results of Fly ash were variable, sometimes it showed better abrasion resistance sometimes not. Silica fume modified repair material and fly ash modified repair material both contained the same amount of polypropylene microfibres as reinforcement, cement and aggregates. The abrasion resistance exhibited by silica fume modified material is far better than fly ash modified material. Therefore it can be said that polypropylene microfibre's contribution to abrasion resistance appears to be negligible.

3) Abrasion rate was compared with age of concrete and exposure time. Test results exhibited that abrasion loss decreases with the increment of age and it increases linearly with exposure duration which is similar to the previous research.
4) Abrasion mass loss is strongly correlated to compressive strength in most cases. With the increment of compressive and flexural strength, abrasion loss decreases linearly. The higher the compressive strength of concrete, the better the abrasion resistance. Fly ash material exhibited slightly different results; compressive strength of fly ash repair materials is higher than latex modified repair material, even though fly ash repair material exhibits higher abrasion than latex modified material. More work is needed in this topic.
5) The method used for evaluating abrasion depth and volume using the 3D scanner and analyzing the data in MATLAB and ArcMap was appropriate. As the resolution was high, it was possible to analyze the data in MATLAB and ArcMap with high accuracy. Utilizing ArcMap to calculate the abraded volume was a good choice as ArcMap was capable to measure projected volume from a reference plane which gave more accurate results.

Overall, calculating abrasion volume in this approach is a new concept and gives a new criteria to compare abrasion resistance of different types of concrete.

6) Depth of abrasion and volume showed a similar relation to the age of concrete as mass loss. But, solely the depth of abrasion will not give an accurate comparison. It is only possible if the position and the area of the water jet impact area were kept the same throughout the test. Therefore, mass loss or volume loss should take into account when comparing the abrasion resistance of concrete as this gives much more information. Most common test methods use abrasion depth as a criterion.

5.2 Recommendations

On the basis of this study, a number of recommendations are made:

1) The test method adopted in this research is suitable for evaluating abrasion resistance due to impact. But still there is significant scope to improve the performance of the abrasion test apparatus. Two types of sand were mixed with water as abrasive materials and these sand mix flows through the pump with water, but it is not possible to determine exactly how much sand was transferred through the pump onto the concrete surface of concrete in the test duration and also it is possible that the amount of sand flow is not equal for all tests. However, it was assumed that sand flow is same for all the experiments as surrounding conditions were kept same. The design of the abrasion test apparatus can be improved by some modification which can ensure constant sand in the pump.
2) Aluminium oxide with a Mohr hardness 9 and fine silica was used as abrasive material. Different sands and other larger particle like gravel can be used to evaluate the impact of different abrasive particles with different hardness on abrasion.

3) As the amount of abrasion mass loss is very small, the difference between the saturation level of concrete sample before and after the test can contribute to the mass loss which was a source of error in this study. This error can be checked by measuring the moisture content of the samples before and after test which will help to evaluate the accurate abrasion loss.
4) Only two types of sand concentrations were used; 400kg/m^3 and 500kg/m^3 to evaluate the impact of abrasive concentration on abrasion which shows higher the concentration higher is the abrasion. Few more different abrasive concentrations with different particle can be used to evaluate the effect of abrasive particle concentration.
5) Ready-made concrete repair materials were used for the study where the limitation was that the amount, percentage of latex polymer, fly ash, silica fume, polypropylene microfibre were fixed. Experiments with different concentration of these materials would help to analyse more accurately on their contribution to abrasion resistance. There is immense scope to use different supplementary materials and fibre reinforcement to evaluate the performance against abrasion resistance.
6) Use of the 3D scanner and evaluating the surface profile, abrasion depth and abrasion volume with the help of MATLAB and ArcMap is a new approach. Better observation of volume loss with more accuracy can be possible by scanning each sample before and after the abrasion test.

5.3 Research Contributions

This experimental study of concrete surface abrasion has made the following research contributions:

The loss of volume is quantified and added to the analysis of abrasion. This quantity is important but has been ignored in previous studies. They have only considered mass loss, abrasion depth and compressive strength.

For the first time, this study introduced 3D scan technology for accurate measurements of volume loss and abrasion depth. The associated data processing methods developed in this study are very efficient and suitable for handling a large of volume of measurements.

6. References

ACI Committee 210, Erosion of Concrete in Hydraulic structure (ACI 210R-03), ACI Manual Concrete Practice, Part 1, American Concrete Institute, Farmington Hill, MI, 2003.

Alexander, M. G., and. Magee, B. J. "Durability Performance of Concrete Containing Condensed Silica Fume." Cement and Concrete Research 29.6 (1999): 917-22.

ArcMap 10.1, http://www.esri.com/software/arcgis (accessed on 27/07/2015), (2012)

ASTM C418-12, Standard Test Method for Abrasion Resistance of Concrete by Sandblasting, ASTM International, West Conshohocken, PA, 2012, www.astm.org

ASTM C779 / C779M-12, Standard Test Method for Abrasion Resistance of Horizontal Concrete Surfaces, ASTM International, West Conshohocken, PA, 2012, www.astm.org

ASTM C944 / C944M-12, Standard Test Method for Abrasion Resistance of Concrete or Mortar Surfaces by the Rotating-Cutter Method, ASTM International, West Conshohocken, PA, 2012, www.astm.org

ASTM C1138M-12, Standard Test Method for Abrasion Resistance of Concrete (Underwater Method), ASTM International, West Conshohocken, PA, 2012, www.astm.org

Bakke, K. J. "Abrasion Resistance." Significance of Tests and Properties of Concrete and Concrete-Making Materials (ASTM STP 169D), ASTM, West Conshohocken, PA (2006): 184-93.

Frizell, K.H, Mefford, B.W.,'' Designing spillways to prevent cavitation damage'', Concrete International (May 1991): 58-64

Gencel, Osman., Ozel, Cengiz., Filiz, Mumin, and Koksal, Fuat. "The Relations between Mechanical Strengths and Abrasive Wear of Concrete Incorporating the Hematite Aggregate." International Journal of Pavement Engineering 13.3 (2012): 235-243.

Grdic, Z. J., Toplicic Curicic, Gordana A., Ristic, N.S. and Despotovic, I. M, "Abrasion Resistance of Concrete Micro-Reinforced with Polypropylene Fibres." Construction and Building Materials 27.1 (2012): 305-12.

Horszczaruk, E. K. "Hydro-Abrasive Erosion of High Performance Fibre-Reinforced Concrete." Wear 267.1–4 (2009): 110-5.

Horszczaruk, Elżbieta. "Abrasion Resistance of High-Strength Concrete in Hydraulic Structures." Wear 259.1–6 (2005): 62-9.

Kumar, R.G., Shamra, U. K. "Standard test methods for determining of abrasion resistance of concrete''. Internation journal of civil engineering research. ISSN 2278-3652 Volume 5, Number 2 (2014), pp. 155-162

Lane, R.O. "Abrasion Resistance." Significance of Tests and Properties of Concrete and Concrete-Making Material (1966): 332-50.

Laplante, P., Aitcin, P. and Vézina D. "Abrasion Resistance of Concrete." Journal of Materials in Civil Engineering 3.1 (1991): 19-28.

Liu, Yu-Wen, Tsong Yen, and Tsao-Hua Hsu. "Abrasion Erosion of Concrete by Water-Borne Sand." Cement and Concrete Research 36.10 (2006): 1814-20.

Liu, Yu-Wen. "Improving the Abrasion Resistance of Hydraulic-Concrete Containing Surface Crack by Adding Silica Fume." Construction and Building Materials 21.5 (2007): 972-7.

Liu, Y.W., Cho, S.W., and Hsu, T.H. ''Impact Abrasion of Hydraulic Structures Concrete'' Journal of Marine Science and Technology, Vol. 20, No. 3, (2012) pp. 253-258.

Momber, A., and Kovacevic, R. "Fundamental Investigations on Concrete Wear by High Velocity Water Flow." Wear 177.1 (1994): 55-62.

Mindess, Sidney., Young, J. F., Darwin, David. Concrete (2nd Ed.) Prentice Hall. Pearson Education, Inc., Upper Saddle River, NJ 07458, USA (2003)

Maya. Autodesk Maya 2015, www.area/autodesk.com/maya2015 (accessed on 27/07/2015),

Naik, T. R., Shiw S. S., and Mohammad M. H. "Abrasion Resistance of Concrete as Influenced by Inclusion of Fly Ash." Cement and Concrete Research 24.2 (1994): 303-12.

Nawy, E. G. Concrete Construction Engineering Handbook. CRC press, 2008.

Nazari, Ali., and Shadi Riahi. "Abrasion Resistance of Concrete Containing SiO_2 and Al_2O_3 Nanoparticles in Different Curing Media." Energy and Buildings 43.10 (2011): 2939-46.

Sadegzadeh, M., Page, CL., and Kettle, RJ. "Surface Microstructure and Abrasion Resistance of Concrete." Cement and Concrete Research 17.4 (1987): 581-90.

Sawyer, J. L. "Wear Tests on Concrete using the German Standard Method of Test and Machine". ASTM Proceedings. 1957.

Shamsai, A., Peroti, S., Rahmani, K., Rahemi, L.,'' Effect of water-cement ratio on abrasive strength porosity and permeability of Nano-silica Concrete.'' World Applied Sciences Journal 17 (8):929-933. (2012).

Siddique, Rafat. "Effect of Fine Aggregate Replacement with Class F Fly Ash on the Abrasion Resistance of Concrete." Cement and Concrete Research 33.11 (2003): 1877-81.

Wang, Xin., Lua, S., Hu, Ya-an., Yuan, Qiang. , Wang, H.S., Zhao, L.H. "High-Speed Flow Erosion on a New Roller Compacted Concrete Dam during Construction." Journal of Hydrodynamics, Ser.B 24.1 (2012): 32-8.

Witte, L.P. and Backstrom, J.E., ‘’Some Properties Affecting the Abrasion Resistance of Air-Entrained Concrete,’’ Proceedings, ASTM International, West Conshohocken, PA. Vol. 51, 1951, P 1141.

Wu, C.H., Liu, Y., Huang, C., Yen, T., Hsu, T.H., ‘’Research on the Abrasion Erosion and Impact Resistance of Fibre Concrete’’ NCHU Research and Development. http://research.nchu.edu.tw/eng (accessed on 27/07/2015)

Wu, C.H., Yen, T., Liu, W.Y., and Hsu, T.H., ‘’The Abrasion Erosion Resistance of Concrete Containing Blast Furnace Slag’’ Taiwan Power Company Report.

Yen, Tsong, Hsu, T-H., Liu, Yu-Wen., Chen, S.H. "Influence of Class F Fly Ash on the abrasion–erosion Resistance of High-Strength Concrete." Construction and Building Materials 21.2 (2007): 458-63.

Yen, T., Hsu, T.H., Liu, Y., Chen S.H., ‘’Influence of class F fly ash on the abrasion–erosion resistance of high-strength concrete ‘’. Construction and Building Materials 02/2007; 21(2-21):458-463.

7. Appendix

A. MATLAB script for rotating concrete surface into a horizontal plane

```
fnameInput = 'Concrete-F3 -v.obj';
      fid = fopen(fnameInput);
      data = textscan(fid, '%s %f %f %f ','HeaderLines',2);
      fclose(fid);
      X=data{2};
      Y=data{3};
      Z=data{4};
      XYZ=[X Y Z];
      xyz0=mean(XYZ);
A=bsxfun(@minus,XYZ,xyz0); %center the data
scatter3(A(:,1),A(:,2),A(:,3));
%% Step 2. Find the direction of most variance using SVD and rotate the data to make that the x axis. (Your data is almost perfectly aligned with the x-axis to begin with).

[U,S,V]=svd(A,0);
A_rot = A*V; %V(:,1) is the direction of most variance
hold on, scatter3(A_rot(:,1),A_rot(:,2),A_rot(:,3));
%% Step 3. Slide the data up the x axis so all the points are x >= 0.

A_final = bsxfun(@minus,A_rot,[min(A_rot(:,1)) 0 0]);
scatter3(A_final(:,1),A_final(:,2),A_final(:,3));
```

B. MATLAB script for plotting various graph

```
 % 3D scanner data
load A_final.txt;
x = A_final(:,1); y = A_final(:,2); z = A_final(:,3);
%load xyz_raw.txt;
%x = xyz_raw(:,1); y = xyz_raw(:,2); z = xyz_raw(:,3);
mid_x = (max(x) + min(x))/2;
mid_y = (max(y) + min(y))/2;

x = x - mid_x;
y = y - mid_y;

% Radius of data inclusion
```

```
r = 40;
mid_x = (max(x) - min(x))/2;
mid_y = (max(y) - min(y))/2;
xr = [-r:1:r];
yr1 = sqrt(r^2 - xr.*xr);
yr2 = -sqrt(r^2 - xr.*xr);

data_pts = size(x,1);

for n = 1: data_pts
   dist = sqrt(x(n)^2 + y(n)^2);
   if dist >= r
      z(n) = NaN;
   end
end

figure(1);
plot(x,y,'+',xr,yr1,'-r',xr,yr2,'-r');
title (['Abrasion depth locations +; ' 'Total number of valid data points = ' num2str(data_pts)]);
xlabel('X (mm)');
ylabel('Y (mm)');
x_max = max(x);
x_min = min(x);
y_max = max(y);
y_min = min(y);
xlim([x_min x_max]);
ylim([y_min y_max]);

figure(2);
plot((1:data_pts)',z,[1 data_pts],[0 0], '-r');
xlabel('Data point from one edge to another');
ylabel('Abrasion depth (mm)');
xlim([1 data_pts]);

figure(4)
xlin = linspace(min(x),max(x),300);
ylin = linspace(min(y),max(y),300);
[Xs,Ys] = meshgrid(xlin,ylin);
f = TriScatteredInterp(x,y,z);
Zs = f(Xs,Ys);
mesh(Xs,Ys,Zs) %interpolated
axis tight; hold on
%plot3(Xs,Ys,Zs,'.','MarkerSize',15) %nonuniform
contour(Xs,Ys,Zs)
xlabel('X (mm)');
ylabel('Y (mm)');
```

```
zlabel('Abrasion depth (mm)');
set(gca,'ZDir','reverse')

%set(gca,'ZDir','reverse')
```

C. MATLAB script for calculating average depth

```
% 3D scanner data
load A_final.txt;
x = A_final(:,1);
y = A_final(:,2);
z = A_final(:,3);
data_pts = size(x,1);
x0 = mean(x);
y0 = mean(y);

figure(1);
plot(x,y,'.');
title (['before; ' 'Total number of valid data points = ' num2str(data_pts)]);
xlabel('X (mm)');
ylabel('Y (mm)');
% Radius of data inclusion
r1 = 40;
r2 = 48;

 sum_z = 0;
cnt = 0;
for n = 1: data_pts
   dist = sqrt((x(n) - x0)^2 + (y(n) - y0)^2);
   if dist >= r1 && dist <= r2;
      sum_z = sum_z + z(n);
      cnt = cnt + 1;
   else
      x(n) = NaN;
      y(n) = NaN;
   end
end
zave = sum_z / cnt

figure(2);
plot(x,y,'.');
title (['after; ' 'Total number of valid data points = ' num2str(data_pts)]);
xlabel('X (mm)');
ylabel('Y (mm)');
```

D. Sample Calculation of SVD of a concrete sample

A_ raw was the dataset obtained from 3D scanner after scanning Fly ash modified repair material sample at the age of 7days. After that whole data was centered so that the center of the whole data set become (0, 0) **A** matrix contains the data after centering. The columns of **A** matrix represent the x, y & z coordinates of vertex points of sample concrete surface, respectively where the number of rows represent the total number of vertex points.

$$\mathbf{A\_raw}=\begin{bmatrix} 7.735 & -1.1944 & 2.7094 \\ 8.23 & -1.1516 & -2.8411 \\ . & . & . \\ . & . & . \\ . & . & . \\ 17.776 & -103.68 & -5.24 \end{bmatrix}$$

$$\mathbf{A_{mn}} = \begin{bmatrix} -6.54 & 50.7296 & 1.0921 \\ -6.046 & 50.7724 & 0.9604 \\ . & . & . \\ . & . & . \\ . & . & . \\ 3.4981 & -51.7634 & -1.4467 \end{bmatrix}$$

The theorem of SVD (singular value decomposition) analysis can be represent like this,

$$\mathbf{A_{mn}} = \mathbf{U_{mn}S_{mm}V_{nn}^{T}}$$

After using SVD function in MATLAB for $\mathbf{A_{mn}}$ matrix, the value of **U, S** and **V** matrix were evaluated which are given below.

$$\mathbf{U_{mn}}=\begin{bmatrix} 0.096 & -7.68\text{e}-05 & -0.0092 \\ .0096 & -1.7217\text{e}-04 & -0.0108 \\ . & . & . \\ . & . & . \\ . & . & . \\ -0.0097 & 6.8172\text{e}+03 & 91.8118 \end{bmatrix}$$

$$\mathbf{S_{mm}}=\begin{bmatrix} 5.344e+03 & 0 & 0 \\ 0 & 5.249e+03 & 0 \\ 0 & 0 & 91.8118 \end{bmatrix}$$

$$\mathbf{V^T}=\begin{bmatrix} -0.1364 & -0.9902 & -0.0316 \\ 0.9899 & -0.1350 & -0.0422 \\ 0.0375 & -0.0370 & 0.9986 \end{bmatrix}$$

So the equation $\mathbf{A_{mn}= U_{mn}\, S_{mm}\, V^T_{nn}}$ becomes like this,

$$\begin{bmatrix} -6.54 & 50.7296 & 1.0921 \\ -6.046 & 50.7724 & 0.9604 \\ . & . & . \\ . & . & . \\ . & . & . \\ 3.4981 & -51.7634 & -1.4467 \end{bmatrix}=$$

$$\begin{bmatrix} 0.096 & -7.68\text{e}-05 & -0.0092 \\ .0096 & -1.7217\text{e}-04 & -0.0108 \\ . & . & . \\ . & . & . \\ . & . & . \\ -0.0097 & 6.8172\text{e}+03 & 91.8118 \end{bmatrix} \begin{bmatrix} 5.344e+03 & 0 & 0 \\ 0 & 5.249e+03 & 0 \\ 0 & 0 & 91.8118 \end{bmatrix} \begin{bmatrix} -0.1364 & -0.9902 & -0.0316 \\ 0.9899 & -0.1350 & -0.0422 \\ 0.0375 & -0.0370 & 0.9986 \end{bmatrix}$$

The main objective of the SVD function was to determine $\mathbf{V_{nn}}$ by which $\mathbf{A_{mn}}$ matrix was multiplied to determine the coordinates of rotated concrete surface.

$$\mathbf{A_{mn}}*\mathbf{V_{nn}} = \begin{bmatrix} 51.1530 & -0.4104 & -0.8426 \\ 51.1226 & -0.9038 & -0.9916 \\ . & . & . \\ . & . & . \\ . & . & . \\ -51.7743 & 3.5787 & 0.6283 \end{bmatrix}$$